Study on Depth-dependent Characteristics in Micro EDM Drilling Based on Observation of Bubble and Debris Behavior

気泡と加工屑の観察に基づく微細深穴の放電加工特性の深さ依存性に関する研究

LI GUODONG

李国棟

Abstract

Electrical discharge machining (EDM) as one of non-conventional machining technologies is widely used in the industry. Its unique virtues in machining conductive materials regardless of the hardness of materials without direct conduct force improve its applications in many fields. With the growing requirements for the micro products, the micro EDM is put forward and its achievements in machining micro features from the shaped micro holes to the complex micro 3D cavities also proves its ability in micro machining.

Micro hole drilling, as one of most important applications and fundamental of the micro EDM, has been researched for many decades. From the achievements in applications, it is successful to the micro hole drilling with EDM. A micro hole with high aspect ratio can be easily obtained with many methods put forward by many researchers. However, in the investigation of the mechanism, it is still a long way for the micro EDM drilling.

In micro EDM drilling, a seemingly simple discharge process contains many complex phenomena from the breakdown of insulated medium to the dispersion system in the gap area. Many methods in pursuing the micro hole with higher aspect ratio mainly depends on the empirical inferences because it is difficult to directly observe the narrow interelectrode gap area. The high-speed camera makes it possible to observe the discharge process based on the specifically designed experiment and such as using transparent workpiece or electrode. However, the detects of the simplified model in published researches are obvious and not suitable to observe the actual micro hole drilling. It is necessary to clarify the gap area based on the actual machining.

In this research, the investigate on the micro EDM drilling is conducted mainly from the following three aspects:

Firstly, the feasibility of observing the interelectrode is explored based on the original compressed sandwich workpiece. The detail of gap area is clarified based on the observation of bubble and debris in SiC and stainless steel SUS304 workpiece. The phenomenon of decreasing machining speed with increase of hole depth is analyzed. Then an improved glued sandwich workpiece is put forward to make use the gap area is totally blocked. The results shown that with increase of hole depth, both bubbles and debris accumulate in the gap area. Bubble will grow up or merge with other bubble to become a big bubble. Debris is not freely distributed in the gap area. They will stick on

the wall of micro hole and surface of micro tool, which decreases the insulated strength of gap area seriously. Thus, the abnormal discharges and short circuits occur frequently, resulting in the frequent retreats of the micro tool. Moreover, the discharge can even occur in debris, leads to the material in workpiece can't be removed and the exist of the machining limitation.

Secondly, the bubble and debris in the actual micro EDM drilling is quantitatively estimated based on the observation of bubbles escaping from the entrance of micro hole. A method is put forward to make the distribution of bubble escaping from the entrance of micro hole orderly by creating a constraint flowing area in the machining area. All the parameters are determined based on the simulation of the velocity filed of the dielectric liquid in COMSOL Multiphysics. The experiments are conducted in the specially debugged equipment to make sure the discharge signals and video can be synchronously recorded and matched. Then a series of solutions are put forward to realize the quantitative estimation on bubble behavior. An image segmentation method based on the digital image processing in MATLAB is used to extract the bubble precisely from the image of the captured video.

In order to instigate the generation of bubble and debris in the single discharge process, the single discharge is observed by using a pair of needle electrodes. It is found that in the breakdown stage only the discharge occurs. The bubble and debris are generated in 10μs after breakdown. The bubble firstly expends then contracts but the contracting time is much longer than the expending time. The melted material is scattered into the dielectric to become debris.

The depth-dependence characteristic of bubbles behavior is quantitatively estimated in the micro hole drilling with EDM. In the normal discharge stage, with the increase of hole depth, the size of bubble has the trend to become larger, the escaping frequency decreases seriously but the flowrate of bubble volume decreases firstly then increases. Two parameters, bubble escaping frequency and bubble flowrate frequency, are used to investigate the bubble behavior in the corresponding discharge frequency. In the consecutive short circuits, once the short circuit starts, the bubble will stop to escape from gap area immediately. Moreover, the debris cluster is observed, which proves that the debris is not freely distributed in the gap area. In the discharge in low open circuit voltage, mass littles bubbles escape from gap area, resulting in the increase of the bubble escaping frequency and flowrate frequency.

Thirdly, a method to improve the machining speed by using the mist jet is put forward. Compared to the conventional water jet, the mist jet with high momentum can flush the gap area strongly and improve the exchange of dielectric liquid in the gap area. The advantages of the mist jet are analyzed from the mechanism and verified by the observation of gap area. An original mist device is designed, fabricated and used in the experiment of micro hole drilling to investigate its performance in micro EDM drilling. It is found that by using the mist jet, the machining speed can be improved significantly. It seems that the machining limitation disappears with mist jet. A deeper micro hole can be obtained in the faster machining speed with the mist jet.

Content

Chapter 1. Introduction

1.1 Background of electrical discharge machining

During the nearly 150 years from the first industrial revolution to the second world war, the mechanical cutting (turning, milling, planning and grinding) is the mainly machining method for the industry products, which depends on cutting the softer material by using a harder tool. Since the nineteen fifties, the rapidly growing requirements of special industry products, such as high accuracy, high temperature and pressure resistance and miniaturization, improve the development of non-conventional machining technologies especially in the defense industry. The challenges for the conventional manufacture mainly focus on the following three aspects:

1. Solutions on machining difficult-to-machine materials. The excellent physical properties of difficult-to-machine materials, such as high hardness, strength, toughness and temperature and pressure resistance, make them irreplaceable in the industry. Therefore, the newly machine method is necessary to realize the machining in them.

2. Solutions on machining the complex special surfaces. Many products work on the extreme circumstances. For instance, the turbine blades and artillery bore works in the high temperature and pressure environment. The surface quality is significantly important.

3. Solutions on the parts with special requirements. For instance, the diesel flue nozzle, inkjet printer nozzle and turbine blades cooling channels.

It is difficult and even impossible to solve the above challenges just depending on the conventional mechanical cutting processes. Therefore, the Non-Traditional Machining (NTM) or Non-Conventional Machining (NCM) is to put forward. Compared to the conventional machining, the NCM provides a totally different thought depending on the unique virtue of every method. The characteristics of NCM are shown as following three aspects [1, 2, 3]:

1. The material removal mainly depends on other form of energy such as luminous energy, chemical electrolysis and thermal energy, not just the mechanical energy.

2. The tool is totally different with that in the conventional mechanical cutting. It can be laser, electron beam or small particles.

3. No direct contract force or the contract force can be ignored.

The electrical discharge machining (EDM) is one of most used NCM. Its two branches,

the sinking EDM and wire EDM, are widely applied in the industry such as fabrication of dies, mouldings, drilling and metal cutting. Its unique virtues are presented in the following three aspects [4,5,6,7,8]:

1. Ability in machining any conductive or semi-conductive materials regardless of hardness of materials.

2. No direct contract force.

3. Ability in machining complex features with high accuracy.

In EDM, the material is removed by the thermal energy generated during the breakdown of gap area. Therefore, the only requirement on the material of workpiece and tool is the electrical conductivity. The breakdown occurs in the gap width of dozens of microns. Therefore, no direct contract force between the workpiece and tool. Moreover, the short gap width also ensures the machining accuracy. By being integrated with CAD/CAM systems [9, 10], very complex 3D features can be generated with simple shaped tools.

The basis of EDM can date from 1770, the erosive effect of discharges is discovered by English chemist Joseph Priestly [8]. In 1943, Lazarenko from Moscow University creatively developed the EDM [4] based on the two creations: the resistance-capacitance type of power supply (RC circuit) and the application of insulted dielectric liquid, which realize the tiny material removal in the discharging by tiny energy releasing during significantly short discharge interval and is widely used at the EDM machine in the 1950s and later served as the model for successive development in EDM [5]. In the same period, based on the work by using electrical discharge to remove broken taps and drills from hydraulic valves, three American employees put forward an electronic-circuit servo system that can automatically keep the proper gap width and avoid the direct contract between the tool with workpiece [6].

Actually, the EDM process is based on the removing material by means of a series of repeated single electrical discharges [11] in the presence of an insulated dielectric liquid [12]. Therefore, an automatic control system is crucial to the continuous processing of EDM, especially in improving the machining efficiency. Until the 1980s with the advent of computer numerical control (CNC), the mature control system for EDM process is developed [7]. Since then, the merits of EDM in machining of conductive material have attract enormous attentions. Many research hotspots have been studied from applications to theory [13, 14, 15] and related manufacturing technologies from sinking

EDM [16] to wire EDM [17,18,19] have been widely used in the industry.

1.2 Mechanism of EDM

The material removal in EDM is based on the discharging corrosion in the pulse discharge between tool with workpiece (cathode, anode) from the breakdown of gap area [4,5,6,7,8,20, 21,22]. A whole discharging process can be distributed into four stages in Fig. 1.1: breakdown of gap area; formation of discharge channel; material removal and medium evaporation; scattering of melt material, bubble expansion and contraction, and recovery of insulation strength.

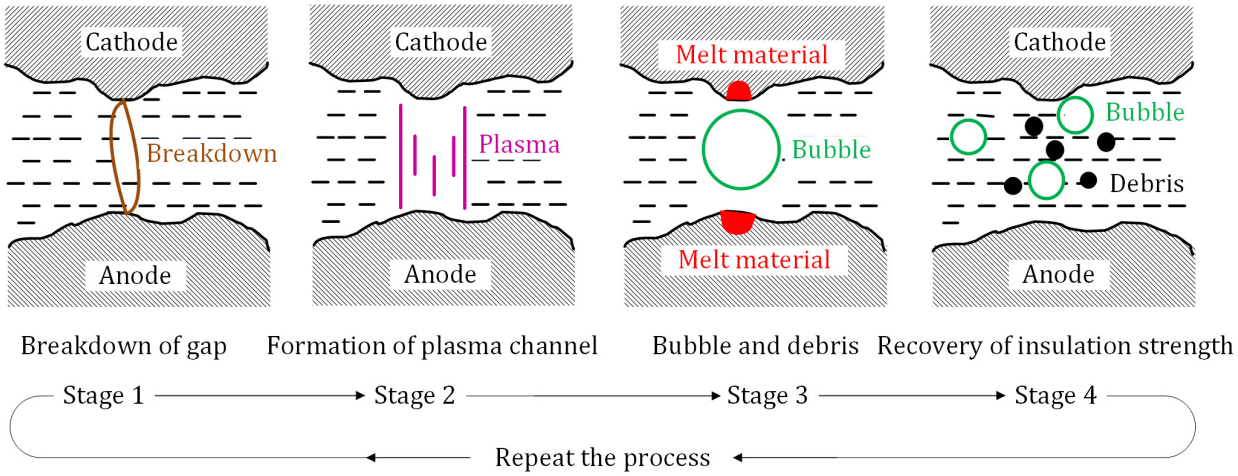

Fig.1.1 Mechanism of EDM process

In order to keep the processing continuous, three basic conditions have to be satisfied:

1. A proper gap width. The proper gap has to be kept between the tool electrode with workpiece. If the gap width is too large, the gap cannot be breakdown and the discharging cannot occur; If the gap width is too short, it is very easy to cause the short circuit and impact between tool electrode with workpiece. Thus, an automatic control is necessary to control the feeding speed of tool electrode and keep the proper gap width. Varieties of servo control systems have been developed by EDM machine manufacturers based on the detection of voltage and current in the gap to satisfy different requirements [23, 24, 25, 26].

2. A proper power supply [24,27,28]. The discharge has to be the pulsed. After the discharging duration, an enough long discharge interval should be kept to make sure the recovery of insulation strength, cool the discharge heat releasing during the discharging and avoid the abnormal discharge, especially the consecutive plasma discharge, which seriously lowers the machining accuracy and increases the tool wear.

3. Insulated media [12, 28, 29, 30]. The discharge should be occurred in the insulated media because the insulated media has high insulation strength, which is condition to make the breakdown occur in significant narrow gap width and insulation recover quickly after the discharge. Generally, the liquid media is widely used in EDM process such as kerosene, tap water and deionized water. The gas media [31, 32] such as air and nitrogen plasma jet [33, 34, 35] have been reported experimentally but many obstacles still exist before the commercial use, for instance, the extremely frequent short circuits in the discharge with air.

The machining system of EDM is shown in Fig. 1.2.

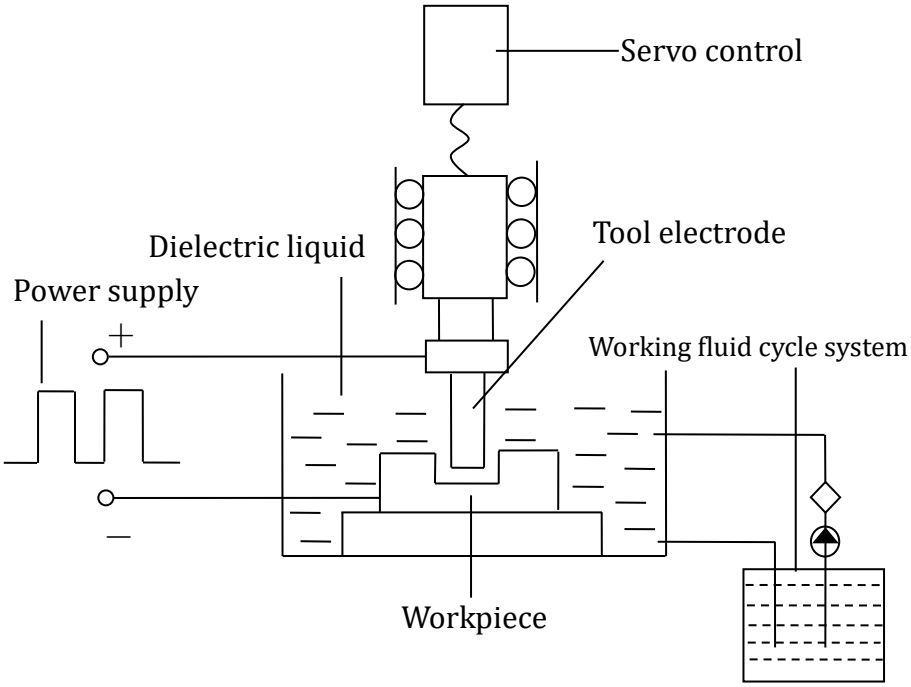

Fig. 1.2 Machining system of EDM

The tool electrode and workpiece are connected to the output terminals of power supply according to the machining requirement. A servo feeding system to control the movement of tool electrode and keep a proper gap width between tool electrode with workpiece. In the machining, when the distance between tool electrode with the workpiece reaches the threshold breakdown distance, the gap area will be breakdown and the discharge will occur. The heat releasing during the discharge melt material in the workpiece to generate the micro crater and tool wear in tool electrode. The material removal amount depends on the physical property of material and energy distribution on cathode and anode. Since the breakdown is much easier to occur in the plot with the weakest insulation strength, namely the spot with shortest distance between cathode and

anode [36, 37, 38, 39], the feature obtained in the workpiece by continuous tiny material removal can accurately duplicate the shapes of tool electrode. Therefore, the EDM has high machining accuracy.

1.3 Micro EDM

1.3.1 Background of micro EDM

With the development of modern manufacture, the requirement of mechanism miniaturization improves the advancement of micromachining technology [40]. For instance, after the introduction of semiconductor devices, electrical circuits become extremely compact. Integrated circuit packages require more and more micro parts and micro features. In automobiles, the fuel injection nozzle forces the design and machining of nozzle towards smaller size and higher accuracy. In medical applications [41], miniaturization of medical tools is one of effective approaches to the inspection and surgery without pain. Therefore, the micro machining is necessary for the satisfaction of rapidly expanding requirements for microproducts.

The EDM has great potential in micromachining [40, 42, 43]. Since the material removal in EDM depends on the repetitive tiny discharge corrosion, it seems easy to realize the micro EDM just by lowering the discharge energy. However, it is more complex in the actual machining. The characteristics of micro EDM is shown in following four aspects [13, 16, 24, 27, 40, 42, 43]:

1. Tiny discharge energy and area. In order to pursue the high accuracy in small products, the single discharge energy has to be enough small to make sure the tiny material removal.

2. Narrow discharge gap. The high machining accuracy require the discharge occurs in narrower gap area compared to the conventional EDM process. Therefore, the feeding control of tool electrode has higher requirement for the servo system.

3. Fabrication of precise micro tool electrode. In conventional EDM, the tool electrode can be finished by the precise mechanical machining micro EDM, then fixed on the EDM machine. However, in micro EDM, the high machining accuracy of micro parts requires precise micro tool electrode. Moreover, the fixture error caused by the second fixture influences the machining accuracy seriously.

The two basic challenges: stably fabricating micro tool accurately and avoiding the

second fixture errors, give a great require the newly design in micro EDM machine that the micro tool has to be fabricated online.

The earliest report about EDM-based micromachining is from Philips Research Laboratory at the end of 1960s [44, 45], van Osenbruggen fabricated a small electrode with diameter of 30μm in a precision EDM machine with dimensional tolerances up to 0.5μm. After this pioneering work, due to the low machining efficiency and poor machining repeatability, the interest in micro EDM was fading away until in the later 1980s, the wire electrode discharge grinding (WEDG) was put forward by Masuzawa T. to fabricate the micro tool electrode [46].

1.3.2 WEDG method for micro electrode fabrication

In 1984, professor Masuzawa from Institute of Industrial Science in the University of Tokyo put forward a creatively method, wire electrode discharge grinding (WEDG) method, to successively solve the fabrication of micro tool electrode, which is widely used in the EDM and micro EDM until now [46].

The schematic of WEDG method is shown in Fig. 1.3. A wire electrode, commonly copper wire, moves slowly along the edge of guide wheel. At the same time, the tool electrode in high rotational speed feeds towards the wire electrode to finish the fabrication of designed tool electrode. The advantages of WEDG method are in the following three aspects:

1. The contract between wire electrode with tool electrode is nearly the point contract or line contract. The tiny contact area leads to the machining in high accuracy. By control the movement of tool electrode, varieties of shaped electrodes can be obtained easily with high accuracy, such as the cylindrical electrode, tapered electrode, square electrode and spiral electrode.

2. WEDG unit is very small and flexible and can be conveniently integrated into the micro EDM machine to realize the online fabrication of tool electrode and avoid the second fixture error.

3. The wear of wire electrode can be totally ignored. The wire electrode is continuously moving along the guide wheel so that every part of wire electrode only has one chance to participate in the discharge and then leave the machining area. Therefore, in every discharge, the wire electrode is unused, which makes sure the tool electrode can be fabricated accurately and avoids the influence of tool wear.

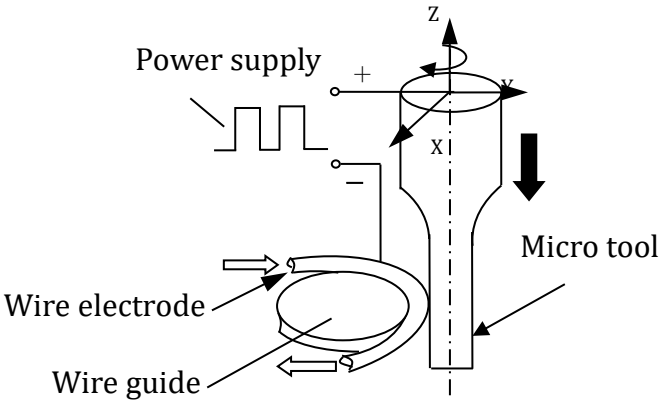

Fig. 1.3 Schematic of WEDG method

1.3.3 Application of micro EDM in 2D features

After the WEDG method is put forward, the application of micro EDM in 2D features has been largely developed. Many micro holes, shaped holes and array holes have been reported. The micro tool electrode with diameter of Φ8μm fabricated by WEDG method [47]is shown in Fig. 1.4. The array holes [46] with diameter of Φ5μm is shown in Fig. 1.5. Complex shaped holes can also be obtained by using the planetary movement combined with the shaped tool electrode [48, 49] as shown in Fig. 1.6.

However, the micro EDM in 3D machining is blocked by a great obstacle, tool wear. The tool wear leads to the poor accuracy of micro tool electrode after many discharges.

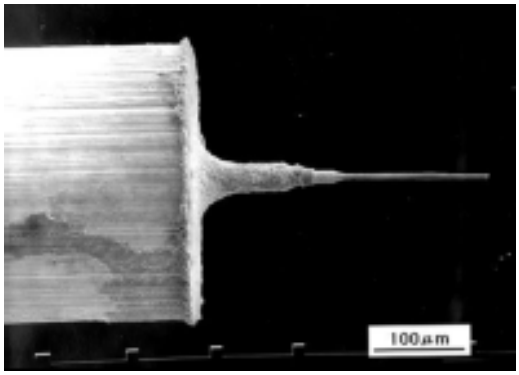

Fig. 1.4 Micro tool electrode fabricated by WEDG method

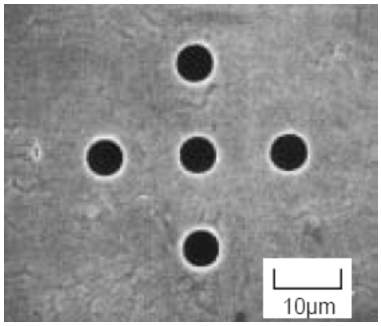

Fig. 1.5 Micro hole with diameter of 5μm

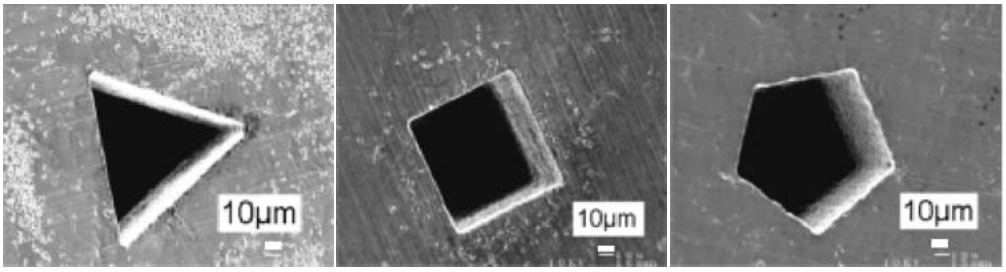

Fig. 1.6 Shaped micro holes

1.4 Application of micro EDM in 3D features

1.4.1 Tool wear [50, 51, 52, 53, 54]

The discharge corrosion in EDM not only removes the material in workpiece but also removes the material in tool electrode. The amount of material removal depends on the energy distribution and material of workpiece and tool electrode [55, 56, 57]. In micro EDM, in order to decrease the tool wear, the material of tool electrode is usually chosen the tungsten or tungsten carbide, which has excellent electric and thermal conductivity, meanwhile has high melt point to decrease the thermal removal in discharge.

The schematic of tool wear is shown in Fig. 1.7. A tool electrode after being fabricated by WEDG method is standard cylinder. In the EDM, due to the tip effect, the electric field in the edge of micro tool is much larger than other area. Therefore, the material in the edge of micro tool is easier to be removed. The tool wear is happened from edge to the center. A cylinder tool electrode may become a taper or needle electrode due to the tool wear. In Fig. 1.7, a is the height of tool wear in bottom; b is the height of tool wear in the edge; C, the tool wear in the side wall.

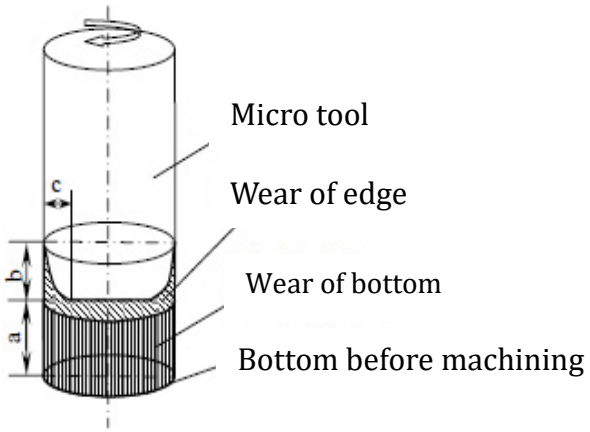

Fig. 1.7 Schematic of tool wear

The tool wear leads a big problem that in the whole EDM machining, the change of tool shapes results in the change of gap width. Moreover, the tool wear is non-uniform so that the detection and prediction is very difficult. Therefore, in 3D machining with EDM, the gradually deteriorated accuracy of tool electrode leads to the poor accuracy.

1.4.2 Uniform wear method

In 1997, the uniform wear method (UWM) was put forward by Z. Yu to solve the tool wear in micro EDM [58]. The thought is that although the tool wear is inevitable in EDM, a proper compensation can be provided to replace the tool wear. In UVW, the 3D feature is conducted layer-by-layer using a simple shaped electrode such as a cylinder tool or square tool. The method is based on the phenomenon that under certain conditions, the shape of electrode tip is recovered after machining one layer. Therefore, before machining, a proper tool path should be designed to determine the number of layers and compensation in each layer. The compensation of each layer can be calculated by the following equation:

$$\Delta Z = L_w(1 + v\frac{S_w}{S_e}) \tag{2.1}$$

Where: L_w, the thickness of each layer; v, the ratio of volume wear of tool electrode and workpiece; S_w, the area of current layer; S_e, the section area of tool electrode.

The equation concludes two parts: the thickness of current layer L_w and the compensation thickness $L_w v S_w / S_e$. Once the tool wear exists, it will be compensated in the next layer. Therefore, by properly design the tool path and distribute the 3D feature into many layers, the 3D machining can be conducted accurately.

A representative 3D feature machined by using UWM is the micro car fabricated by Z. Yu. The CAD design of micro car is shown in Fig. 1.8. The tool path for the car body and roof is shown in Fig. 1.9. The tool path for the car wheel is shown in Fig. 1.10.

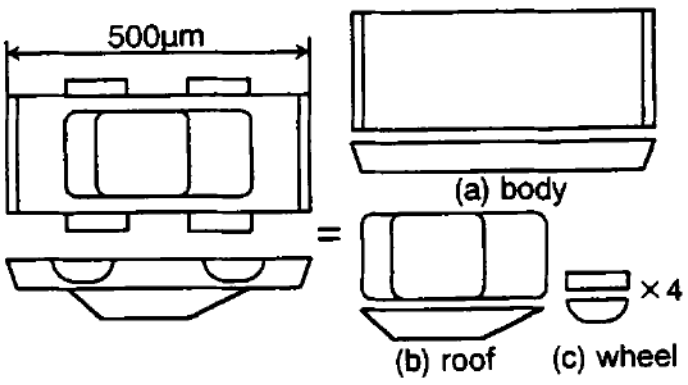

Fig. 1.8 Components of a micro car mold

Fig. 1.9 Tool paths for machining parts of body and roof (X-Y plane)

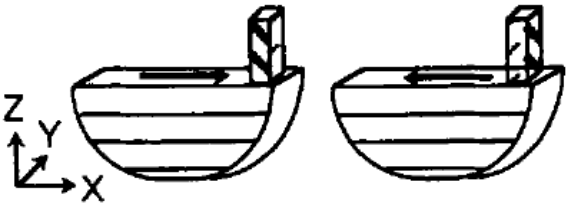

Fig. 1.10 Tool paths for machining of wheels

The SEM image of micro car mold is shown in Fig. 1.11. The micro tools for car roof and wheel before machining are shown in Fig. 1.12 (a) and (b) respectively. The tool for car roof after machining is shown in Fig. 1.12 (c). It is found that the edge of micro tool after machining is still very sharp and the tool wear seems to completely compensated. Z. Yu also obtained a press micro car model by using the car mold. It also indicated the micro EDM can be used in the micro mold fabrication.

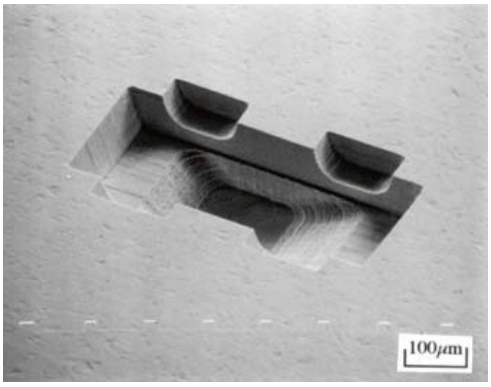

Fig. 1.11 Micro car mold

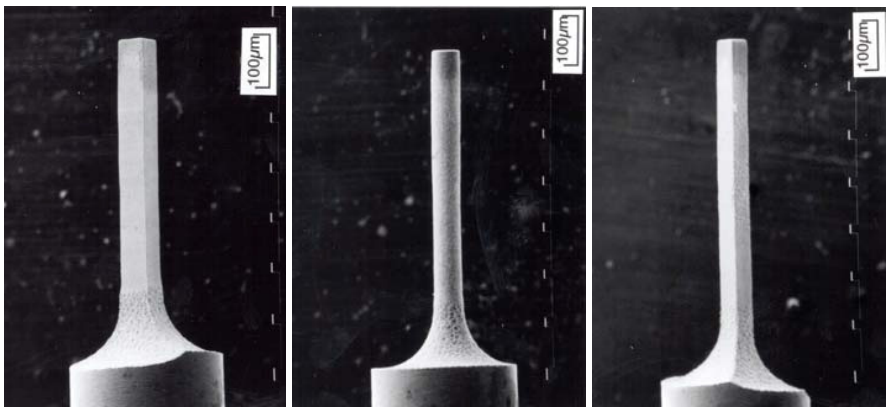

(a) For car roof (b) For car wheel (c) Tool after machining

Fig. 1.12 Tool electrode used in micro car

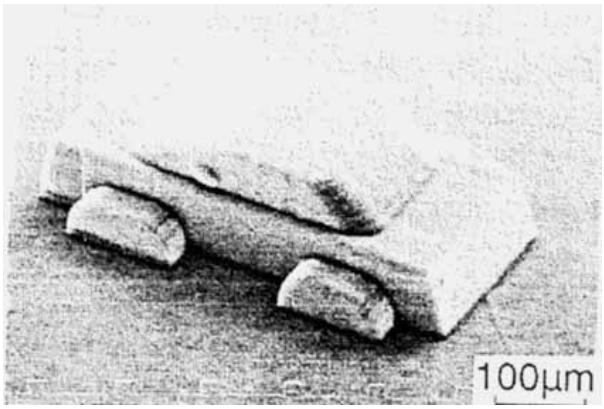

Fig. 1.13 Press molding of a microcar model

1.4.3 3D features machined by micro EDM

After the UWM is put forward, the 3D features fabrication by micro EDM is widely used in the machining of die, mold [59] and micro punching [60, 61]. Later, in order to solve the limitation of generating 3D complex cavities due to lack of necessary Computer Aided Design and Manufacturing (CAD/CAM) systems to generate the tool paths, Z. Yu and K. Rajurkar proposed an approach to integrate UWM with a CAD/CAM system [9]. It is more convenient for the 3D features fabrication with the CAD/CAM system. The tool path of 3D complex feature can be easy generated by the CAD/CAM software. Moreover, the tool path, thickness of layer and compensation thickness can be optimized by the CAD/CAM system so that the machining speed and accuracy can be improved significantly.

A complex cavity designed by CAD is shown in Fig. 1.14 then the tool paths are regenerated using the uniform wear method followed by the compensation of electrode wear method followed by the compensation of electrode wear in the NC codes.

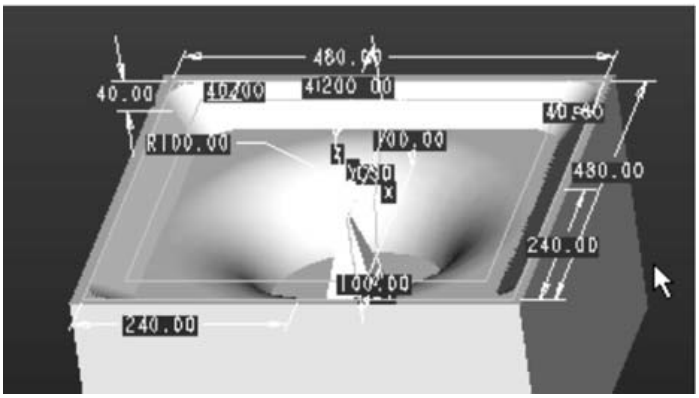

Fig. 1.14 CAD design of a complex cavity

In order to improve the precision of the machined surface and obtain a more uniform electrode wear, the two set of tool paths is designed and generated by the CAD. The cut angle for each subsequent layer is changed, which means that the electrode moves along

the tool path (cut angle 0°) in Fig. 1.15 (a) to machine one layer, and then moves along the tool path (cut angle 90°) in Fig. 1.15 (b) to machine the next layer. The machined cavity is shown in Fig. 1.16 (a) and the micro tool electrode after machining is shown in Fig. 1.16 (b).

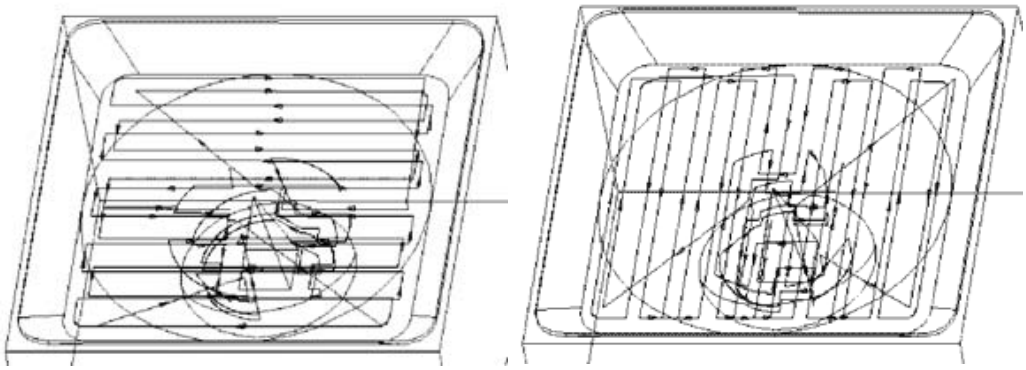

(a) Cut angle 0° (b) Cut angle 90°

Fig. 1.15 Tool paths

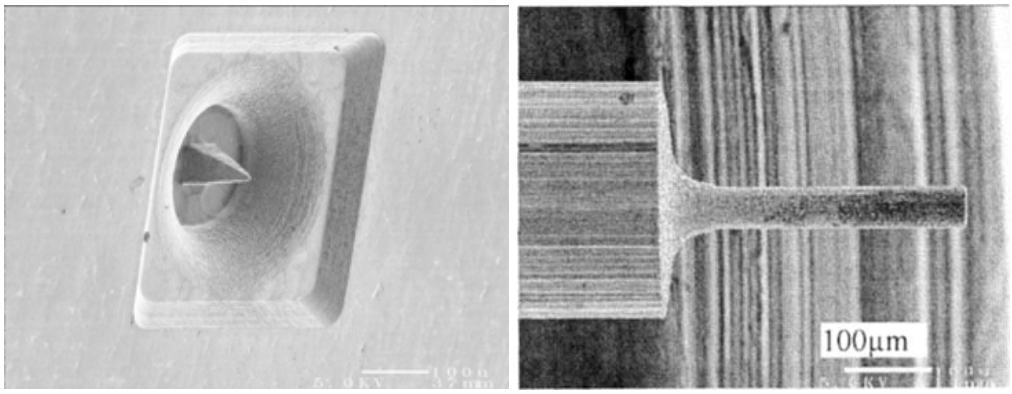

Fig. 1.16 Machined cavity and micro tool after machining

By integrated with CAD/CAM system, the 3D machining by micro EDM is very easy and almost arbitrary 3D features can be machined by micro EDM [62]as shown in Fig. 1.17.

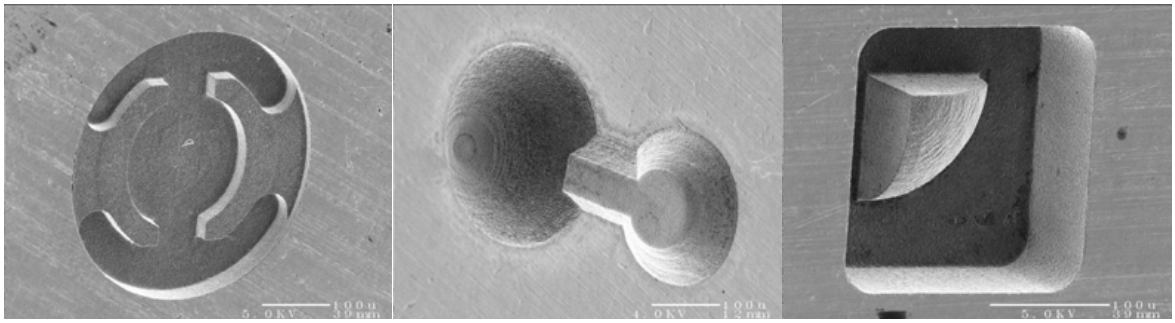

Fig. 1.17 Arbitrary 3D cavities

1.5 Micro hole drilling

Micro hole drilling, as one of most important applications and fundamental of micro

EDM, has been researched for many decades. As the statistical analysis in the manufacture, around 50-70% of all production time is spent making holes. Since the 2D and 3D machining by micro EDM is usually conducted in the layer-by-layer machining or a whole forming-electrode, the micro hole drilling is the base of above process. On the other hand, the micro drilling is a simper process compared to the 2D or 3D machining by micro EDM. Therefore, the basic procedure of micro EDM is always started from the micro hole drilling.

1.5.1 Obstacle in micro blind hole drilling

In micro hole drilling, the high AR (aspect ratio: the ratio of hole depth with hole diameter) is always pursued. However, after the experiments, many researchers find that it is very difficult to obtain a blind hole with high AR. After reaching a certain depth, the machining speed decreases seriously then the micro tool starts to retreat, which is called limitation of feeding depth in our research [33].

The phenomenon of feeding limit of the tool electrode, commonly exists in the micro EDM drilling. The reasons for the decreasing machining speed are owing to the gradually deteriorating environment in the views of most researchers although the details in the gap area still unclear, such as the conductive debris accumulation and concentration, tool wear, and low exchanging rate of dielectric liquid. Moreover, the scale of micro hole is so small that the viscous effect of liquid dielectric and capillary action also makes the exchange of dielectric difficult as shown in Fig. 1.18.

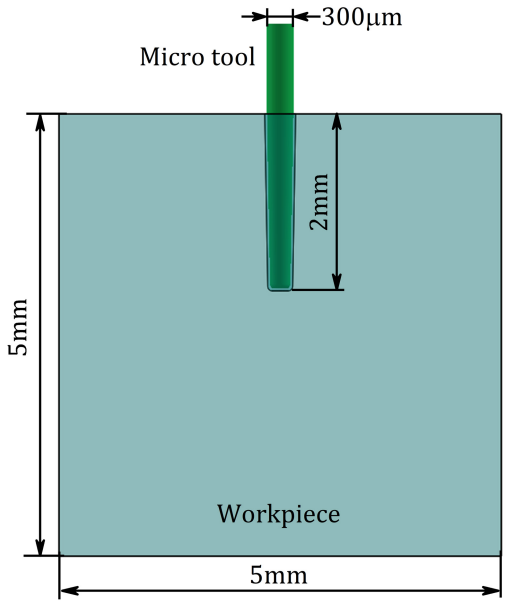

Fig. 1.18 Scale of micro hole

In micro hole drilling, the scale of micro hole makes exchange of dielectric liquid and

debris exhaust difficult due to the influence of surface tension, vicious resistance and capillary action. Mass debris accumulates in the gap area may decrease the insulation strength of gap area and cause the abnormal discharges, finally resulting in the frequent retreat of micro tool and decrease of machining speed.

Accumulation of conductive debris weakens the insulated strength of dielectric liquid. Tool wear leads to the uneven gap width. Moreover, the enlarging bubble occupancy area squeezes the space of dielectric liquid in the narrow gap area, furtherly improving the debris concentration. Therefore, the exhaust of debris, exchange of dielectric liquid and recovery of insulation strength of gap area play decisive roles in maintaining stable machining state in EDM process.

1.5.2 Methods to improve the AR of micro hole

In the conventional micro blind hole drilling by micro EDM with a solid micro rod, there is no effective self-flushing way except the bubble movement and micro tool rotation. Many researches were focused on the point of improving the flushing process to enhance the debris exhaustion and dielectric liquid exchange. Several novel methods put forward have largely improved the aspect ratio (ratio of the depth and diameter) of micro hole such as the ultrasonic vibration [65, 67, 68], helical tools [66] and planetary movement [67].

Wataru Natsu investigated the machining characteristic of micro EDM with ultrasonically vibrated machining fluid under ultra-small discharge energy [68]. The schematic is shown in Fig. 1.19 (a) and the curve of average feed rate is shown in Fig. 1.19 (b). Results shows that by using the ultrasonic vibration the feed rate of micro rate can be improved significantly.

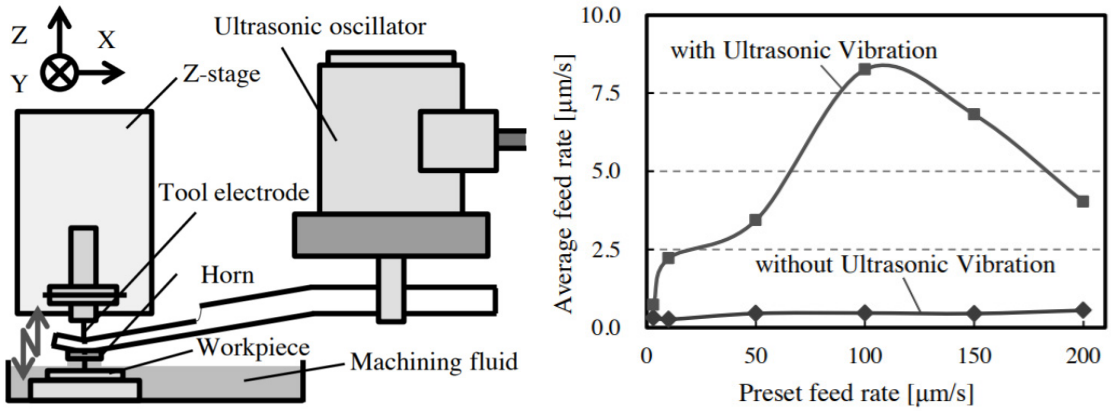

(a) Schematic of setup (b) Curve of feed rate

Fig. 1.19 Micro hole drilling with ultrasonic vibration

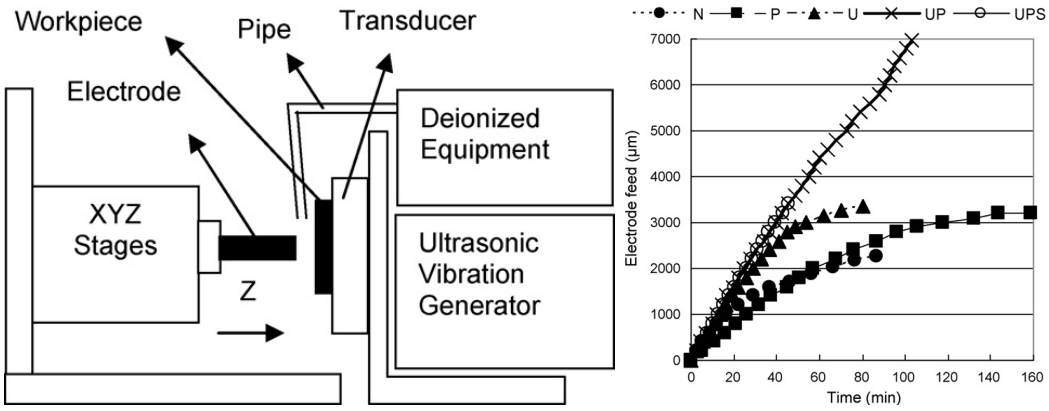

(a) Schematic of setup (b) Feed depth of micro tool

Fig. 1.20 Micro hole drilling with ultrasonic vibration and planetary movement (N, the normal state; P: planetary movement; U: ultrasonic vibration; UP: ultrasonic+planetary movement+feed depth of 6.97mm; UPS: ultrasonic+planetary movement+feed depth of 3.4mm)

Z. Yu combined the ultrasonic vibration with planetary movement of electrode to obtain a micro hole with aspect ratio of 29 [67]. The schematic of setup and feed depth of micro tool is shown in Fig. 1.20 (a) and (b) respectively. Results shows that by combining ultrasonic vibration with planetary movement, the AR can be improved significantly.

J. Hung used the hollow electrode to machine the micro hole with EDM [66]. The hollow electrode is shown in Fig. 1.21

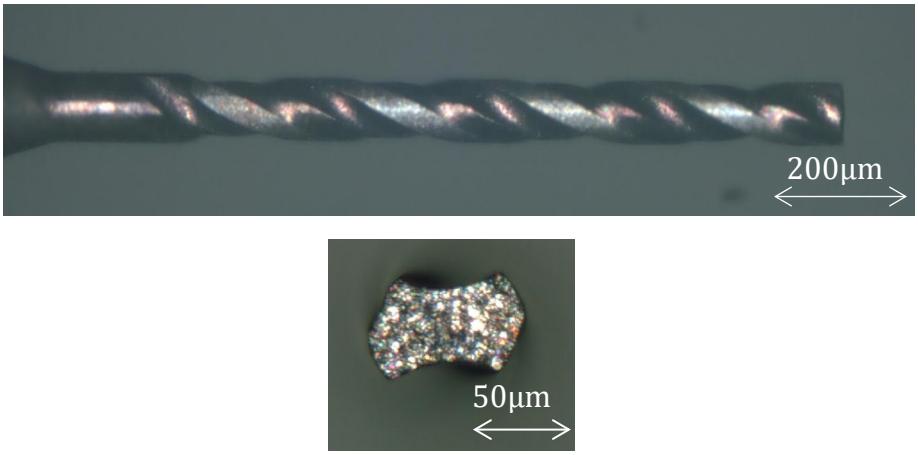

Fig. 1.21 Hollow tool electrode

However, it is difficult to obtain micro hole with an aspect ratio larger than 30 by using the solid electrode in the methods mentioned above. With the advancement of manufacturing electrode technology, the commercial tube electrode shown in Fig. 1.22 (a) was applied in micro hole drilling with internal flushing method. The machining of micro hole with an aspect ratio larger than 120 [69] shown in Fig. 1.23 has been reported by

using the tube electrode with insulted sidewall [69, 70] shown in Fig. 1.22 (b).

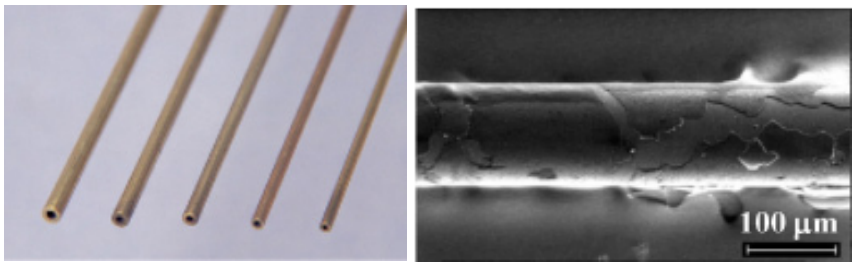

(a) Copper tube electrode (b) Insulated coat

Fig. 1.22 Tube electrode

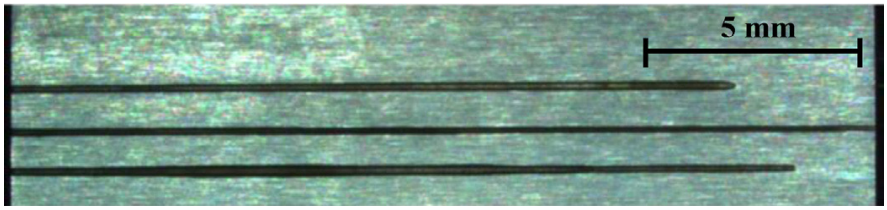

Fig. 1.23 Micro hole with high AR

1.6 Observation of gap area by high-speed camera

Many researchers also tried to investigate the mechanism of discharge process. In early 1972, I. Mitsutomo observed the bubble in EDM and found the bubble expansion [71] shown in Fig. 1.24. In 1987, J. Miyajima et al. used the transparent plastic disk to observe the gap area and found that the gap area was mostly occupied by bubbles [72]. In 2008, S. Hayakawa et al. used a special tool electrode, plastic flat plate with metal wire inserts, to observe the behavior of bubble and debris in the single discharge [73].

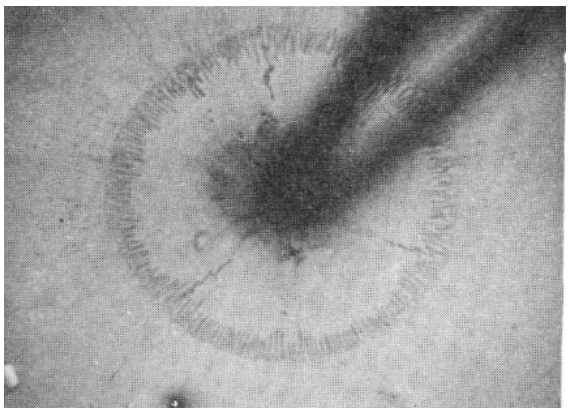

Fig. 1.24 Bubble expansion

It was found the bubble expansion and contraction (shown in Fig. 1.25 (a)) during discharge duration, meanwhile, the debris was scattered from the discharge point in parallel flat gap space (shown in Fig. 1.25 (b)). In 2012, J. Wang et al. used the similar

method to observe the behavior of bubble and debris during consecutive pulse discharges and analyze the mechanism [74]. Later, a simulation model was put forward to verify the observation results [75].

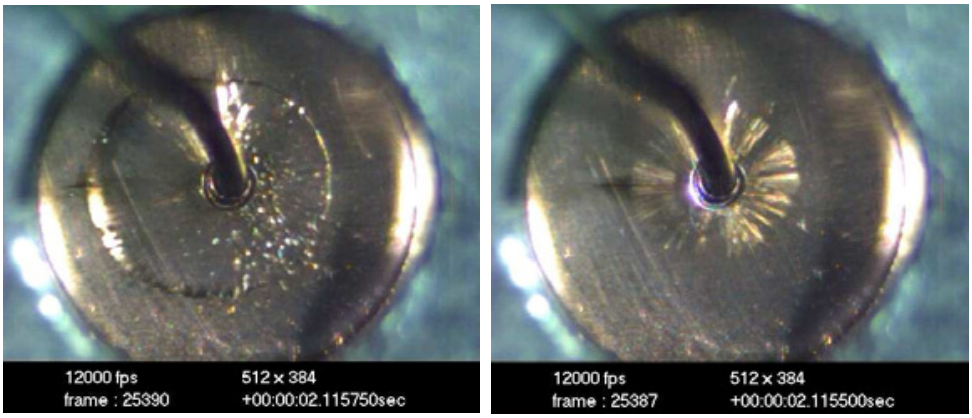

(a) Bubble expansion and contraction (b) Debris scattering

Fig. 1.25 Behavior of bubble debris

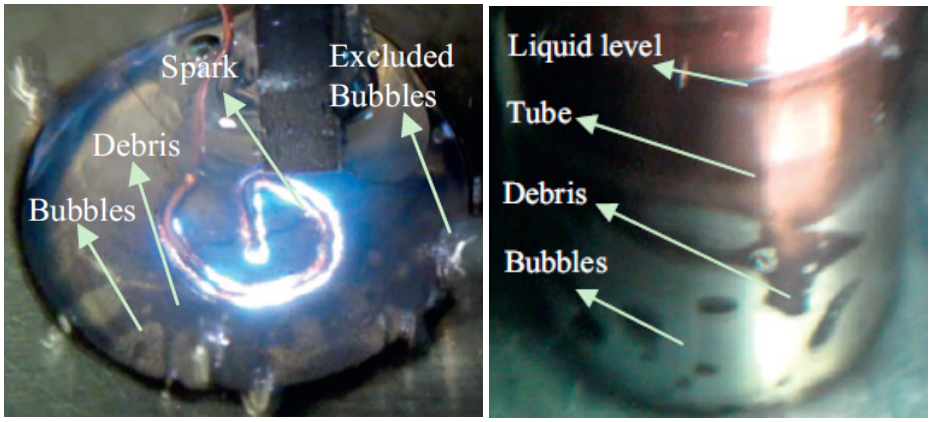

(a) Consecutive discharge (b) Bubble and debris

Fig. 1.26 Observation of bubble and debris in consecutive discharge

With the advancement of high-speed camera, the observation of gap area with high frame rate become possible. Many new insights of EDM have been clarified to explain the complex phenomenon in the interelectrode gap area which is hardly observed before. However, direct observation of gap area is still difficult because the tool electrode and workpiece are not transparent. In 2013, M. Kunieda et al. firstly used the gap area of EDM with transparent SiC electrode [76] and later in 2014 quantitatively described and compared the diameter of plasma heat source with the discharge crater by using the transparent Ga_2O_3 electrode [77], which has higher spectral transmissivity than SiC. The transmission of SiC and Ga_2O_3 is shown in Fig. 1.27. The image of arc plasma and crater is shown in Fig. 1.28.

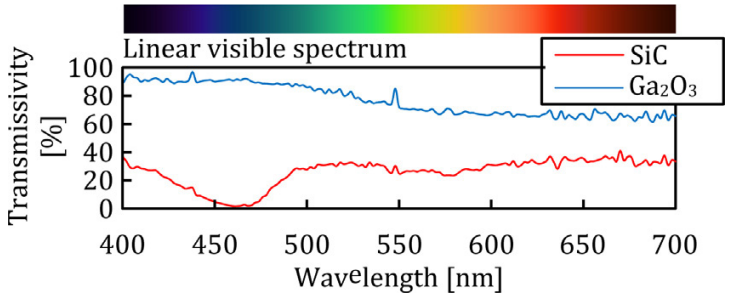

Fig. 1.27 Spectral transmission of SiC and Ga2O3 single crystals

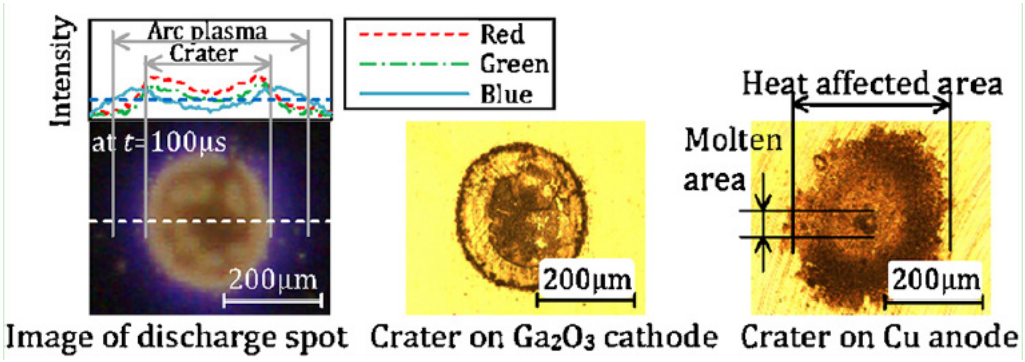

Fig. 1.28 Relationship between diameters of plasma and crater

In 2015, T. Kitamura and M. Kunieda still used the transparent SiC workpiece observe the bubble and discharge spot then discuss the relationship between bubble and discharge locations [78] as shown in Fig. 1.29.

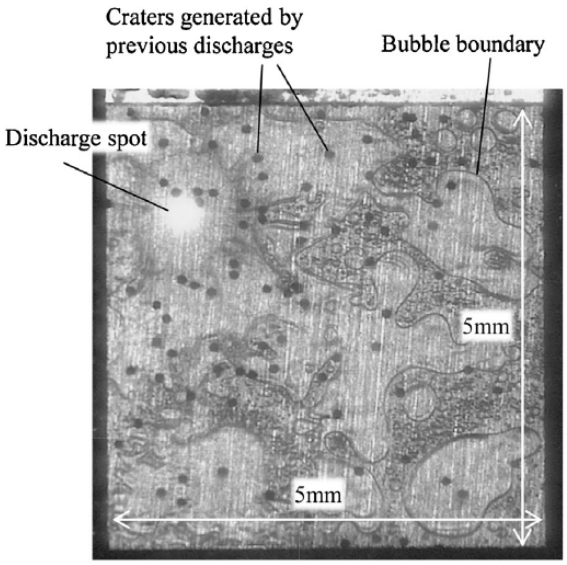

Fig. 1.29 High-speed video frames of EDM gap phenomena

Although these researches all pointed out that the bubble behavior plays a significant role on EDM drilling, the experiments were carried out under specific conditions which were not the same with the real machining process.

Actually, the investigation on the bubble behavior is difficult in micro EDM under the conditions the same with the real machining conditions. Firstly, it is difficult to observe

the gap area directly for a long time. Secondly, it is hard to quantitatively estimate bubble behavior since bubbles' moving and deforming in the narrow gap area.

1.7 Background of the Research

According to the summary no the previous researches, it is found that the drilling micro hole with micro EDM has been improved significantly and many effective and convenient methods have been put forward to obtain micro hole with high AR. However, many problems still exist:

1. The lack of reasonable explanations on the deteriorated environment.

The decrease of machining speed is attributed to the deteriorated environment. However, there is no clear definition to exactly describe or explain the deteriorated environment. In this research, the deteriorated environment is summarized into two layers of implications:

1) In the mechanism. The changes of whole EDM process after many discharges mainly three aspects: Material removal leads to the generation of debris and tool wear; Dielectric liquid evaporation leads to the generation of bubble; Discharge heat releasing leads to changes of temperature of gap area. Moreover, the changes in above three aspects influence each other. For instance: the discharge heat releasing may influence the size of bubble; The change of bubble size may squeeze the debris and leads to the debris concentration in the limited space of gap area; The concentrated debris decreases the insulated strength of gap area seriously and leads to the frequent discharge in low open circuit voltage or short circuit even the consecutive short circuit, resulting in abnormal discharges; The abnormal discharges influence the discharge heat releasing and the generation of bubble, which is back to the beginning. Therefore, the actual micro hole drilling is a very complex process.

In general, the changes are mainly shown in following three aspects: debris accumulation and concentration; bubble behavior; tool wear.

2) Results in discharges. These changes mentioned above eventually are reflected on the discharges. Firstly, debris accumulation and concentration decrease the insulated strength seriously so that the breakdown of gap area can occur more easily. The abnormal discharge states occur frequently, which mainly include discharge in low open circuit voltage, frequent short circuit and consecutive short circuit. Secondly, the reported research indicated that the most of gap area was occupied by the bubble. It reveals that

the bubble may not escape from gap area immediately so that they may stay in the gap area to become a big bubble. Therefore, the space for the debris may be squeezed, resulting in the debris accumulation and concentration. Moreover, the insulation strength of gas is much lower than the liquid. The large bubble occupancy area may change the insulation strength of gap area; Thirdly, tool wear leads to non-uniform gap width. Actually, because the electric field is not uniform due to the tip effect, the probability of discharge in the spot with larger electric intensity is higher than the spot with smaller electric intensity even if the gap with is uniform in the whole gap area. A cylinder tool electrode may become a tapper or needle electrode, which means that the gap area is enlarged seriously and the discharge may occur in larger area.

The increase of abnormal discharges increases the probability of short circuit, which is detected by the servo system to make the tool electrode retreat frequently. Therefore, the machining speed decreases.

However, the above inferences just depend on the empirical understanding of the mechanism of micro EDM. So far, no evidence has been presented to verify the explanation. It is necessary to observe the gap area of micro hole drilling directly, present the details in the gap area and verify the explanation.

2. The difficulty in observing the gap area directly. Although many observations have been done to observe the gap area, there are many defects in these methods. For instance, the excellent optical visibility of transparent material SiC or Ga_2O_3 is very suitable to observe the gap area. However, the observations based on transparent material were only carried out in a very short time because the transparent material became opaque after destruction of crystallographic texture by discharge plasma. Therefore, the results can't explain the phenomenon of gap area after a period of time. The observation of bubble and debris based on the transparent adhesive material is not consistent with the actual machining because the adhesive material is not conductive. This method ignores the influence of electric field on conductive debris. So far, no results have been reported in direct observation of blind hole drilling to explain the depth-dependence characteristics of bubble, debris and discharge.

The direct observation on the gap area is difficult. Firstly, it is impossible to observe the whole gap area with a shape of test tube; Secondly, it is difficult to quantitatively estimate on the behavior of bubble and debris in the corresponding discharge state. The bubble has complex physics properties in the narrow gap area such as fluidity, deformability,

viscosity and their variation characteristics in thermo-shock during discharging. The debris generated in machining conductive material is conductive, which may absorb ions in the gap area to become the colloid and influenced by the electric field.

1.8 Research purpose

In this research, based on the previous researches in the micro hole drilling, the purpose is focus on the following three aspects:

1. Put forward to a method to observe the interelectrode gap area directly by the high-speed camera during the long-time micro hole drilling with micro EDM to investigate the depth-dependent characteristics of bubble and debris and clarify their influences on the abnormal discharges.

2. Explore the feasibility of quantitative estimation on the bubble and debris in micro hole drilling to investigate the reasons for the decrease of machining speed with increase of hole depth

3. After the clarification of the deteriorated environment based on research on term 1 and 2, try to put forward a method to prevent the deterioration of environment and improve the machining speed in micro hole drilling.

1.9 Dissertation structure

The dissertation is arranged from following 5 chapters:

In chapter 1, the introduction and background of the research are presented. Firstly, the introduction and development from EDM to micro EDM are presented based on the key breakthroughs at that time. Then the background of micro EDM drilling is introduced from principle, machining to the application. The principle and many key factors such as fabrication of micro tool, tool electrode and gap control are explained. Based on analyzation and summarization on the current researches in micro EDM drilling, the research purpose is put forward that investigate the micro EDM drilling based on the bubble and debris.

In chapter 2, firstly all the machining devices used in the following chapters are presented and introduced. Secondly, the phenomenon of decreasing machining speed is investigated and confirmed. In order to clarify the reasons for the decreasing machining speed due to retreat of micro tool, the discharges signals in different machining speed were recorded and analyzed coupled with the servo control of NC system, which controls

the movement of micro tool, especially the discharge signals in a retreat process is analyzed. Results show that the reasons are due to the abnormal discharges mainly pointing to the consecutive short circuit and discharges in low open circuit voltage. It is indicated that the behavior of debris and bubble play a key role in decreasing the insulation strength of dielectric even links the cathode and anode. Therefore, it is necessary to observe and clarify the details in the gap area.

In chapter 3, the interelectrode gap area of micro EDM is clarified based on the direct observation on the interelectrode area depending on the original sandwich workpiece. Two methods, using hollow glass pipe and sandwich workpiece, are put forward to explore the feasibility of direct observation on the gap area. Results show that based on the original sandwich workpiece, the observation is feasible. Then an improved sandwich workpiece by is put forward to overcome the open-ended gap area in compressed sandwich workpiece and used in the observation of gap area. The behavior of bubble based on the SiC workpiece and behavior of debris based on the stainless steel SUS304 workpiece are observed and analyzed. Finally, in the foundation of observation, the influence of bubble and debris and influence of tool wear on the micro EDM drilling are analyzed and the deteriorated environment is explained

In Chapter 4, investigation is done for the quantitative estimation of bubble behavior in actual micro hole drilling. A series of solutions from experimental equipment to the measure of bubble size are put forward and presented. Firstly, a method is put forward to make the distribution of bubble escaping from entrance of micro hole orderly. Then many parameters are determined based on the simulation of velocity field of dielectric liquid in the upper surface of micro hole. A set of solutions are put forward to deal with problems in the date processing.

In Chapter 5, three aspects are presented. Firstly, the generation of bubble and debris is clarified based on the observation of single discharge by using a pair of needle electrode. The whole single discharge process is analyzed in the corresponding discharge signal. Secondly, the depth-dependent characteristic of bubble behavior in micro EDM drilling is quantitively estimated in different discharge states (normal discharge, consecutive short circuit and discharge in low open circuit voltage) based on the series solutions put forward in Chapter 3. Thirdly, the quality of debris in different hole depth is measured by an ultra-micro balance. At last, based on the quantitative estimation of bubble and debris, their influences on the micro EDM drilling are summarized.

In chapter 6, based on the clarification on the behavior of bubble and debris from chapter 2 to 4, a method of improving the machining speed in micro EDM drilling is put forward by using the mist jet. Firstly, the disadvantages by using deionized water is analyzed based on the previous researches. Then the advantages of mist jet are presented. An original mist device is designed, fabricated and used in the micro EDM drilling. In order to clarify the reason of improving machining speed by using mist jet, the observation of interelectrode in micro hole drilling with mist jet is done and result is analyzed.

In chapter 7, the main achievements in this research are summarized to the final conclusions. The understanding of micro EDM drilling is presented.

Chapter 2. Exploration on feasibility of observing the interelectrode gap area in micro EDM drilling

In micro EDM drilling, the machining speed decreases with the increase of hole depth. The reasons are generally owing to the gradually deteriorated environment of gap area. However, the details of complex interelectrode phenomenon is still not clear due to the difficulty in directly observing on the micro-scale gap area. In this chapter, firstly, the phenomenon of decreasing machining speed in micro hole drilling was confirmed coupled with the analyzation on control strategy in micro EDM machine, which controls the feed and retreat of micro tool in the machining. Secondly, the feasibility of direct observation on interelectrode gap area was explored by several proposed methods to find an suitable method to directly observe the interelectrode gap area in micro EDM drilling.

2.1 Introduction

Micro EDM is very suitable for drilling micro EDM in conductive materials such as the inkjet print nozzle, diesel fuel injection nozzle and turbine blades cooling channels due to its unique virtues in the aspects of high accuracy, no direct contact force and regardless of hardness of conductive workpieces.

Although the micro hole drilling with EDM has been studied for many decades, an obstacle still exists that decreasing machining speed with increase of hole depth due to the frequent abnormal discharges and short circuits. In most views, the reasons are attributed to the gradually deteriorating environment of gap area, such as the conductive debris accumulation and concentration, tool wear and low exchanging rate of dielectric liquid in the narrow gap area. Accumulation of conductive debris weakens the insulated strength of dielectric liquid. Tool wear leads to the uneven gap width. Moreover, the enlarging bubble occupancy area squeezes the space of dielectric liquid in the narrow gap area, furtherly improving the debris concentration. Therefore, the exhaust of debris, exchange of dielectric liquid and recovery of insulation strength of gap area play decisive roles in maintaining stable machining state in EDM process.

Since there is no effective self-flushing way except the bubble movement and micro tool rotation in the conventional blind hole drilling of EDM with a solid micro rod, many researchers focused on the point of improving the flushing process to enhance the debris exhaust and dielectric liquid exchange. Several proposed methods have largely improved

the aspect ratio (ratio of the depth and diameter) of micro hole such as the ultrasonic vibration, helical tools and planetary movement. However, it is still difficult to obtain micro hole with an aspect ratio larger than 30 by using the methods mentioned above.

With the advancement of manufacturing electrode technology, the commercial tube electrode was applied in micro hole drilling with internal flushing method. The micro hole with an aspect ratio larger than 120 has been reported by using the tube electrode with insulated sidewall. the decreasing machining speed with increase of hole depth scale of micro hole (generally the diameter is less than 500μm) makes it difficult to directly observe the interelectrode gap area and capture the clear images due to the limitation of finite performance of high-speed camera. Moreover, the observation in high magnification requires enough illumination for the camera lens to get a clear vision on the observation area.

Meanwhile, with the advancement of high-speed camera, many researchers tried to explain the complex phenomenon in interelectrode gap area by observing the gap area directly, which was hardly observed before. Many new insights of EDM have been clarified in this way. Kitamura and Kunieda applied the transparent electrode (material of SiC or Ga2O3) to observe the plasma in EDM, later investigated the relationship between bubble and discharge location and discussed the probability of discharge occurrence. Ikeda et al. observed the behavior of bubble generated between parallel flat plates in the single pulse discharge and found the oscillation of bubble. Miyajima et al. used the transparent plastic disk to observe the gap area and found that the gap area was mostly occupied by bubbles. However, the observations based on transparent material were only carried out in a very short time because the transparent material became opaque after destruction of crystallographic texture by the discharge plasma. Wang et al. observed the gap area directly and described the movement of bubble and debris by means of a simplified tool electrode made of heat-melt adhesive with a copper wire inside and later proposed a simulation model to confirm the observation results. Although these researches all pointed out that the bubble behavior plays a significant role on EDM drilling, the experiments were carried out under specific conditions which were not the same with the real machining process.

Actually, the investigation on the bubble behavior is difficult in micro EDM under the conditions the same with the real machining conditions. Firstly, it is difficult to observe the gap area directly for a long time. Secondly, it is hard to quantitatively estimate bubble

behavior since bubbles' moving and deforming in the narrow gap area.

In this chapter, firstly, the phenomenon of decreasing machining speed in micro hole drilling was confirmed, coupled with the analyzation on control strategy in micro EDM machine, which controls the feed and retreat of micro tool in the machining. Secondly, the feasibility of direct observation on interelectrode gap area was explored by several proposed methods to find a suitable method to observe the interelectrode gap area in micro EDM drilling.

2.2 Experimental devices

2.2.1 Micro EDM machine

The micro hole drilling was designed to be conducted in the micro EDM machine (MG-ED82W, Panasonic) with a numerical control (NC) system (MG-NC82) shown in Fig. 2.1. The micro EDM machine has high accuracy and can be used to machine the micro hole from 15μm to 300μm, array holes with specific interval and 3D micro features. It mainly includes a rotating spindle, NC XY table and NC discharge unit.

Fig. 2.1 Micro EDM machine

The rotating spindle is mounted on the Z axis with 3000rpm and driven by a DC motor.

The micro tool is fixed on a special holder then mounted on the rotating spindle. The tool holder has high-class fit with the spindle and can be conveniently installed and dismantled on the spindle before and after machining regardless of the second fixture positioning errors. The schematics is shown in Fig. 2.2.

The X-Y table and Z axis are located by the glass grating with the axial minimum resolution of 0.1μm. The largest moving distance for X, Y, Z axis is 500mm, 50mm and 50mm respectively.

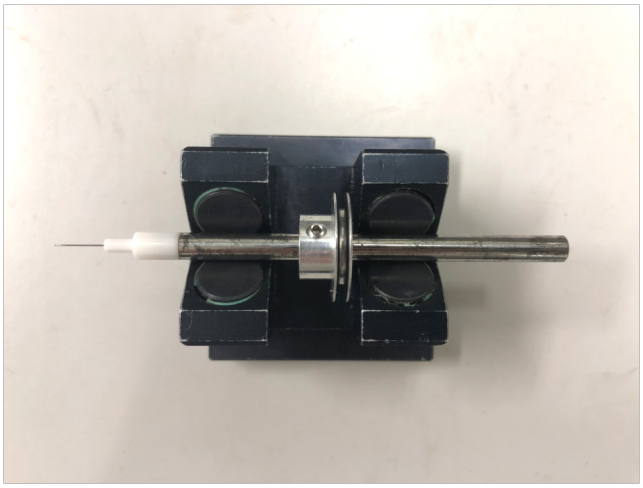

Fig. 2.2 Micro tool holeder

In the micro EDM machine, the RC circuit is adopt shown in Fig. 2.3, where E, power supply; R (1000Ω), current limiting resistor; R' (100Ω), protective resistance; $C_{1,2,3,4}$ (3300pF, 220pF, 100pF, 10pF), a set of capacitances.

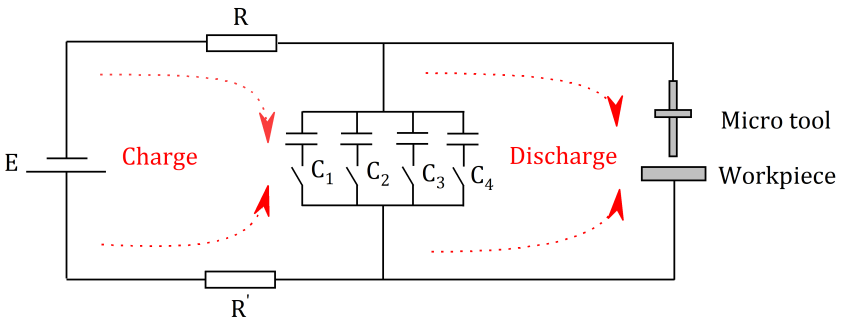

Fig. 2.3 RC circuit in micro EDM machine

The discharge duration in RC circuit is significant short (108ns) as shown in Fig. 2.4.

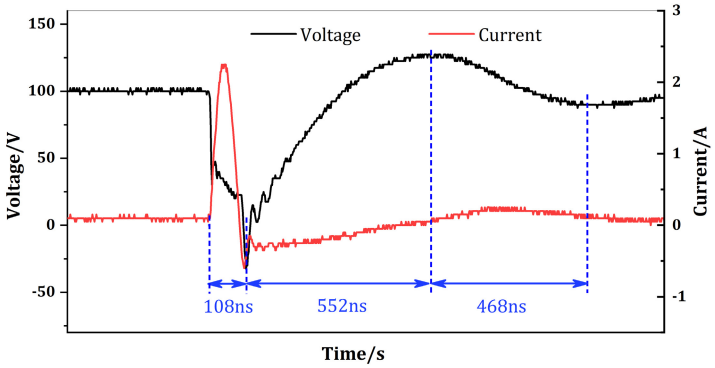

Fig. 2.4 Discharge duration and interval in RC circuit

(Open circuit voltage 100V; Capacitance 3300pF)

In electrotechnics, the charging of capacitance obeys the equation 2.1:

$$V_t = E(1 - e^{-t/[(R+R')C]}) \quad (2.1)$$

where, V_t, voltage of capacitance at time t; t, charging time.

The charging time depends on the time constant RC. According to the equation 1, the completely charging needs infinite time. The relationship between charging time t with charging voltage V_t is shown in Table 2.1. Normally, it was thought when t≈3RC, the charging process has been almost finished.

Table 2.1 Charging voltage V_t in time t

t	Vt
(R+R')C	0.63E
2(R+R')C	0.86E
3(R+R')C	0.95E
4(R+R')C	0.98E
5(R+R')C	0.99E

According to the calculation, the charging time is about 10.89μs, which is much larger than that obtained in the experiment (1.02μs).

In the discharging process, it obeys the equation 2.2:

$$V_t = Ee^{-t/(R_g C)} \quad (2.2)$$

where, R_c, the resistance of gap in breakdown process. The resistance can be calculated by the equation 2.3:

$$R = \rho L/S \quad (2.3)$$

where, ρ, the resistivity; L, the length of the sample; S, the cross section of sample.

In this research, the dielectric is the deionized water. The resistivity is 2×10^5 Ω·m. L is the gap width, about 20μm. S represents the area of discharging area, which is different to measured. However, according the measured result from the oscilloscope, the discharge time is about 108ns. Thus, the resistance in the discharging process is nearly close to 0Ω.

Since the mechanism of breakdown has not been clarified so far, the above analyzation indicates that the theory of charge-discharge of capacitance in electrotechnics is not suitable to explain the breakdown process in micro EDM.

2.2.2 Micro tool fabrication discharge machine

The micro tool is fabricated by the WEDG unit (introduced in section 1.3 chapter 1) in a micro tool fabrication discharge machine, a supporting equipment for the micro EDM machine, shown in Fig. 2.5. It has the similar structure with the micro EDM machine expect following several differences:

1. Dielectric media. In the fabrication of micro tool, to avoid the thermal deformation caused by the discharge heat, the tip of micro tool, waiting to be processed, should be sunk in the media during the machining to disperse the discharge heat effectively. Therefore, the oil base media such as kerosene is usually used to prevent the electrolysis action in water base media. While in micro EDM machining, the water base media is inclined to be used such as deionized water because the smaller discharge gap can be obtained and machining accuracy can be improved. To avoid the electrolysis action, generally the water base medium is injected onto the machining area by a nozzle to make sure the medium can be exchanged quickly and prevent the accumulation of ions.

2. Polarity of cathode and anode. In the fabrication of micro tool, the micro tool is the workpiece so that it should be set to the anode and the moving copper wire is the cathode. However, it is totally opposite in the micro EDM. Actually, the cathode and anode can be switched according to the different experiments. The above discussion is in the normal case.

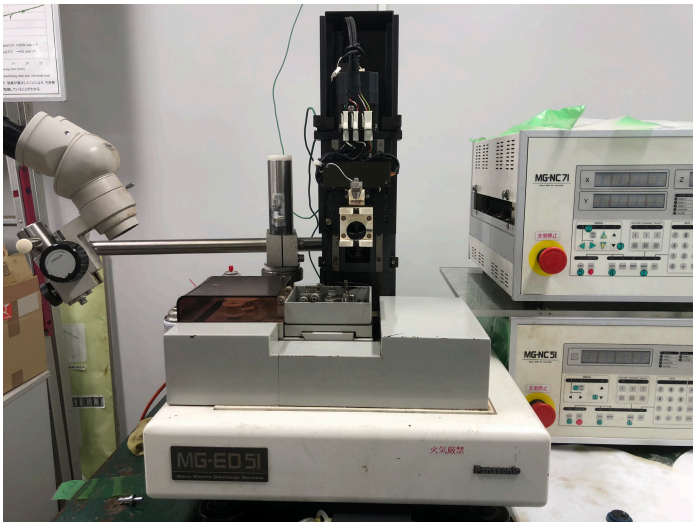

Fig. 2.5 Micro tool fabrication machine

2.2.3 Data recording, measurement and observation

In the micro EDM machine, only the shell is grounding and the cathode is not grounding. In order to record the voltage signal accurately, the voltage signals of cathode and anode

are both input into a suspended oscilloscope (TBS2000, Tektronix).

The significantly short discharge duration in RC circuit shown in Fig. 2.1 Section 2.2.1 requires a current sensor with high frequency response for the accurately recording of discharge current. Therefore, a high-frequency, bidirectional current probe (CT-1, Tektronix) shown is used to detect the high frequency current signals in discharging.

The size of micro tool and micro hole is measured by a multi-function micro scope (VW9000, Keyence) shown in Fig. 2.7. It not only can be used in the measurement but also in observation. The long working distance lens (VH-Z50L) shown in Fig. 2.8 supports the observation on the interelectrode gap area.

Fig. 2.7 VW9000 (Keyence)

Fig. 2.8 Lens with long working distance

Another high-speed camera (HX-3, NAC) shown in Fig. 2.9 is also been used in the observation because it has higher frame rate and the maximum speed can reach 1.3Mfps.

Fig. 2.9 High-speed camera (HX-3, NAC)

A laser sensor (LK-G80, Keyence) is used to detect the movement of Z axis and record the feed depth of micro tool. The figure of laser sensor and controller is shown in Fig. 2.10. The measuring range is ±15mm and reposition accuracy is 0.2μm.

Fig. 2.10 Laser sensor and controller

2.3 Investigation on decreasing machining speed in micro EDM drilling

2.3.1 Phenomenon of decreasing machining speed in micro EDM drilling

In micro hole drilling, the high AR (aspect ratio: the ratio of hole depth with hole diameter) is always pursued. However, in the experiments, many researchers found that it was very difficult to obtain a blind hole with high AR. After a certain depth, the machining speed decreases seriously and the micro tool retreated frequently. The phenomenon was confirmed in this section. The experiment of drilling micro hole has been conducted. The experimental conditions are shown in Table 2.2 and the feed depth recorded by laser sensor is shown in Fig. 2.11.

Table 2.2. Machining conditions

Items	Parameters
Tool electrode	Φ300μm
Material of tool	Tungsten
Tool feed rate	3μm/s
Open circuit voltage	110V
Capacitance	1000pF
Dielectric liquid	Deionized water jet
Workpiece	Stainless steel SUS304

It was found that the machining speed gradually decreases with increase of hole depth. The feed limit exists and after that the micro tool retreats seriously. Then the micro tool fluctuates around 0.9mm in the range of 200μm for a long time. The phenomenon of feeding limit of the tool electrode, called limitation of feeding depth in our research [33], commonly exists in the micro EDM drilling.

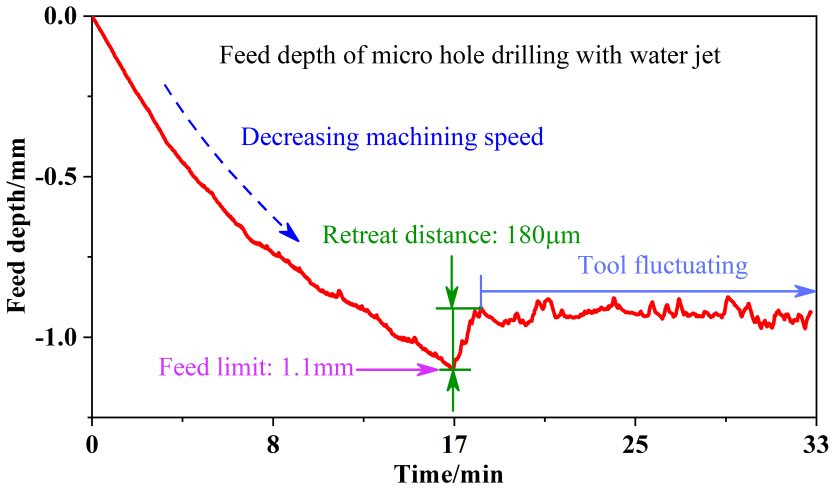

Fig. 2.11 Feed depth of micro blind hole drilling

2.3.2 Strategy of NC system on the movement of micro tool

The movement of micro tool such as feeding and retreating is controlled by the NC system. The control strategy is that the micro tool feeds at a desired feeding speed in the control program and retreats until the quantity of electricity (integration of short circuit current) reaches the threshold value during a certain period of time. The schematics is shown in Fig. 2.12.

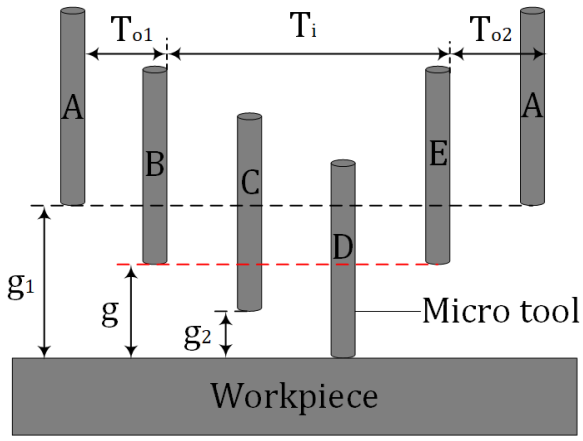

Fig. 2.12 A discharge circle

In the period of no discharge, the open voltage of capacitance is kept in the full charge state and the micro tool moves toward the workpiece. In the state of short circuits, the voltage difference of anode and cathode will almost decrease to zero and the current of short circuit increases quickly. The micro tool will retreat until the short circuit disappears. Then the energy of capacitance will be fully released and the micro tool moves away from the workpiece.

In a discharge circle, there are two stages:

(1) Stage 1- no discharge: $g1>g$, the tool feeds;

(2) Stage 2- in discharge: $g2<=g$, the discharge or short circuits occurs.

As shown in Fig. 2.12, a discharge circle includes the stages from A to E. In a new circle, the tool will start to feed in stage A, which is the end of the last circle. Since the gap width g_1 is much larger than the threshold breakdown distance g, the voltage of gap area is still in full charge state and no discharge happens. Thus, the tool keeps feeding towards the workpiece. T is the period of a discharge circle, including T_i and T_o. T_i is the time of gap area in discharge. T_o is the time of gap area out of discharge, including two parts: T_{o1} and T_{o2}.

When the tool reaches the position in stage B, the discharge occurs with the breakdown of gap area. The energy stored in the capacitance is released. The tool will keep feeding until the quantity of electricity reaches the threshold value during stage B to D. Then the tool will retreat until the quantity of electricity lowers than the threshold value from stage D to A.

The signals of voltage and current in a discharge circle are shown in Fig. 2.13.

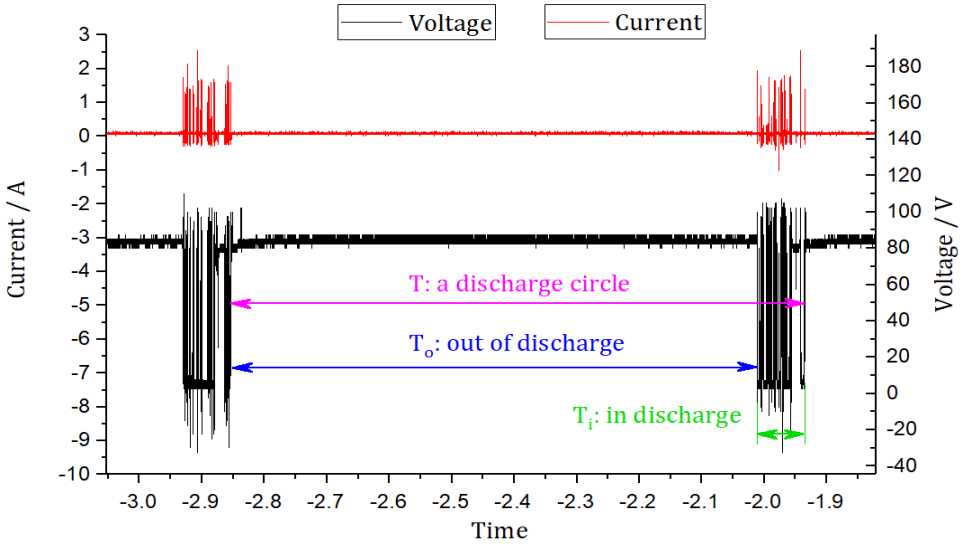

Fig. 2.13 Signals of voltage and current in a discharge circle

It is found that during T_i lots of discharges occur, which is due to the control strategy of NC. Because in the normal discharge, the current is too small to reach the threshold and trigger the retreat of micro tool until the short circuit appear. The discharge signals in the short circuit is shown in Fig. 2.14. Once the discharge occurs, the value of current increase quickly and the micro tool retreat immediately. In approaching the short circuit, the gap width is less than the threshold breakdown distance, resulting in the appearance of lots of discharges. As shown in Fig. 2.14, high order discharges in low voltage occur before the short circuit.

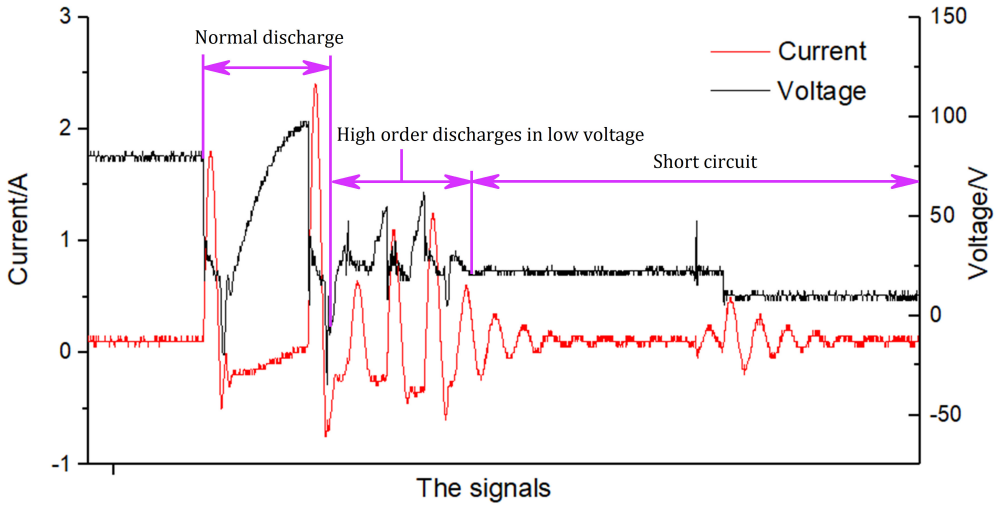

Fig. 2.14 Signals of voltage and current in short circuit

2.4 Characteristics of discharge signals in different discharge states

In micro hole drilling with EDM, the deteriorating environment of gap area is also

reflected in the discharge signals because the byproducts will influence the discharge process, for example, the accumulation of conductive debris will decrease the insulation strength of dielectric liquid seriously and cause abnormal discharges. To clarify the reason for the decreasing machining speed with increase of hole depth, it is necessary to investigate the discharge signals in different machining states. Therefore, in this section, the discharge signals during different discharge states in the micro hole drilling have been recorded and investigated, especially the discharge signals in a retreat process has been investigated and the reasons for decreasing machining speed has analyzed.

2.4.1 Experimental equipment and conditions

The experiment is designed to drill micro hole by EDM in RC circuit. The schematics of experimental equipment is shown in Fig. 2.15 and the machining conditions are shown in Table 2.3. Micro hole drilling is carried out with micro-EDM machine (MG-ED71, Panasonic) with an RC discharge power supply. The Laser sensor (LK-G80, Keyence) is used to record the feed depth of micro tool and the data are collected by the dedicated software and saved in the control computer. The current signal is detected by the bidirectional current probe (CT-1, Tektronix) and recorded in the oscilloscope. The voltage signal of cathode and anode is also input into oscilloscope to match with the current signals.

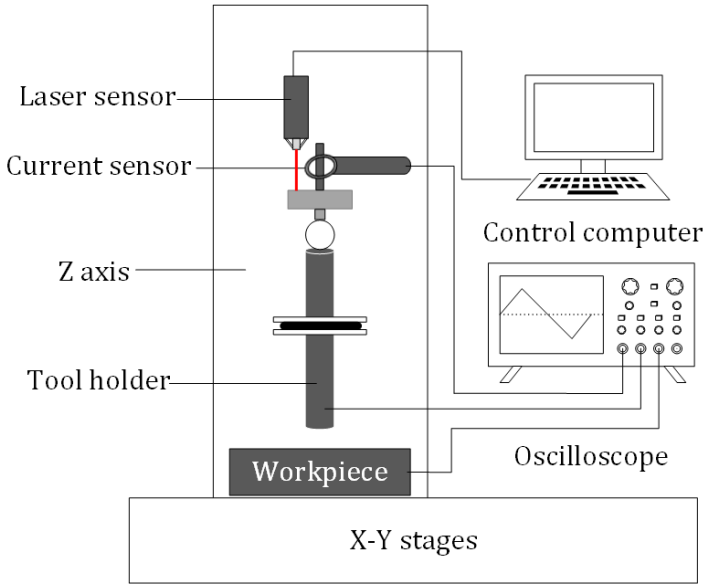

Fig. 2.15 Experimental experiment

Table 2.3. Machining conditions

Items	Parameters
Tool electrode	Φ300μm
Material of tool	Tungsten
Tool feed rate	5μm/s
Open circuit voltage	110V
Capacitance	1000pF
Dielectric liquid	Deionized water jet
Workpiece	Stainless steel SUS304

2.4.2 Signals of voltage and current in different discharge states

The experiment of drilling micro hole was done and the feed curve was recorded and shown in Fig. 2.16. The trend of feed curve is same with that in Fig. 2.11 that with increase of hole depth the machining speed decreases seriously. In the last stage of machining, the micro tool fluctuates around 1 mm and the retreat process occurs repeatedly.

The normal discharge signals in the drilling of micro hole is shown in Fig. 2.17. The regular discharge circle explained in Fig. 2.12 Section 2.3.2 can be observed distinctly, although the period of discharge circle is not constant.

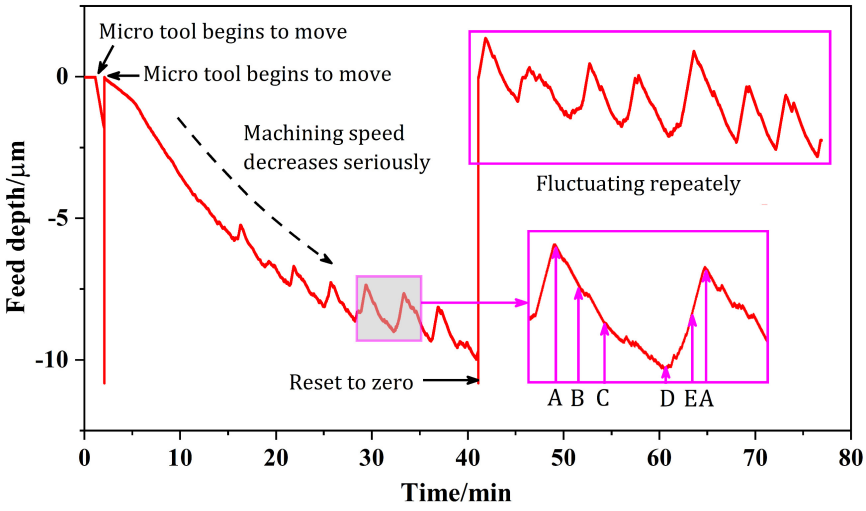

Fig. 2.16 Feed depth of micro hole

With the increase of hole depth, the environment of gap area has been deteriorated. The discharge occurs more frequently in large area so that the discharge circle is totally irregular as shown in Fig. 2.18. Moreover, the signals of discharge in low open circuit voltage is shown in Fig. 2.19. The predefined fully open voltage is 110 but the discharge

occurs in 75V, which may because the debris accumulation and concentration decrease the insulated strength of gap area so that the gap area can be breakdown in low open circuit voltage.

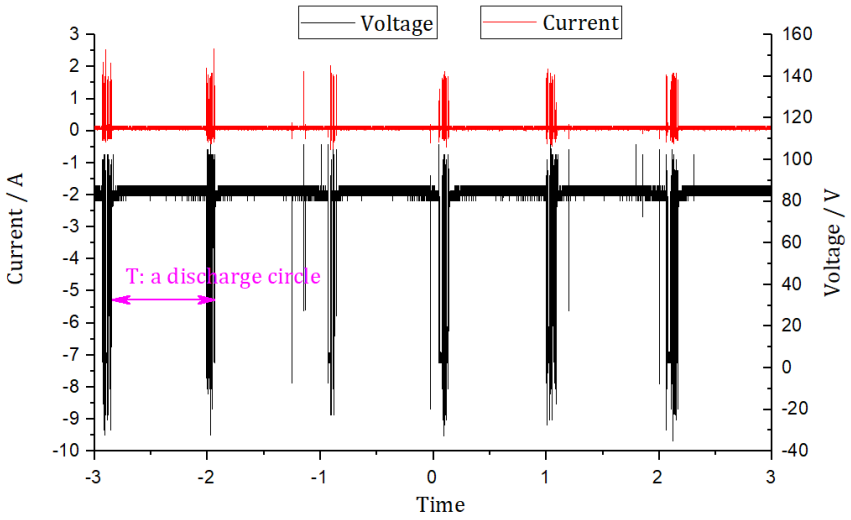

Fig. 2.17 A discharge signal in the normal discharge state

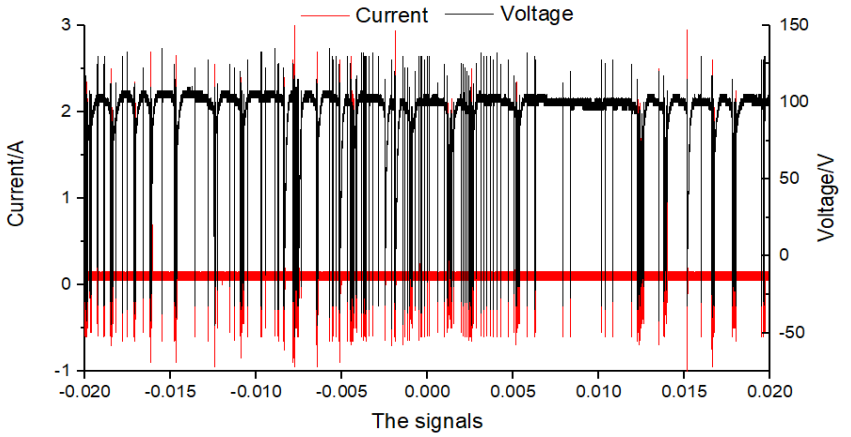

Fig. 2.18 Irregular discharge signals

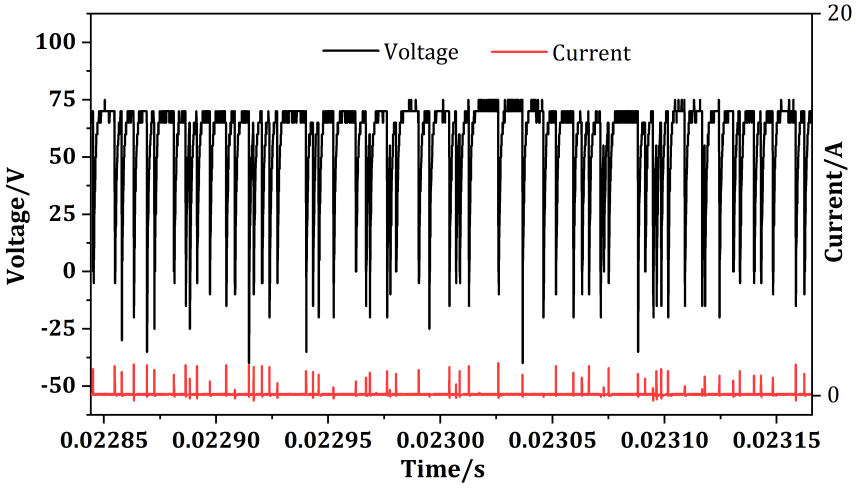

Fig. 2.19 Signals of discharge in low open circuit voltage

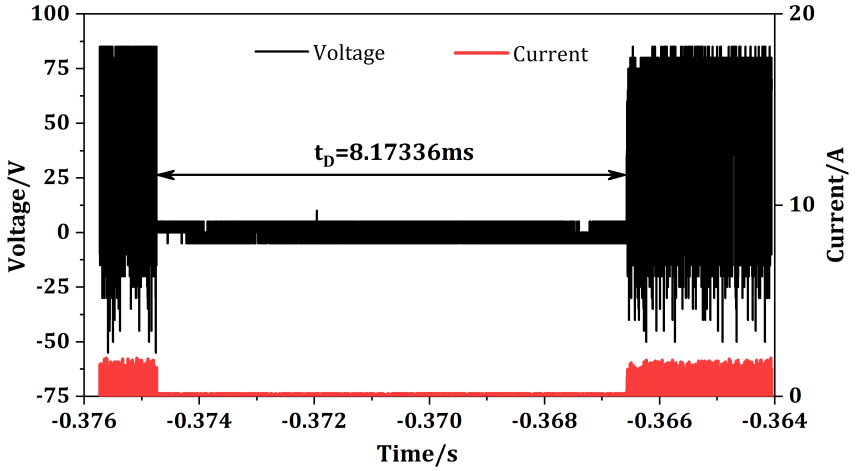

Fig. 2.20 Signals of consecutive short circuit

On the other hand, consecutive short circuit occur frequently and duration of short circuit become longer in deeper hole depth as shown in Fig. 2.20. The current value become 0 in the short circuit because the bidirectional current probe (CT-1, Tektronix) is specifically used to detect the high frequency current signals in discharge.

2.4.3 Discharge signals during a retreat process

As shown in Fig. 2.16, the retreat process repeats in the last stage of machining and the distance is much larger than the threshold breakdown distance. In order to investigate the reasons for the retreat of micro tool, the signals of voltage and current in a retreat process are captured shown in Fig. 2.21 by the oscilloscope. The whole retreat process is distributed into five stages from A to E, same with the labels in Fig. 2.12.

It is found that the in the stage A shown in Fig. 2.21 (a), the voltage of gap area is the full-charged open circuit voltage. Then with the feeding of micro tool, regular discharge occurs as shown in Fig. 2.21 (b), which is described in Fig. 2.17 that the gap area in discharge and out of discharge can be found distinctly. With the feeding of micro tool, in stage B, the discharge becomes more frequently and mass discharges in low open circuit voltage occur as shown in Fig. 2.21 (c). It indicates that the insulation strength of gap area decreased seriously. Then the consecutive short circuits happened when the micro tool reaches the stage D and the tool kept retreating as shown in Fig. 2.21 (d) until the consecutive short circuits disappeared and the voltage of gap area recovered to the full-charged voltage in Fig. 2.21 (e), which is the starting of the next retreat circle.

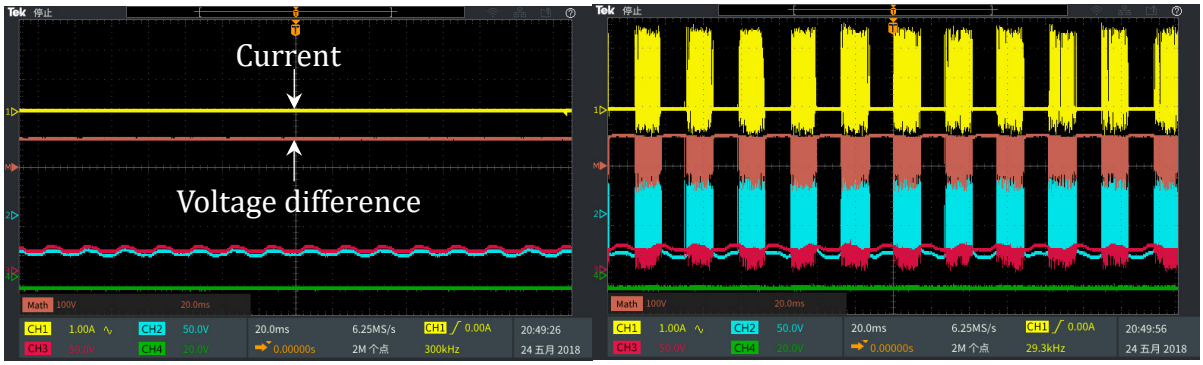

(a) Stage A: No discharge (b) Stage B: regular discharge circle

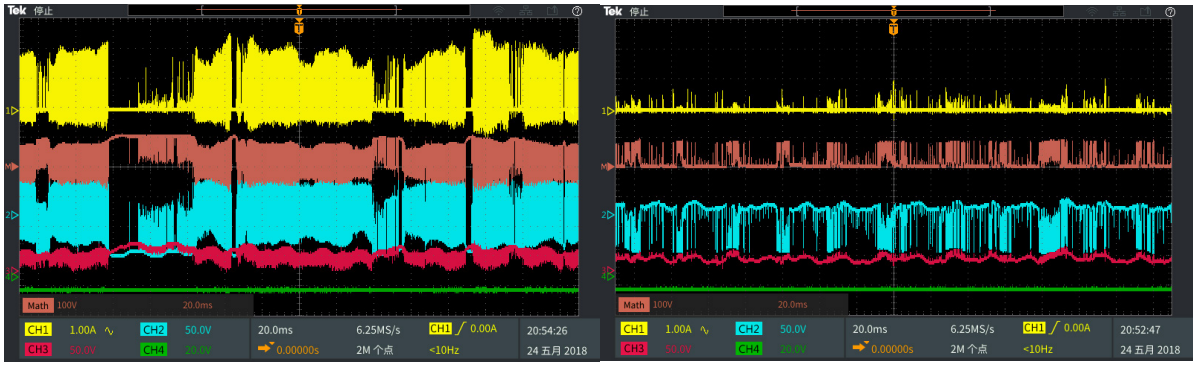

(c) Stage C: In low open circuit voltage (d) Stage D and E: Frequent short circuit

(e) Stage A: No discharge

Fig. 2.21 Discharge signals in the retreat process

The retreat distance in the retreat process in Fig. 2.10 is about 380μm, which is much larger than the threshold discharge gap width (about 10-20μm). The consecutive short circuits existing in such a long distance indicates there should be conductive media between the cathode and anode. The most likely medium is the debris that accumulates in the gap area and links the cathode with anode.

Above all, it is obvious that the decrease of machining speed with increase of hole depth is owing to abnormal discharges in the deteriorated discharging environment, resulting in the frequent retreat of micro hole. It is necessary to observe the interelectrode gap area to clarify the reasons for the deteriorated environment.

2.5 Conclusions

In micro EDM, no matter the experimental conditions and the design of NC system are both designed for the ideal machining, where no tool wear and contamination of dielectric liquid. However, in the actual machining, the machining environment is gradually deteriorating and not consistent with the initial machining conditions. Therefore, the abnormal machining states occur and the micro tool will retreat frequently, eventually resulting in the decrease of machining speed.

Generally, the machining states can be distributed into the normal machining state and abnormal machining states. The normal machining state, the elf-evident is that the discharge is in normal state or ideal state, which just occur in the initial machining stage. The abnormal machining states, however, there is no clear definition to descript. In this chapter, it is summarized into the discharges in low open circuit voltage and consecutive short circuit.

In order to clarify the reasons for the decreasing machining, firstly, the phenomenon of decreasing machining speed is confirmed and discussed. It was found that with increase of hole depth, the machining speed decreases gradually. After the machining limit, the retreat of micro tool repeats frequently and the machining speed is nearly 0. It is evident that low machining speed is due to the frequent retreat of micro tool. Since the movement of micro tool is control by the NC system, secondly, the control strategy of NC system was investigated and the discharge circle was clarified. It indicated that the retreat of micro tool is due to the short circuit.

To furtherly verify discharge signals in different machining states, the micro hole drilling was conducted and discharges signals in different machining states were recorded and analyzed, especially in a retreat process. The results showed that with increase of hole depth, the discharge circle became irregular and discharges occurred more frequently. The more frequent discharges indicated that the insulation strength of gap area has decreased seriously. In the last stage of machining, the fluctuation of micro tool is due to the frequent retreat. The discharge signals in a retreat process indicated that the consecutive short circuits frequently occurred, which can be inferred that the cathode and anode were always linked during the retreating process. The reason maybe due to the accumulation conductive debris.

However, the details in the gap area have never been reported, for instance, the reasons

for the decrease of insulation strength of gap area and behavior of debris due to the difficulty in direct observation on the gap area. The reported observations were conducted in the special-designed experiment or by using simplified method, which were not consistence with the actual machining conditions. Therefore, in the next chapter, the new methods were put forward to observe the gap area and clarify the details in the gap area.

Chapter 3. Clarification on the interelectrode gap area of micro EDM drilling by direct observation

It is difficult to observe the narrow gap area directly in the whole drilling process due to limitation of observation method and the performance of high-speed camera. Therefore, the details in the gap area is unclear. Depending on the empirical inference, many researchers think that the deteriorated environment is the reason for the decrease of machining speed, which is mainly presented in the following two aspects [27, 48, 63, 64, 65, 66, 67, 68]:

1. Lack of effective self-flushing method to improve the exchange of dielectric liquid.
2. Debris accumulation cause the deterioration of environment.

In this chapter, the feasibility to observe the interelectrode gap area was explored based on two methods: using hollow glass pipe and sandwich workpiece. The results showed that using sandwich workpiece was capable method and the gap area in two kinds of workpiece, single crystal SiC and stainless steel SUS304, was observed. Considering the disadvantage of open-ended gap area in sandwich workpiece resulting in the leak of debris and dielectric, which is not consistent with actual machining, an improved sandwich workpiece was made and observation was conducted. Results showed that by using the improved workpiece, the drilling process is nearly similar to the actual micro hole drilling. The behavior of bubble, debris and characteristics of discharges were investigated and analyzed. Moreover, in the observation with SiC workpiece, the profile of micro hole can be observed clearly. The dependent characteristics of profile of micro hole was investigated. Based on this, the influence of tool wear in micro hole drilling was analyzed.

3.1 Observation of gap area by using the hollow glass pipe

3.1.1 Experimental method

The difficulty to observe the gap area is due to the majority of workpieces is not transparent. The requirements for clear observation on the narrow gap area such as high magnification and illumination intensity cannot be satisfied due to the limited performance of high-speed camera. In the other hand, the high illumination intensity larger than 1000nit will heat the machining area even melt the tank made of PMMA. Therefore, the transparent workpiece such as SiC or Ga_2O_3 was used in the reported

observation. However, the observations based on transparent material were only carried out in a very short time because the transparent material became opaque after destruction of crystallographic texture by the discharge plasma.

A method is put forward for the observation. The schematics is shown in Fig. 3.1. A special anode is made by using the transparent glass pipe and tool electrode of Tungsten. The parameters of all parts are shown in Table 3.1. A Tungsten electrode is glued together with the glass pipe with the resin adhesive, which is served as the anode. Anode Tungsten electrode is inserted into the hollow glass pipe to be served as the cathode. In order to make sure the gap area is similar to the actual machining, the inner diameter of hollow glass is 340μm so that the gap width is 20μm, which is similar to the actual micro hole drilling in the conditions of Table. 2.3. The glass pipe after inserting the anode is shown in Fig. 3.2.

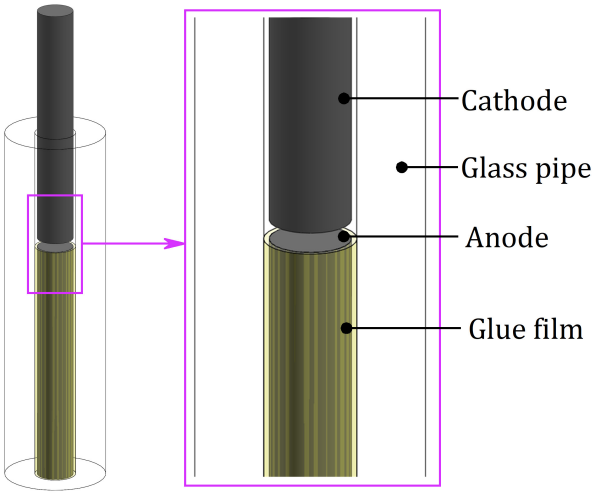

Fig. 3.1 Schematics of workpiece using glass pipe

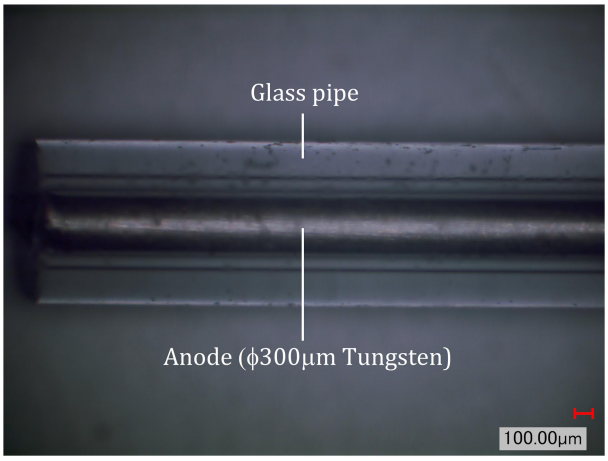

Fig. 3.2 Glass pipe with anode

Table 3.1 Parameters for all parts

Items	Parameters
Cathode	Φ300μm Tungsten rod
Anode	Φ300μm Tungsten rod
Inner diameter	340μm
Outer diameter	840μm
Glue film	Resin adhesive

3.1.2 Experimental equipment and conditions

The schematics of setup is shown in Fig. 3.3. The high-speed camera (VW9000, Keyence) is used to observe the gap area. The anode is fixed on the tank of XY stages.

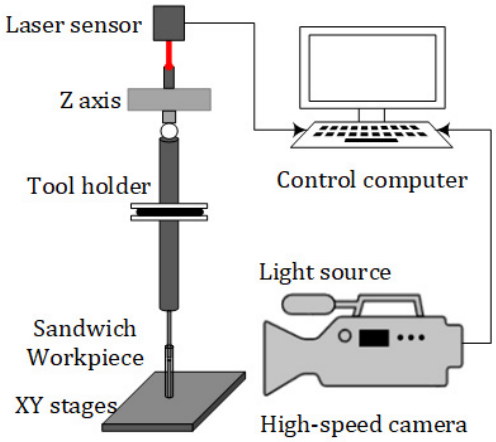

Fig. 3.3 Schematics of setup

The schematics of tank is shown in Fig. 3.4. Two fixture blocks made of transparent PMMA are used to fix the glass pipe. There is a good perpendicularity between the fixture block with metal base to assure installation accuracy of glass pipe.

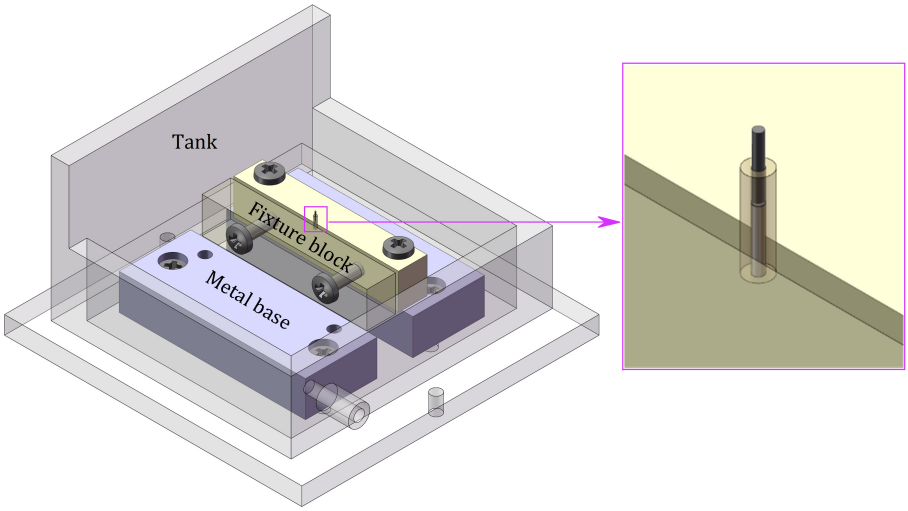

Fig. 3.4 Schematics of fixed glass pipe

The experimental conditions are shown in Table 3.2. Due to the viscous effect of deionized water, it maybe cannot flow into the narrow gap area with width of 40μm. Therefore, the high pressure of air is used to flush the deionized water to make sure the gap area is full of deionized water.

Table 3.2. Machining conditions

Items	Parameters
Tool electrode	Φ300μm
Material of tool	Tungsten
Tool feed rate	5μm/s
Open circuit voltage	110V
Capacitance	1000pF
Dielectric liquid	Deionized water jet
Anode	Tungsten
Pressure of air	0.65-0.8Mpa

3.1.3 Results and discussion

The machining area before machining is shown in Fig. 3.5. In Fig. 3.5 (a) without dielectric supply, the cathode and anode can be observed clearly. In Fig. 3.5 (b) with the dielectric supply, the surrounding of glass pipe is coved by the deionized water.

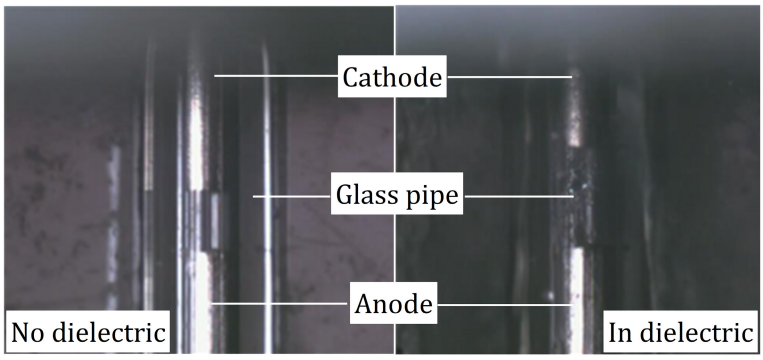

(a) No dielectric (b) In dielectric

Fig. 3.5 Machining area before machining

The gap area in feed depth of 60μm, 325μm, 690μm and 1380μm is shown in Fig. 3.6 (a), (b), (c) and (d) respectively.

Since the melt point of the glue film is much lower than the Tungsten, it is firstly melted in the discharge as shown in Fig. 3.6 (a). With the increase of feed depth, the melted glue film is enlarged and the mixture of bubble and water is formed near the discharge area as

shown in Fig. 3.6 (b).

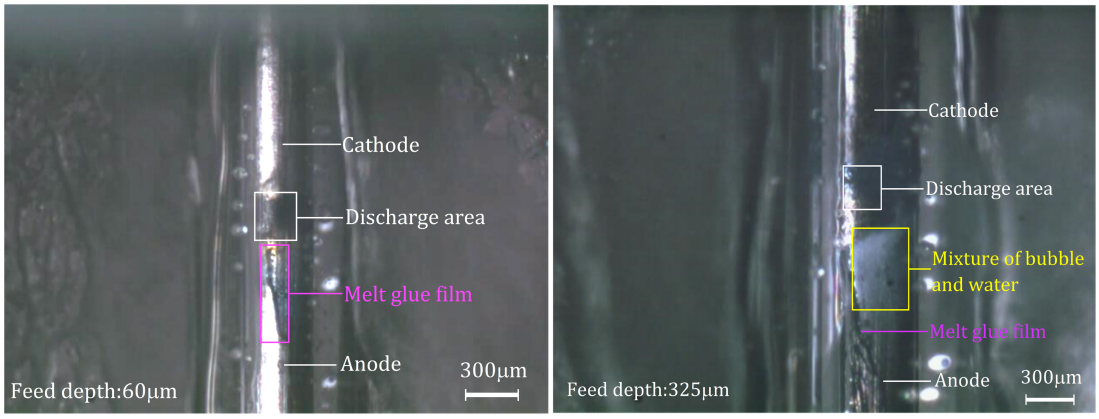

(a) Feed depth 60μm (b) Feed depth 325μm

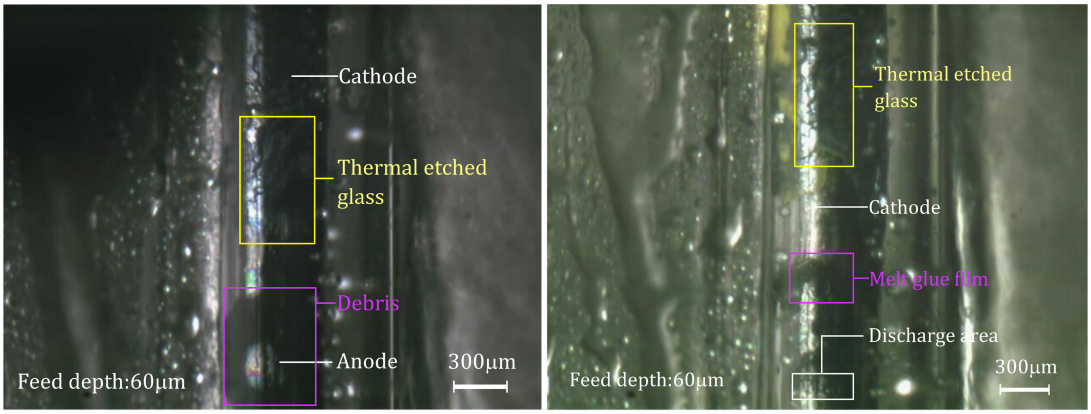

(c) Feed depth 690μm (d) Feed depth 1380μm

Fig. 3.6 Gap area in different hole depths

The temperature of discharge plasma can reach 6000-8000K so that the glass pipe is also etched in the long time machining as shown in Fig. 3.6 (c). In the other hand, the accumulated debris contaminates the dielectric liquid in the gap area. In Fig. 3.6 (d) with feed depth of 1380μm, the etched area of glass pipe is enlarged. Moreover, sometimes the thermal etching even breaks the glass pipe as shown in Fig. 3.7.

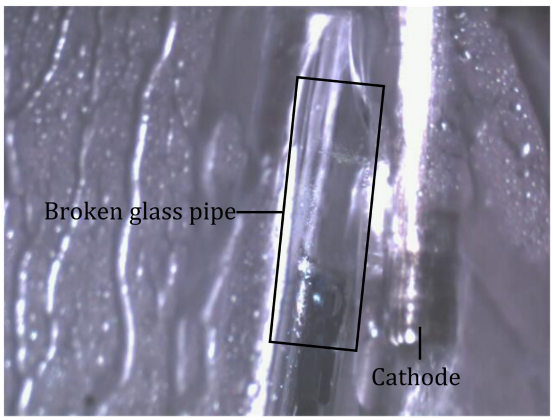

Fig. 3.7 Broken glass pipe due to thermal etching

It is found that the glue film and glass pipe cannot suffer the discharge plasma with high temperature. Therefore, the gap area is enlarged and transparent glass pipe was etched resulting in the poor visibility of machining area. Since there is none of transparent material can resist the high temperature of discharge plasma (6000-8000K), the problems mentioned above cannot be solved so far. Thus, this method is not suitable to observe the gap area.

3.2 Observation of gap area by using sandwich workpiece

3.2.1 Method to observe the interelectrode gap area

In this section, the second method is put forward for the long-time observation of gap area from the side wall, by using an original sandwich workpiece. The schematic is shown in Fig. 3.8, where R is radius of micro tool, g is the width of gap area. The high-speed camera is focus on the observation area A. The micro tool with the diameter equal to the thickness of the sheet workpiece is used. During the discharging, the material in the gap area with the cross-section area of $\pi(r+g)^2$ will be completely removed so that the details of gap area can be observed through the window B of side wall.

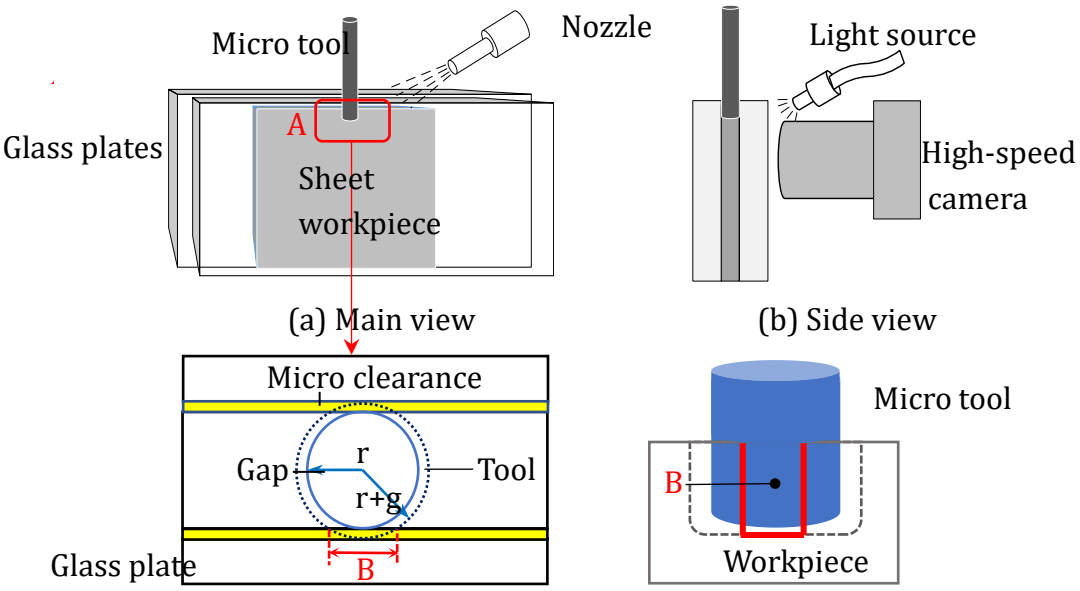

Fig. 3.8 Method for observing the gap area

3.2.2 Experimental equipment and conditions

The original sandwich workpiece is shown in Fig. 3.9. The sheet workpiece with thickness of 300μm is pressed by two pieces of glass plates from both sides then they are

fixed together with the bolt. The material of sheet workpiece is chosen the transparent SiC workpiece to investigate the feasibility of observing the interelectrode directly.

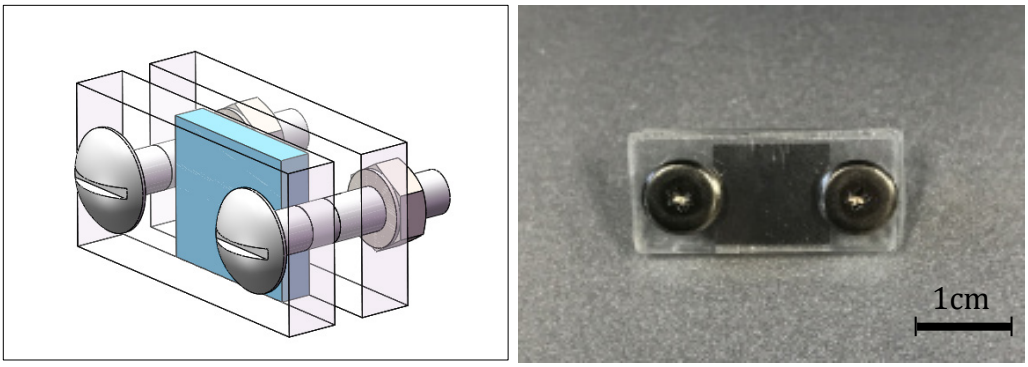

Fig. 3.9 Original sandwich workpiece

Table 3.3. Machining conditions

Items	Parameters
Tool electrode	Φ300μm
Material of tool	Tungsten
Tool feed rate	5μm/s
Open circuit voltage	110V
Capacitance	1000pF
Dielectric liquid	Deionized water jet
Workpiece	SiC

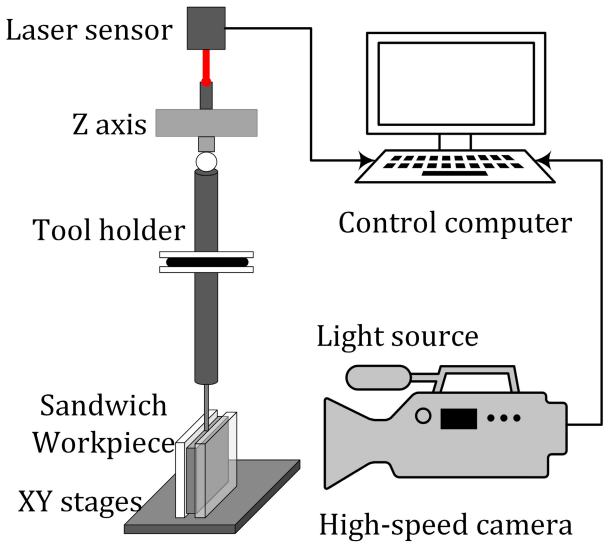

Fig. 3.10 Experimental equipment

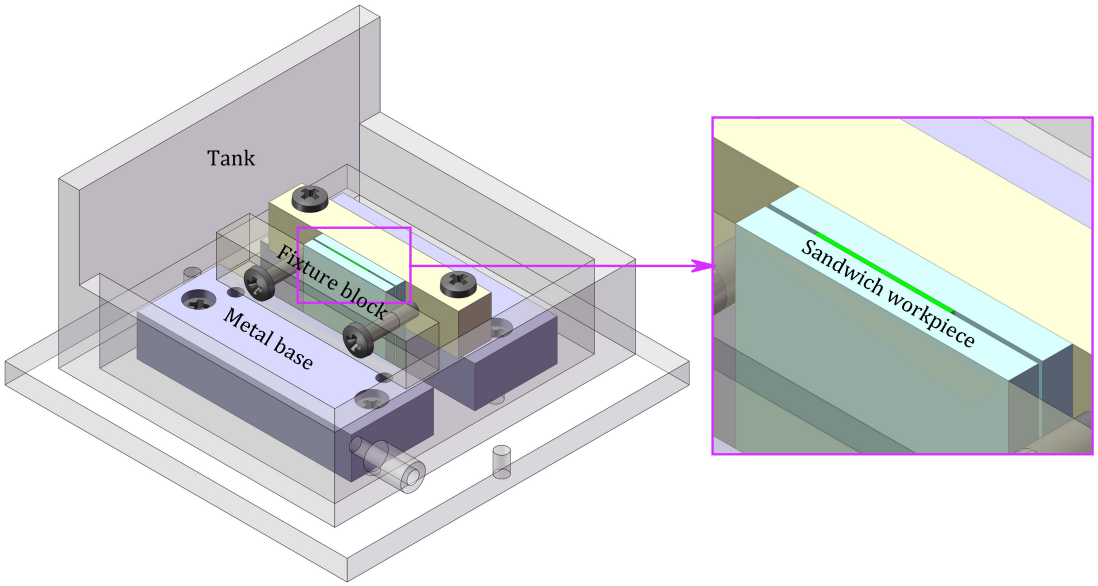

Fig. 3.11 Schematics of fixed sandwich workpiece

The machining conditions and experimental equipment is shown in Table 3.3 and Fig. 3.10 respectively. The high-speed camera (VW9000, Keyence) and a high magnification lens with long working distance (VH-Z50L) are applied to observe the interelectrode gap area. The sandwich workpiece is fixed on the tank of XY stages as shown in Fig. 3.11.

3.2.3 Details in the interelectrode gap area with SiC workpiece

The interelectrode gap area is shown in Fig. 3.12 (a), its schematic is shown in Fig. 3.12 (b). It is found that the gap area can be clearly through the window in the side wall of gap area. Many little bubbles overflow out of gap area.

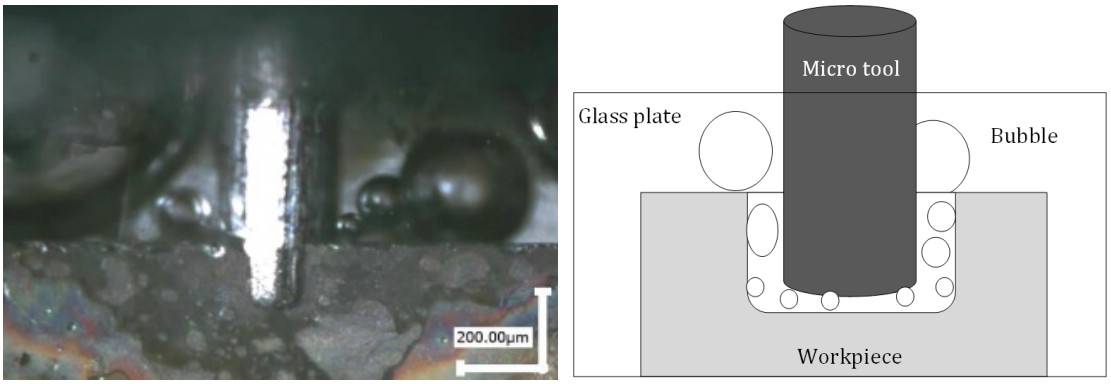

(a) Image of gap area (b) Schematics

Fig. 3.12 Bubble in the beginning of machining (×500, 4000fps)

In the deeper hole depth, the growth of bubble is observed. In Fig. 3.13 (a), a little bubble is observed then grows up in Fig. 3.13 (b) and become a very large bubble in Fig. 3.13 (c).

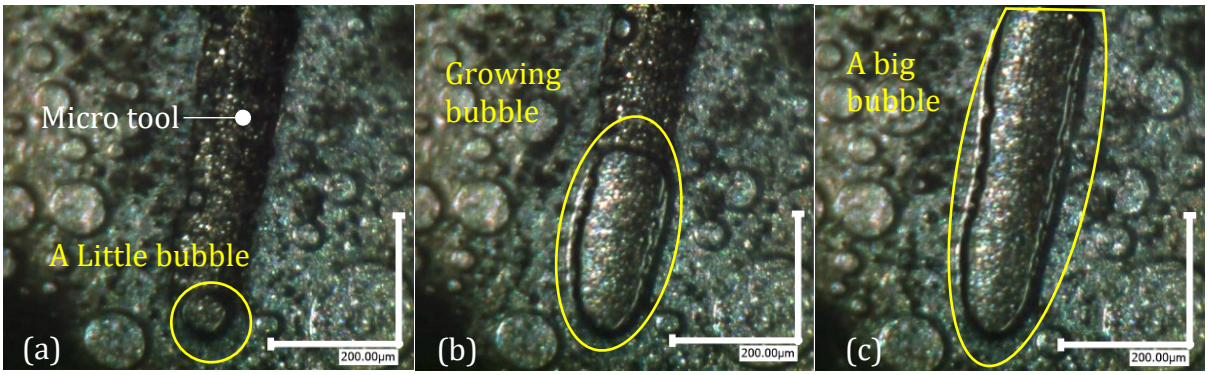

Fig. 3.13 Growth of bubble in the gap area (×400, 4000fps)

Moreover, the mergence of bubble is also observed. Two bubbles in Fig. 3.14 (a) merge to become a big bubble in Fig 3.14 (b). Then the big bubble grows up to become a larger bubble in Fig. 3.14 (c).

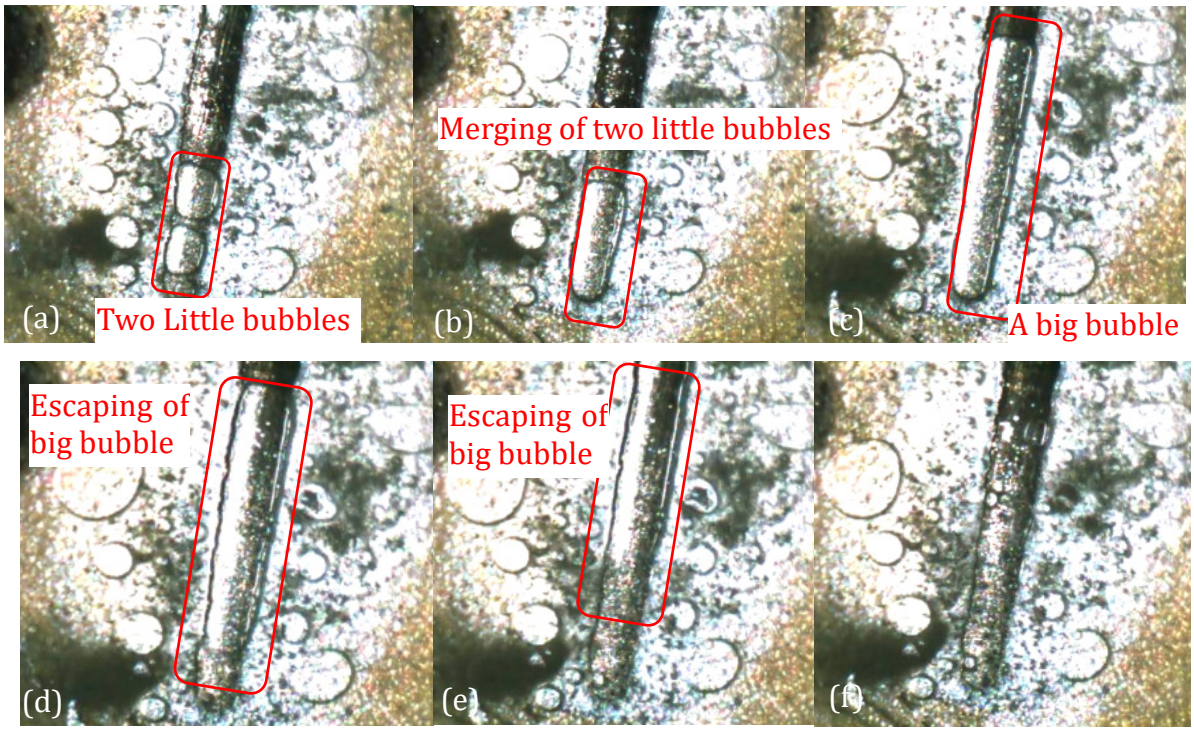

Fig. 3.14 Mergence of little bubbles

Finally, the big bubble escapes from the gap area from Fig. 3.14 (d) to (e). It indicates that with the increase of hole depth, the bubble can't escape from gap area immediately. The little bubble generated in the bottom of gap area may grow up or merge with other bubbles to become a larger bubble then escapes from gap area slowly.

It is found that the method by using the sandwich workpiece is feasible to directly observe the interelectrode gap area. In the next part, the gap area in the stainless steel SUS304 workpiece will be observed.

3.2.4 Details of gap area with stainless steel SUS304 workpiece

In order to investigate the gap area of micro hole with commonly used metal workpiece. The observation in gap area with stainless steel SUS304 workpiece is observed by using the method put forward before, which has been proved to be feasible in the observation of interelectrode gap area. The experiment equipment and conditions are same with those in Fig. 3.10 and Table 3.3.

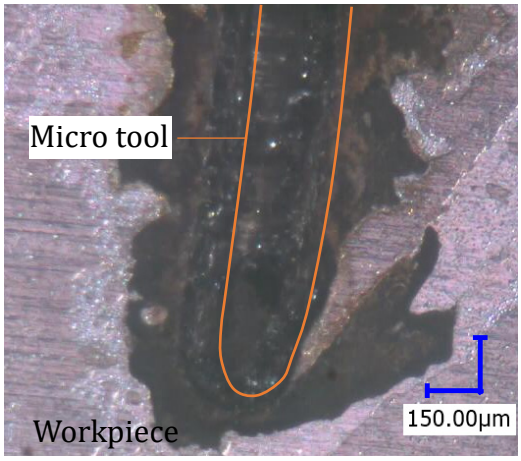

Fig. 3.15 Gap area in micro hole drilling with stainless steel SUS304

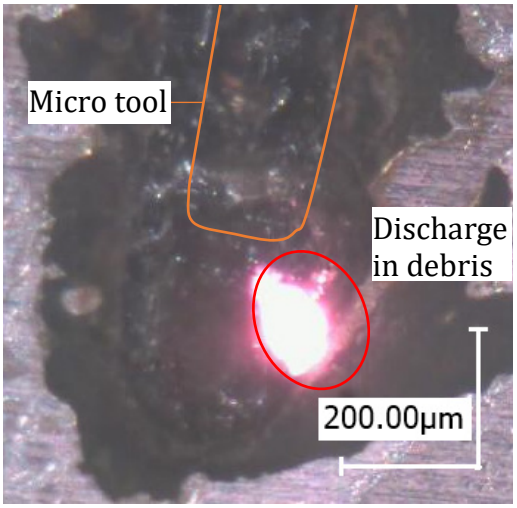

Fig. 3.16 Discharge in debris

The image of gap area is shown in Fig. 3.15. It is found that compared to the SiC workpiece, more debris accumulate in the gap area. Much debris accumulates in the gap area, sticks to the wall of micro hole and surface of micro tool. Moreover, the discharge in debris is observed as shown in Fig. 3.16. It indicated that the debris is not freely distributed in the gap area, it participates in the discharges process, which is may be the reason for the retreat of micro tool when it reaches the feeding limitation. The debris on the gap area replace the workpiece to participate in the discharge so that the material of

workpiece can't be removed.

3.3 Improved sandwich workpiece in observation of gap area

Although the inter-gap area can be observed directly by using the method put forward, there is a big detect for the sandwich workpiece that the workpiece is not totally blocked, thus there is micro clearance between the sheet workpiece with the glass plates. Therefore, the debris will leak out from gap area and enter into the micro clearance, which is not consistent with the actual micro hole drilling. Thus, the sandwich workpiece is improved in this section. The gap area is also observed by using the improved sandwich workpiece.

In the improved sandwich workpiece, the sheet workpiece is glued with the glass plate from both sides by the transparent resin adhesive. The schematics is shown in Fig. 3.17. The improved sandwich workpiece based on the SiC workpiece is shown in Fig. 3.18.

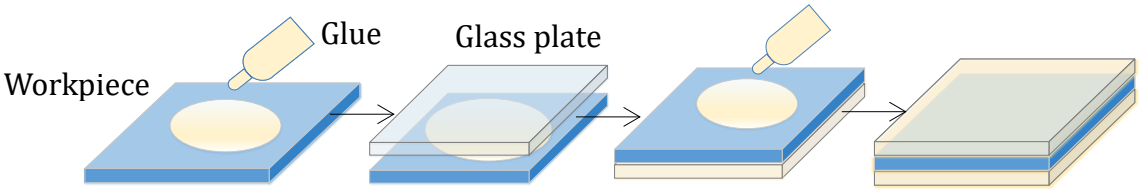

Fig. 3.17 Steps for the improved sandwich workpiece

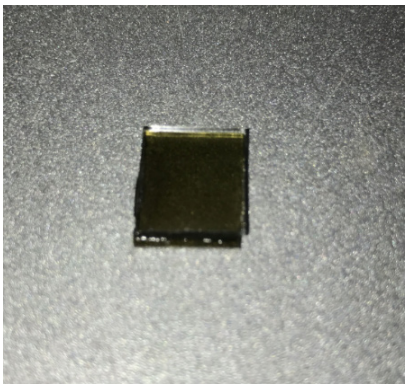

Fig. 3.18 SiC sandwich workpiece

The method for the observation is same with method presented in section 3.2.1 as shown in Fig. 3.19. The thickness of workpiece is equal to the diameter of micro tool. The interelectrode can be observed though the window A in the side wall of micro hole.

In addition, the thickness of glue film should be close to the width of discharge gap to avoid enlarging the micro hole because the melting point of resin adhesive is much lower than the stainless steel SUS304. One example of the thickness of glue film was is shown in Fig. 3.20, which is measured from three locations by a surface profiler (CV-3100S4/MM,

Mitutoyo). It is found that the thickness of glue film is similar to the gap width [32] in the condition of Table 3.2.

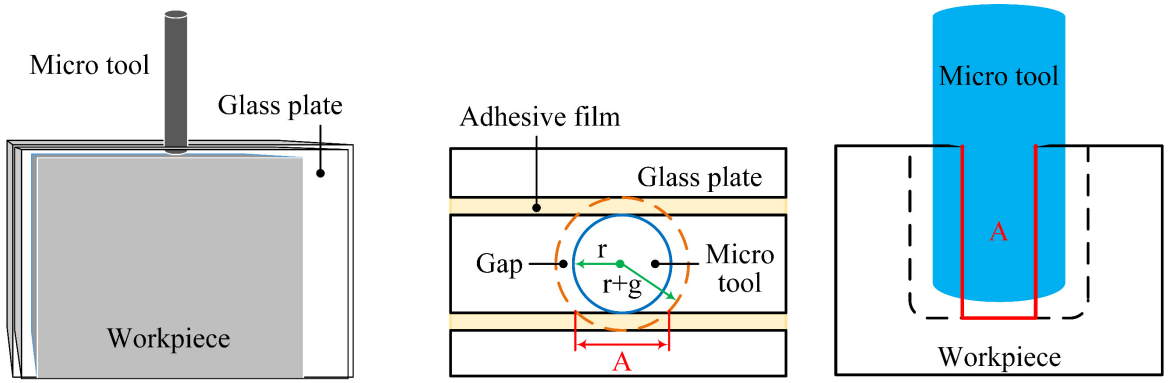

(a) Sandwich workpiece (b) Top view (c) Window A for observation

Fig. 3.19 Sandwich workpiece applied in observation

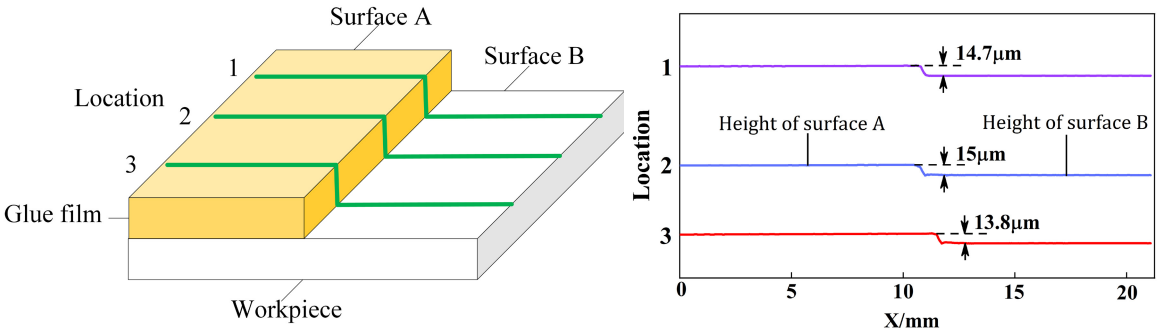

Fig. 3.20 Thickness of glue film.

3.3.1 Observation of gap area with SiC sandwich workpiece

The image of gap area with SiC sandwich workpiece is shown in Fig. 3.20. It is found that no debris leaks out from the gap area as shown in Fig. 3.13 and 3.14.

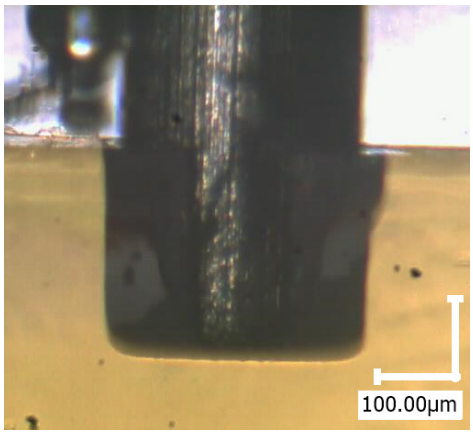

Fig. 3.20 Image of gap area with SiC sandwich workpiece

The mergence of bubble is also observed as shown in Fig. 3.21. Two little bubbles in Fig. 3.21 (a) merge together to become a big bubble Fig. 3.21 (b).

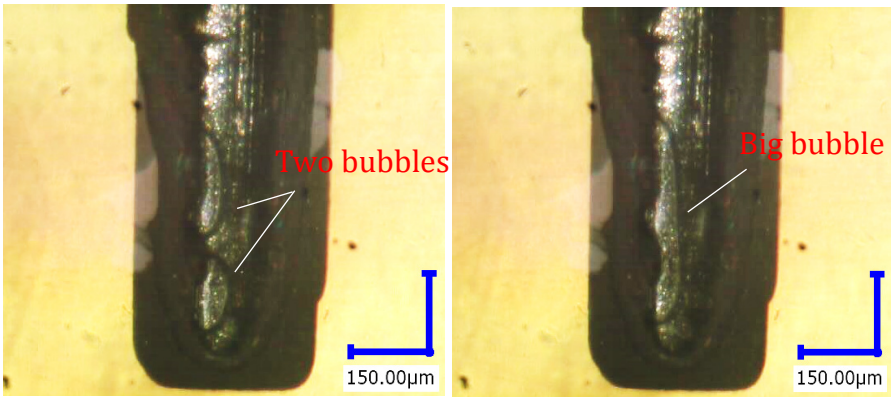

(a) t (b) t+0.2011s

Fig. 3.21 Merging of two bubbles

(t, a certain machining time; Feed depth: 1117μm)

In addition, with the increase of hole depth, more bubbles accumulate in the gap area and the bubble occupancy area becomes larger as shown in Fig. 3.22. In feed depth of 500μm, only a small part of gap area is occupied by the bubble. But in depth of 1149μm, a large bubble covers the gap area.

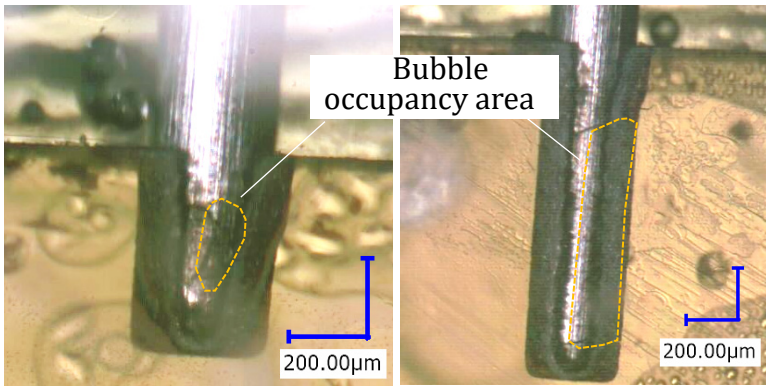

(a) Feed depth: 500μm (b) Feed depth: 1149μm

Fig. 3.22 Bubble occupancy area

Moreover, more discharges occur in deeper hole depth as shown in Fig. 3.23. In the depth of 423μm, the discharge only occurs in the bottom of micro hole but in the feed depth of 1117μm, many discharges sparks are captured in a same image, which means that in a short period time, many discharges occur. The accumulation of debris decreased the insulation strength of gap area significantly. It makes the discharge occurs more frequently and easily.

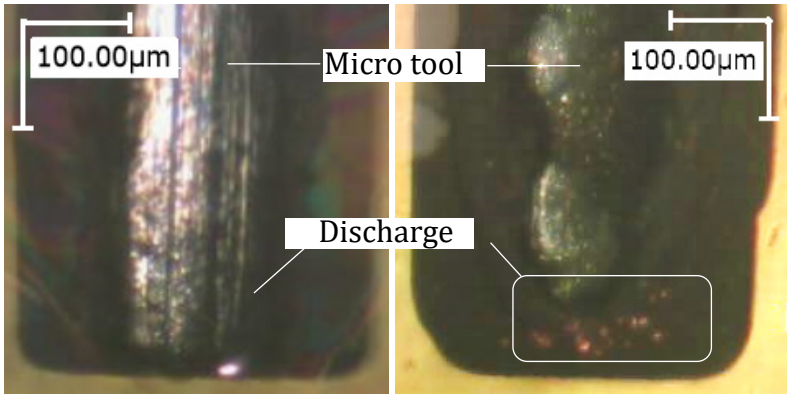

(a) Feed depth: 423μm (b) Feed depth: 1117μm

Fig. 3.23 Discharge in SiC

3.3.2 Observation of gap area with stainless steel SUS304 sandwich workpiece

It is found that at the beginning many little bubbles occurred in the gap area. The generation rate of bubble and the speed overflowing out of the gap area are very fast. Because the melting point of glue is much lower than that of the stainless steel SUS304, it is firstly removed in the machining as shown in Fig. 3.24 (b).

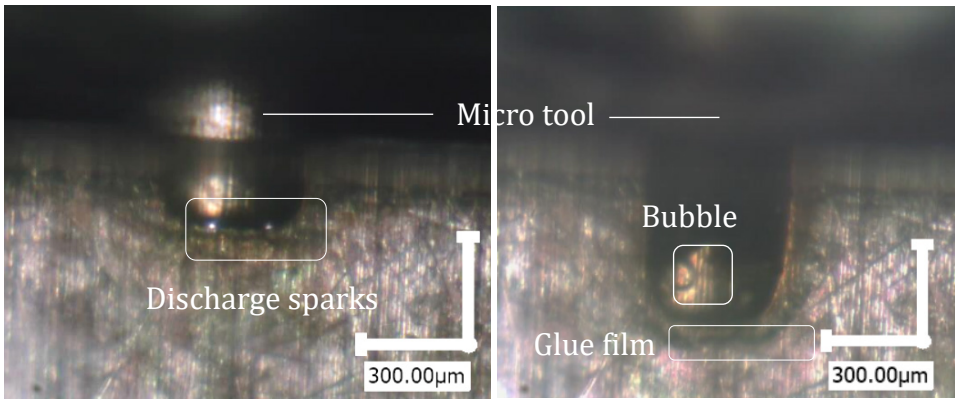

(a) Feed depth: 180μm (b) Feed depth: 400μm

Fig. 3.24. Observation of gap area

The debris accumulates with increase of hole depth, leading to the frequent short circuits and the retreat of tool because of abnormal discharges, such as the discharge between the debris and tool as the Fig. 3.25 showed.

Since the accumulation of debris, at the last stage of the machining, the gap area is nearly full of the debris. They block the gap area and prevents the movement of bubbles. Therefore, the bubble grows up and become bigger and bigger, then overflows the gap area slowly as the Fig. 3.26 showed. Sometimes the gap area is totally blocked by the debris, the bubble will deform its shape to overflow the gap area slowly as the shown in Fig. 3.27.

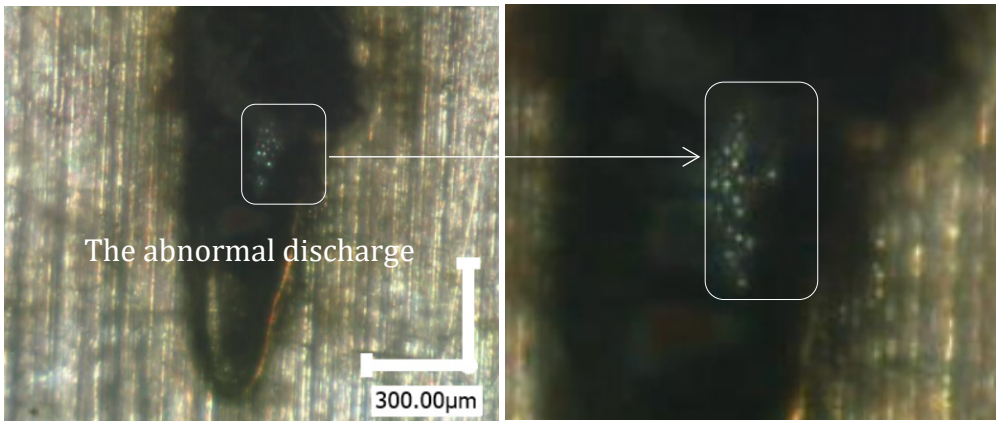

(a) Abnormal discharge (b) Large version

Fig. 3.25. Abnormal discharge in the gap area

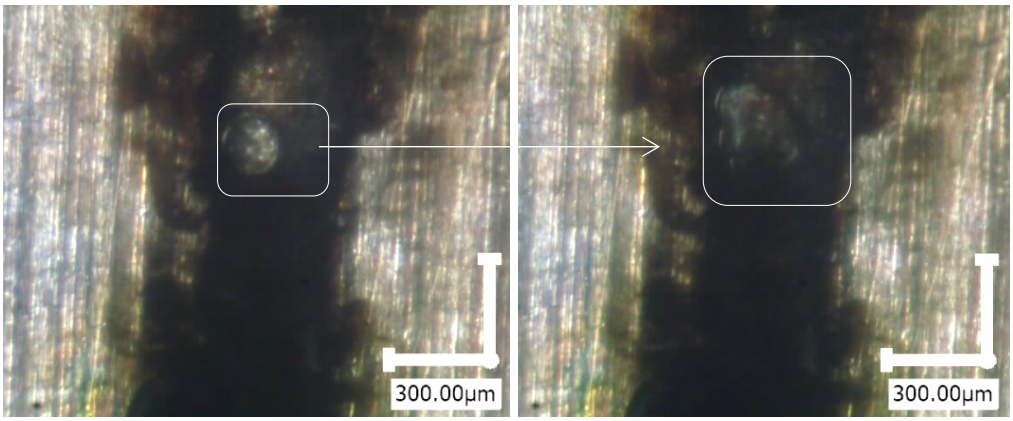

(a) Little bubble (b) Growing bubble

Fig. 3.26. Growth of bubble

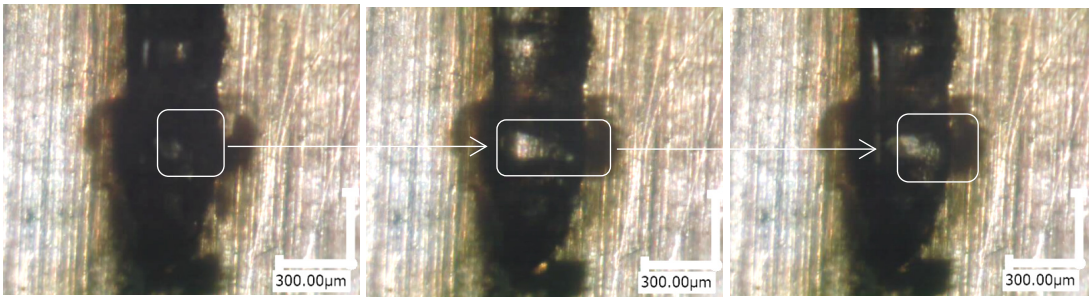

Fig. 3.27. Deformation of bubble

Above all, it is found that in the deep depth of micro hole, more debris accumulates in the gap area and the speed of bubble overflowing out of the gap area become slow. The key to improve the machining speed is to find the effective to exhaust the debris in the gap area.

3.4 Influence of tool wear on the micro EDM drilling

3.4.1 Introduction

During micro EDM, in the heating of the hyperthermal discharge plasma (approximately 6000-8000K), the materials of both cathode and anode will be instantly melted and become the scattering debris. The material removal of micro tool is commonly called tool wear. In the processing of micro EDM, actually the continuous replications of features of the micro tool onto the workpiece, the machining accuracy is difficult to be guaranteed since the original features of the micro tool is continuously machined. This phenomenon of tool wear is a big obstacle in the early research of EDM, and clearly exposed in the 3D cavity machining, in which a tapered electrode tip, far away from the original cylinder electrode tip, is formed in the lay-to layer machining, eventually resulting in the poor machining accuracy. Therefore, in micro EDM, the minimization of the tool wear is the permanent pursue in micro EDM, which is also reflected in the selection of material of tool electrode that normally the material with high temperature resistance is chosen for the micro tool such as tungsten or tungsten carbide.

Nevertheless, other views are thought that although the use of materials with high temperature resistance definitely decreases the tool wear, the discharge heat may accumulate in the tip of the cathode and gap area, rise the temperature of gap area and cause the thermal breakdown. On the contrary, the use of materials of excellent thermal conductivity, such as copper, is able to transfer the discharge heat promptly, decrease the accumulation of discharge heat and maintain the good heat balance of the gap area.

In fact, the mechanism of tool wear is still unknown since it concerns the mechanism of the breakdown process and the energy distribution during the discharging process. In the actual machining, the tool wear is able to be predicted by performing the pre-processing for the specific machining. Moreover, various methods of minimizing the tool wear are proved to be effective and adopted in the industry, such as the use of refractory metals, thin-walled tube electrode and the uniform wear method.

According to the experimental instances, the tool wear is non-uniform, which is firstly started from the edge then to the central part. One possible explanation is that the tip effect enlarges the electric field of the edge in comparison to the central part. A general description on the characteristics of tool wear varying with hole depth is still missing.

In this section, the depth-dependent characteristics of tool wear is investigated based on the real-time observation of the profile of the micro hole in the transparent SiC single crystal. The machining characteristic of micro EDM, replicating the feature of the micro tool onto the workpiece, ensures that the shape of the machining area is nearly same with

the outline of the micro tool. Real-timely observing the profile of micro hole in different hole depth reveals the change of the tool wear varying with the hole depth.

3.4.2. Experiments method

The observation of the profile of the micro hole in SiC single crystal was performed. The experimental equipment and sandwich workpiece are same as that in the Fig. 3.10 of the section 3.2.1 and the Fig. 3.18 of the section 3.3.1 respectively. The improved SiC sandwich workpiece not only provides the excellent optical visibility for observation but also prevents the leak of the debris to provide a sharp observation on the edge of the profile of the micro hole.

3.4.3 Results and analyzation

The profiles of the micro hole in different hole depth were shown in Fig. 3.28. The profiles of the micro tool can be distinguished clearly from the unprocessed part as shown in Fig. 3.29.

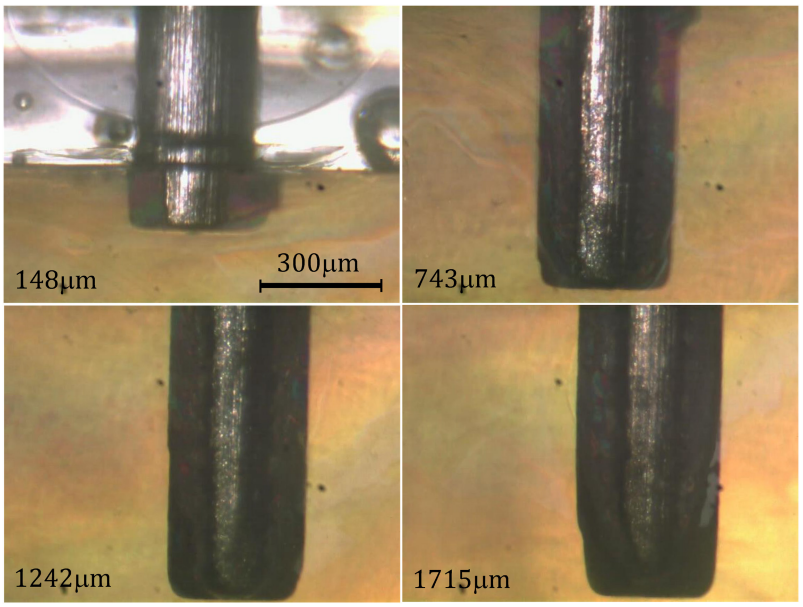

Fig. 3.28. Profiles of the micro hole in different hole depths

The profile of the micro hole can be tracked by the function of the point tracking in the SOLIDWORKS and extracted as shown in Fig. 3.29. After flattening all the profiles in different hole depths, the depth-dependent characteristics of material removal varying with the tool wear can be clearly visible as shown in Fig. 3.30. A series of the profiles are flatted together depending on the feed depth. The final profile of the micro hole (red line in Fig. 3.30) is extracted from the image captured in the end of the machine, which can reveal the real profile of micro hole in the final stage. The good consistency between the

profile formed by the flatted profiles in different feed depth with that extracted from the image in the end of machine reveals that the arrangement of these profiles is reliable and they can imply the variations of material removal with the tool wear.

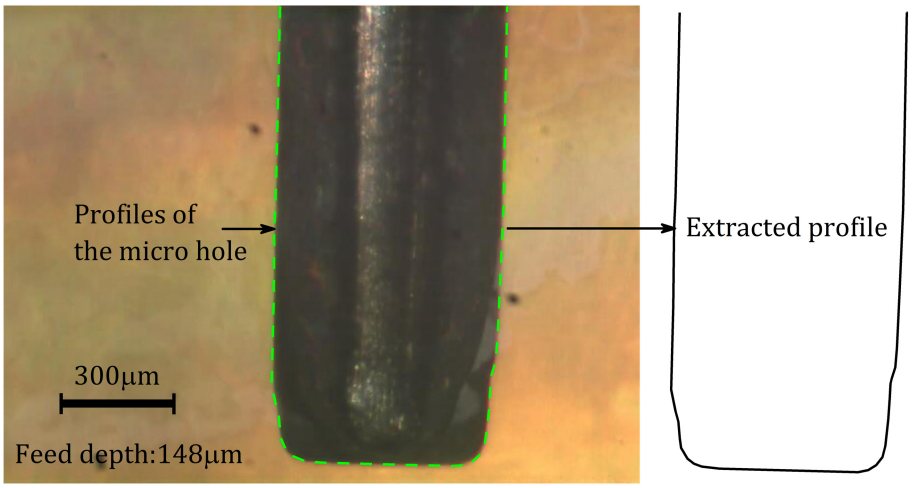

Fig. 3.29 Extracting the profile of the micro hole

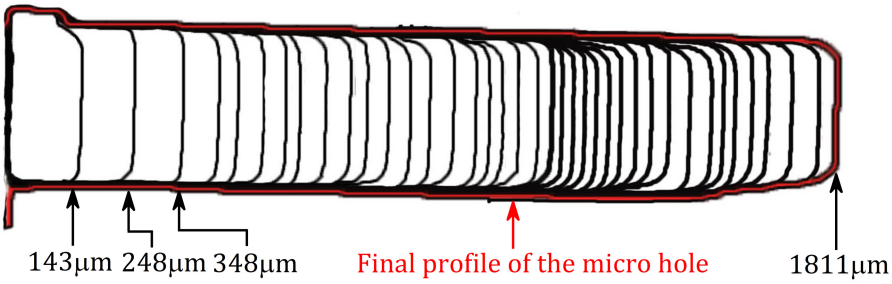

Fig. 3.30 Flattened profiles of the micro hole in different hole depth

The result shows that with the increase of the hole depth, the potential discharge area gradually converts from the bottom of the micro tool to the side wall of micro tool due to the tool wear making the cylinder electrode become the taper electrode and enlarging the potential discharge area seriously.

The micro tool used to drill the micro hole with the feed depth of 1.5mm and 3.2mm is shown in Fig. 3.31 (a) and (b) respectively. As mentioned before, in deeper feed depth, the profile of micro hole gradually converts from the shape of cylinder to tapper. The same method as put forward before is to track the edge of the micro tool and extract the profile of the micro hole, which is presented in Fig. 3.32 (a) and (b) respectively.

It is found that the tool wear is uneven in following two aspects:

1. In a same micro tool, the tool wear in different parts of the micro tool is different;

2. In different feed depths, the tool wear is different.

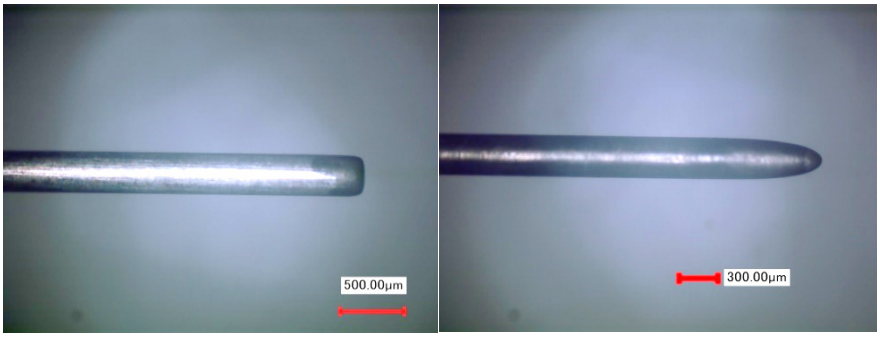

(a) Feed depth of 1.2mm (b) Feed depth of 3.2mm

Fig. 3.31 Micro tool after drilling the micro holes with different hole depth

As the comparison of profiles of micro tools in Fig. 3.32, in a same micro tool (tool$_a$ or tool$_b$), the tool wear in the left side and right side is different: $L_1 \neq L'_1$, $L_2 \neq L'_2$; Between the tool$_a$ with tool$_b$, the tool wear of the tool$_b$ is much larger than that of the tool$_a$, which implies that the tool wear increase seriously with the increase of the feed depth.

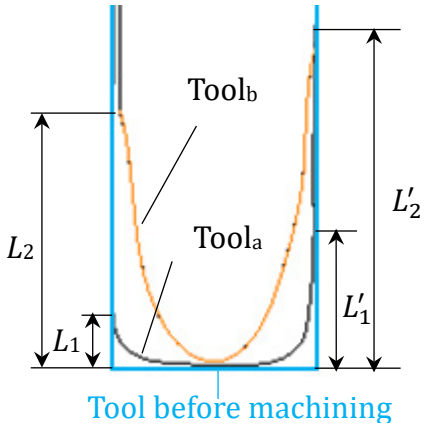

Fig. 3.32 Profiles of the micro tools

It can be assumed that in the two cases the micro tool with the profile in Fig. 3.32 further proceeds a tiny distance H, the potential discharge area is totally different as shown in Fig. 3.33. In case of the micro tool$_a$, the potential discharge area with a shape close to a round table reveals that the discharge mainly occurs in the bottom of the micro tool. However, in the case of the micro tool$_b$, it can be destined that the discharge in the cone potential discharge area mainly occurs in the side of the micro tool.

In order to visibly present the potential discharge area in two cases, the 3D model of the potential discharge area is built in the SOLIDWORKS based on the left part of the profile in Fig. 3.32 as shown in Fig. 3.34.

The results show that the uneven tool wear leads to an uneven discharge gap and eventually enlarges the potential discharge area. As shown in Fig. 3.33, the cone potential discharge area in Fig. 3.33 (b) increases the possibility of the short circuits and abnormal

discharges compared the round table one in Fig. 3.33 (a) when mass debris will accumulate in the gap area as analyzed in section 3.2 and 3.3.

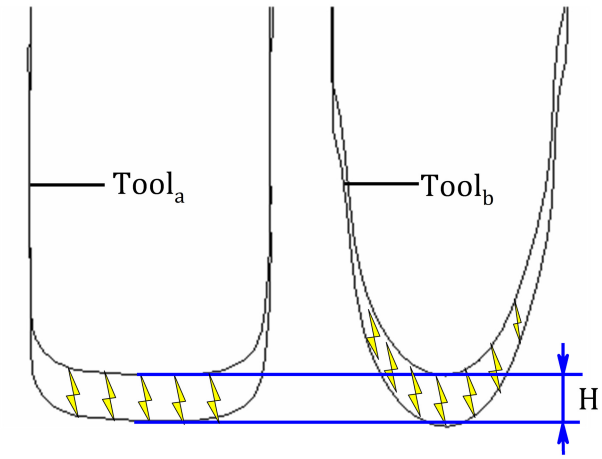

Fig. 3.33 Potential discharge area in further proceeding distance H

With the increase of the feed depth, the uneven tool wear causes the changes of shape of the micro tool. The discharge area gradually converts from the bottom of micro tool to the side wall of the micro tool. The uneven gap width eventually leads to the uneven material removal in the workpiece. As shown in Fig. 3.30, the uneven tool wear in the side wall of the micro tool cause the loss of symmetry for the material removal. It is obvious that the symmetric line of the bottom of the micro tool ceaselessly fluctuates around the rotation center line of the micro tool. The uneven gap width increases the uncertainty of discharging location due to the uneven insulation strength of gap area especially the movement and accumulation of the conductive debris. Eventually, the short circuits and abnormal discharges occur frequently. Therefore, the serious tool wear always accompanies with the low machining speed and machining accuracy.

3.5 Conclusions

The discharge environment is definitely deteriorated with the increase of hole depth. The direct evidence is the change of the discharge circle from regular to unregular. The phenomenon of decreasing machining speed in micro EDM drilling is because of the frequent retreat of the micro tool. The detection on the discharge signals during a big retreat process indicates that the gap area between the cathode and anode is electrically connected in the whole retreat process. The only possible explanation is the behavior of the dissociative debris like movement, adsorption and accumulation in the gap area, resulting in the seriously low insulation strength of the gap area by building the electric

bridge or linking the cathode with anode directly.

The observation on the interelectrode also verifies the inference. In the observation of the interelectrode gap area with stainless steel SUS304 workpiece, mass debris is observed to accumulate in the gap area, stick on the surface of the cathode and anode and even participate in the discharging process. Obviously, the debris is not freely distributed in the gap area and will be influenced by the complex phenomena such as the electric field and the viscous effect on the dispersion system of gap area. The decreasing insulation strength of the gap area is the reason for the machining limitation in micro hole drilling, such as the discharge in debris and the electric bridge. The participation of debris in the discharge process replace the role of the workpiece and results in the decrease of material removal of the workpiece in the micro EDM.

The bubble behavior of the mergence and upgrowth indicates that the bubble will incline to accumulate in the gap area with increase of hole depth. Since there is no other way to flush and mix the gap area expect the rotation of the micro tool, the less bubbles escaping from the gap area will weaken the flushing effect on the gap area to lead that dielectric liquid can't exchange immediately and debris will accumulate in the gap area. Moreover, inclination of less bubble escaping from the micro hole will increase the bubble occupancy area in the narrow gap area, decrease the space for the dielectric liquid and debris and increase the possibility of debris concentration, which also decrease the insulation strength of the gap area because normally the insulation strength of the gas is much smaller than that of the liquid.

In the other hand, the tool wear also plays a key role in deteriorating the environment of the gap area accompanying with the behavior of the bubble and debris. The different tool wear on the bottom and the side wall of the micro tool forms the uneven gap width in the gap area, which further aggravates the uncertainty of the discharge location accompanying with the complex behavior of the bubble and debris. For instance, in the uneven gap area, the debris is inclined to concentrate towards the spot with narrower gap width where the stronger electric field exists. Furtherly, considering the enlarging bubble occupancy area in the uneven gap area, there is the great possibility for the debris concentration to initiate the phenomenon of the electric bridge and short circuit. Therefore, the abnormal discharge states such as the discharge in low open circuit, arc discharge and especially the frequent short circuits frequently exist in the deteriorated gap area.

Overall, with the increase of the hole depth, it can be concluded that the gradually deteriorating environment with the increase of the hole depth is inevitable result of the distinctive mechanism of the micro EDM. The micro EDM depends on the thermal erosion effect to remove materials. The ultra-high temperature of the discharge plasma is capable to any known metal materials, likewise, the material of the cathode can also be instantly melted in the discharging process. Hence, firstly, the tool wear is inevitable in the micro EDM; The narrow gap area where the discharge occurs guarantees the high machining accuracy of the micro EDM. However, in the narrow gap area, which actually can be treated as a complex dispersive system, the escape of bubble and exist of debris is destined to be difficulty due to the viscous effect and capillary action. Therefore, the large bubble occupancy area and accumulation of debris are also both inevitable. Eventually, tool wear and the behavior of bubble and debris make it possible for the abnormal discharge by decreasing the insulation strength of the gap area.

Chapter 4. Feasibility in quantitively estimation on the behavior of bubble and debris

In micro EDM, the narrow discharge gap has two sides. On the one hand, it ensures the occurrence of the discharge under the controllable small discharge energy and maintains the machining accuracy through the tiny material removal. On the other hand, like a double-edged sword, it also raises the difficulty in the exchange of the dielectric liquid and exclusion of byproducts such as the debris and bubble, which will deteriorate the machining environment and result in the poor machining accuracy and low machining speed.

The concern for the behavior of bubble is mainly focused on its complex physics prosperities: fluidity, deformability, viscosity, and their variations under the thermo-shock during discharging. Therefore, it is a great challenge to quantitatively evaluate the behavior of the bubble. Moreover, more complex interelectrode phenomena are likely to be caused in the inference of the published reports. For example, in the condition that the most of the gap area is occupied by bubbles [76, 78], the discharge is inclined to occur in gas nor the liquid medium because generally the insulation strength of the pure liquid is much larger than the gas [80], which is likely to be one of reasons for the weak insulation strength of the gap area in the long-time drilling with the micro EDM. Bubble movement and deformation is the main way for the debris exclusion since no other ways for stirring the gap area except the tool rotation. However, the debris is more likely to be concentrated owing to the large bubble occupancy area in gap area.

The evaluation on the influence of the behavior of the bubble and debris on the deteriorated environment in micro hole drilling with EDM stops at the description of the complex interelectrode phenomena based on the empirical understanding.

For the sake of the clarification of the bubble behavior in the interelectrode, the direct observation of the gap area has been done with an originally designed sandwich workpiece and a high-speed camera, and some phenomena have been presented in detail in the previous chapters such as the upgrowth and mergence of bubbles, the discharge in debris and the emergence of the large bubble occupancy area in deeper hole depth. However, limited by the experimental equipment and method, the quantitatively estimation on bubble behavior is still difficult because only a part of gap area can be observed with a special designed sandwich workpiece, which is not the same as the actual

experiment in a solid workpiece. In addition, the ultra-short discharge duration, shorter than 1μs in micro EDM with RC circuit, also makes it difficult for matching the voltage waveform of ultra-high sampling frequency with the high frame rate video, let alone analyzing the relationship between bubble behavior with discharge waveform.

So far, the study on the clarification of the behavior of the bubble and debris just stops on the description of the complex interelectrode phenomena. By contrast, the behavior of the debris seems so complicated that few published reports concern except the exploration on the measurement of the scale of the debris.

In this chapter, the feasibility of the quantitative estimation on the behavior of the bubble and debris is investigated. A method is put forward to quantitatively measure the size and number of the bubble escaping from the micro hole in the premise of no influence on the drilling process. Moreover, a series of solutions from the experimental equipment to the data processing are put forward to realize the quantitative evaluation on the behavior of the bubble and debris.

4.1 Method to observe bubbles escaping from the micro hole

The bubble behavior in the interelectrode of the micro hole drilling has been presented in the previous chapters. Nevertheless, it is difficult to quantitatively estimate the behavior of the bubble because the gap area with the shape of a text tube is impossible to be observed totally where only a part of the bubble can be observed. However, no matter how complex of the bubble behavior in the interelectrode, finally the bubbles will escape from the micro hole through the only exit, the entrance of the micro hole. Therefore, if the bubbles escaping from the entrance of the micro hole can be counted, the quantitative estimation on the bubble behavior is possible.

In the conventional micro hole drilling, the bubble escapes from micro hole disorderly as shown in Fig. 4.1 (a), which is impossible to be observed and measured. The first is to order the distribution of the bubble escaping from the micro hole to make it convenient to be observed and counted. A method was put forward to arrange the bubble orderly as shown in Fig. 4.2 (b) and create a suitable observation area for the high-speed camera.

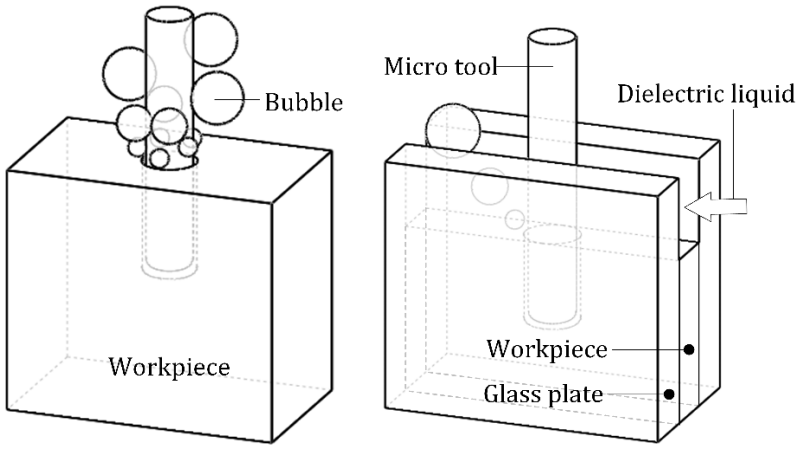

(a) In conventional state (b) In ordered state

Fig. 4.1 Distribution of bubble

The schematics of method and setup are shown in Fig. 4.2 and Fig. 4.3 respectively. A sheet workpiece of stainless steel SUS304 is vertically fixed by a self-designed workpiece holder supported by the XY stages. There is a good perpendicularity between the workpiece holder with XY stages to assure installation accuracy of workpiece. Two pieces of glass plates are used to press the sheet workpiece from both sides then fixed together by two little clamps. Therefore, a channel is created between the two glass plates. When the dielectric liquid is gently spurted towards the channel, a constraint flowing area is formed due to the constraint of glass plates to the dielectric liquid as shown in Fig. 4.1 (b). The thought is to sweep the bubble away immediately once the bubble escapes from the micro hole by the gently flowing dielectric liquid with a proper velocity. Moreover, the constraint flowing area with the dielectric liquid of uniform thickness is necessary for the narrow focusing length of the high-speed camera.

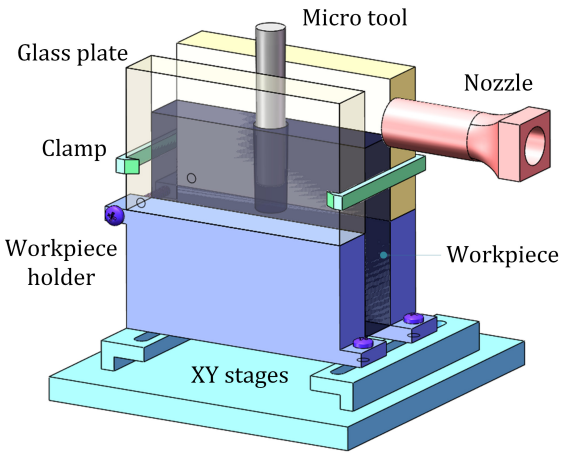

Fig. 4.2 Schematic of setup

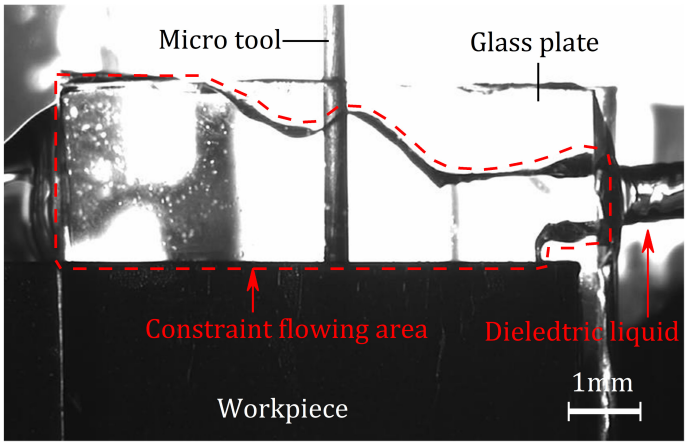

Fig. 4.3 Constraint flowing area

4.2 Experimental equipment

The experimental equipment and signal transmissions among the devices are shown in Fig. 4.4. The stainless steel SUS304 sheet workpiece or the needle electrode acted as the anode are fixed in the XY stages according to the different experiments. The whole experiments are carried on the micro EDM machine (MG-ED71, Panasonic) with a RC circuit, which is more sensitive to the state of gap area compared to gate control of the transistor type pulse generator. A high-speed camera (HX3, NAC) focuses on the constraint flowing area and is used to observe bubbles or the discharge spot. A laser sensor (LK-G80, Keyence) is for detecting the position of Z axis. The control computer controls the machining and real-timely displays the observed video and the feed depth of micro tool received from the high-speed camera and laser sensor respectively. A high-frequency, bidirectional current probe (CT-1, Tektronix) is used to detect the high frequency current signals in discharging. Since the discharge duration in the RC circuit is significantly short, in order to record the voltage and current waveforms more accurately, they are both input into the oscilloscope (TBS2000, Tektronix) with a ultra-high sampling frequency, 1GS/s. The quantitative estimation on bubble behavior in different discharge states require the synchronous recording of the voltage/current waveforms and the observed video. Thus, a trigger signal (a falling-edge of the voltage pulse) is used to synchronously trigger the oscilloscope and the high-speed camera, which is sent out by the oscilloscope by pressing the “Force trigger” button. Moreover, in order to make it more convenient to match the video with waveforms of voltage/current in the later data processing, the signal of the video frame sent out by the high-speed camera is also input into the oscilloscope, triggered and saved together with voltage and current waveforms.

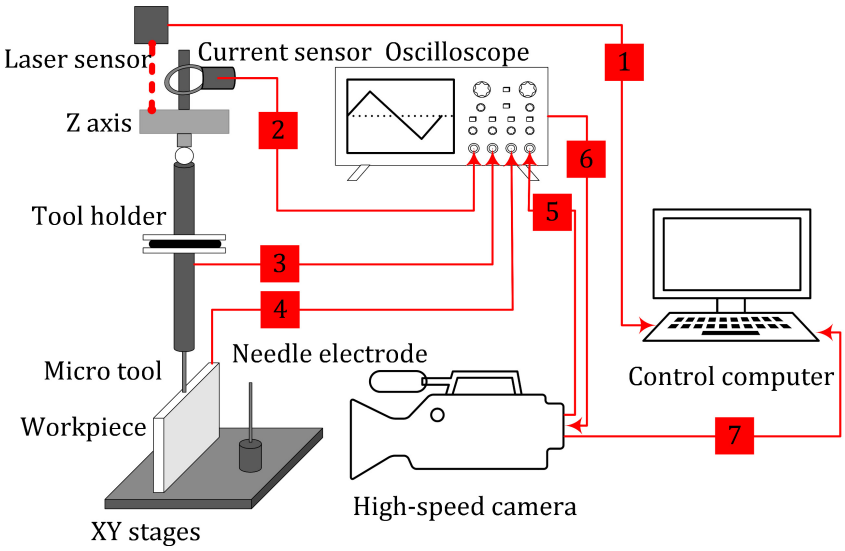

Fig. 4.4 Schematic of experimental equipment

→ : Signal transmission direction

1: Displacement signal from laser sensor

2: Current signal from current sensor

3: Voltage signal of cathode

4: Voltage signal of anode

5: Frame signal from high-speed camera

6: Trigger signal from oscilloscope

7: Digital video signal from high-speed camera

4.3 Determination of parameters for the flow field of the dielectric liquid based on simulation

In this section, the analysis and determination of the parameters of the velocity field used in experiment of blind hole drilling are explained. The schematic of the vertical view of the machining area is shown in Fig. 4.5. Two requirements have to be satisfied to ensure the clear observation of the bubbles escaping from the micro hole: First, the bubble should be flushed away immediately once it escapes from micro hole to avoid staying in the constraint flowing area or merging with other bubbles; Second, the movement of the flushed bubble should be kept in the focus area shown in Fig. 4.5 to avoid defocusing. The bubble that is outside of the focus area can still be observed by the high-speed camera, but its edge is fuzzy due to defocusing, which is not convenient for the measurement. Since the bubble movement near the entrance of the micro hole is significantly influenced

by the flow field of the dielectric liquid in the constraint flowing area, it is necessary to investigate the distribution of the flow field and determine the proper parameters for the flow field to meet the requirements for bubble flushing.

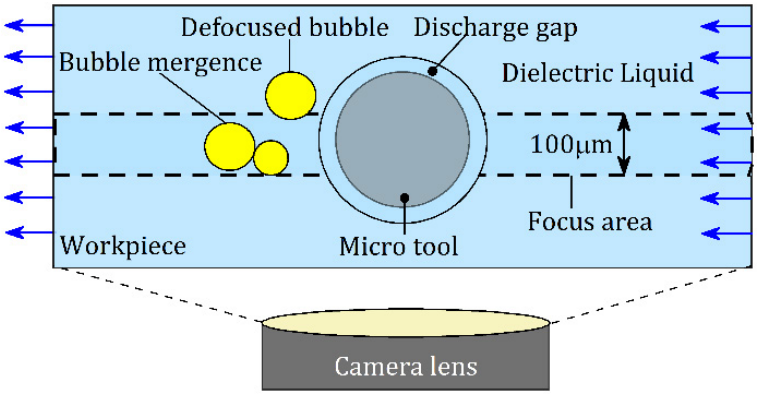

Fig. 4.5 Vertical view of machining area

4.3.1 Simulation model based on COMSOL Multiphysics

To investigate the flow field of the dielectric liquid in the constraint flowing area, a 2D multi-physics model was established with COMSOL Multiphysics based on laminar flow coupled with rotating machinery physics. The geometry of the model is shown in Fig. 4.6. The length of the workpiece is set to 2mm, which is enough for the development of flow field. The width of the discharge gap is set to 25μm based on our previous experiment of drilling deep micro holes with EDM [23]. The entrance and exit of the fluid are set in the right and left wall of the workpiece respectively.

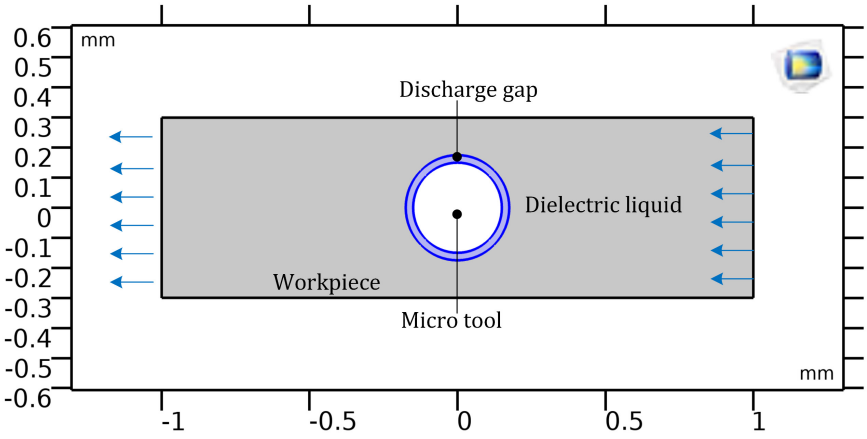

Fig. 4.6 Geometry of simulation model

The domain of the discharge gap is set as the rotating domain to accurately model the flow of liquid surrounding the micro tool in a rotating coordinate system. The domain of workpiece is not rotated and expressed in the fixed material coordinate system. The rotating and fixed parted are coupled together by an identity pair, where a flux continuity

boundary condition is applied. The edge of the micro tool is set to the rotating boundary.

The flow is described by the Navier-Stokes equations and mass conservation equation as shown in equations 1 and 2:

$$\rho\,\partial \boldsymbol{u}/\partial t + \rho(\boldsymbol{u}\cdot\nabla)\boldsymbol{u} = \nabla\cdot[-p\boldsymbol{I} + \mu(\boldsymbol{\nabla}u + (\boldsymbol{\nabla}\boldsymbol{u})^{T})] + \boldsymbol{F} \quad (1)$$

$$\nabla\cdot\boldsymbol{u} = \boldsymbol{0} \quad (2)$$

where, $\boldsymbol{u}$ denotes the velocity (m/s), ρ is the density (kg/m^3), μ is the dynamic viscosity (Pa·s), and p is the pressure (Pa), T is the absolute temperature (K), $\boldsymbol{F}$ is the volumetric force (N), and $\boldsymbol{I}$ is the identity matrix. The parameters of the simulation are shown in Table 2. The flow field was investigated under the influence of three key factors: the rotational direction of the micro tool, the thickness of the sheet workpiece and the entrance velocity of the dielectric liquid.

Table 4.1 Parameters for multi-physics field simulation

Items	Parameters	Unit
Tool rotational speed	3000	rpm
Tool rotational direction	Clockwise, anti-clockwise	
Dielectric liquid	Deionized water	
Entrance velocity of liquid	0.05, 0.1, 0.25, 0.5, 0.56	m/s
Thickness of workpiece	0.6, 0.8	mm
Diameter of micro tool	300	μm
Width of discharge gap	25	μm

4.3.2 Influence of the rotational direction of the micro tool on the flow field

The flow fields at different rotational directions of the micro tool are shown in Fig. 4.7. The arrows in streamlines are arranged in equal time. The flow field with an entrance velocity of 0.05m/s develops adequately in 0.02s and becomes steady under a total simulation time of 0.05s. The initial flow is separated into two streams due to the blocking of the micro tool. Influenced by the viscous effect, the fluid flowing in the direction that is the same as the tangential velocity of the micro tool will be accelerated. Otherwise, it will be decelerated. Loss of symmetry for the flow field due to rotation of the micro tool will lead to the appearance of reflux on the lower side of the low velocity area. Bubbles in the accelerated area can be flushed away more quickly than those in the decelerated area. Since the camera is placed on the front of workpiece shown in Fig. 7, the accelerated area

in Fig. 9 (b) cannot be observed due to the blocking of the micro tool. Thus, in the experiment, the rotational direction of micro tool was set clockwise, as shown in Fig. 9 (a).

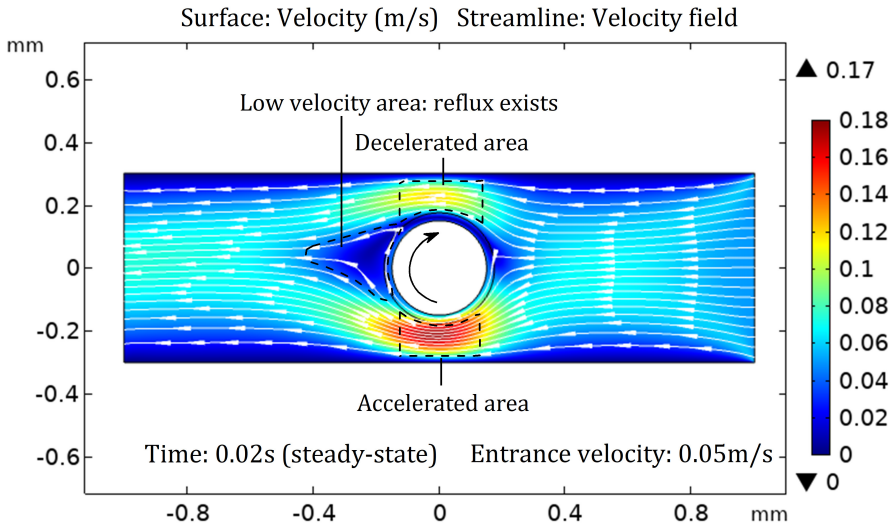

(a) Clockwise

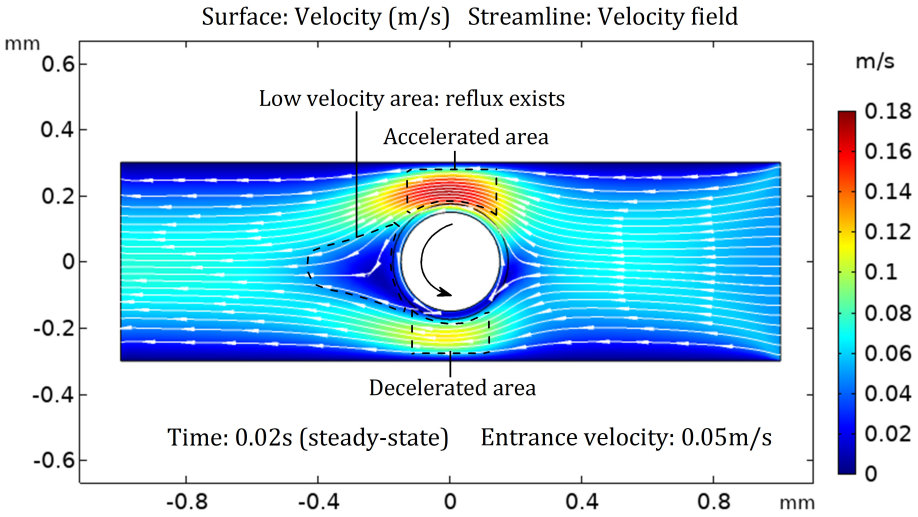

(b) Anti-clockwise

Fig. 4.7 Flow fields at different rotational directions of the micro tool

4.3.3 Influence of the entrance velocity of the dielectric liquid on the flow field

The flow fields at different entrance velocities are shown in Fig. 4.8. The streamline contour reveals the distribution of the flow field. The flow field reaches a steady state in 0.02s under the total simulation time of 0.05s when the entrance velocity is less than 0.56m/s. With increase of the entrance velocity, the effect of rotation of the micro tool is weakened and the flow field is inclined to be symmetrical. Nevertheless, the low velocity area becomes larger to form a tongue-like recirculation zone, where many vortexes exist.

When the entrance velocity reaches 0.56m/s, the wakes of two streams exhibit shedding. The shedding wave of each stream is enough to disturb the other. Therefore, the near-wake flow field becomes disordered, as shown in the Fig. 10 (e) and (f).

To flush the bubble away effectively, the entrance velocity of the dielectric liquid should not be very large to avoid the enlarging of the low velocity area and shedding wakes in the larger entrance velocity.

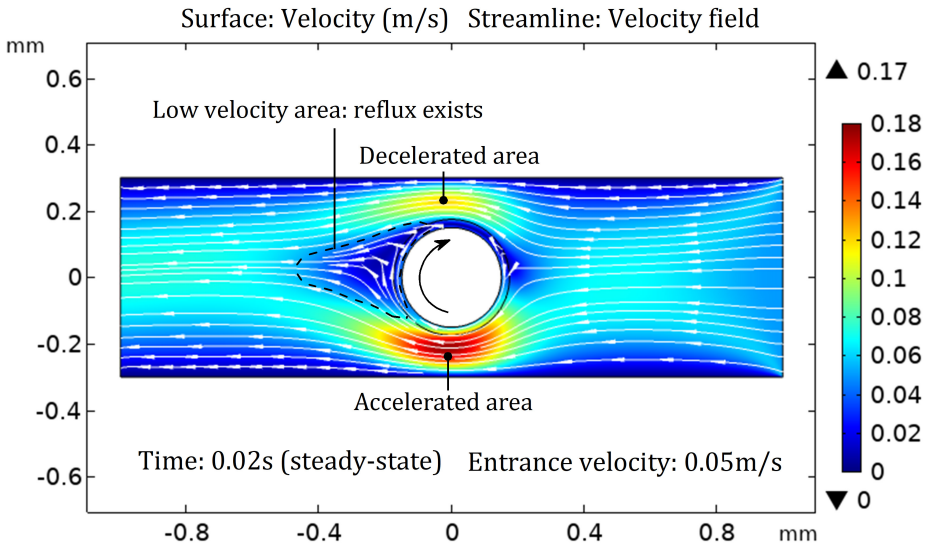

(a) Entrance velocity: 0.05m/s

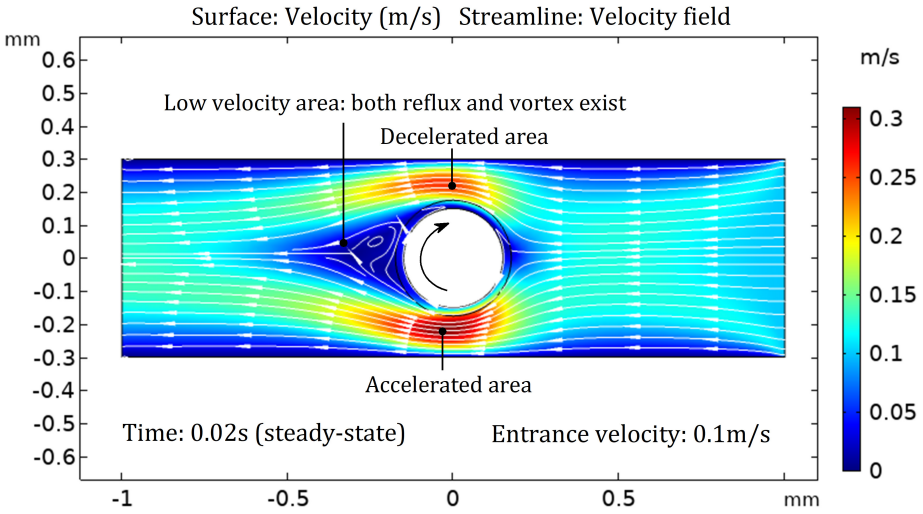

(b) Entrance velocity: 0.1m/s

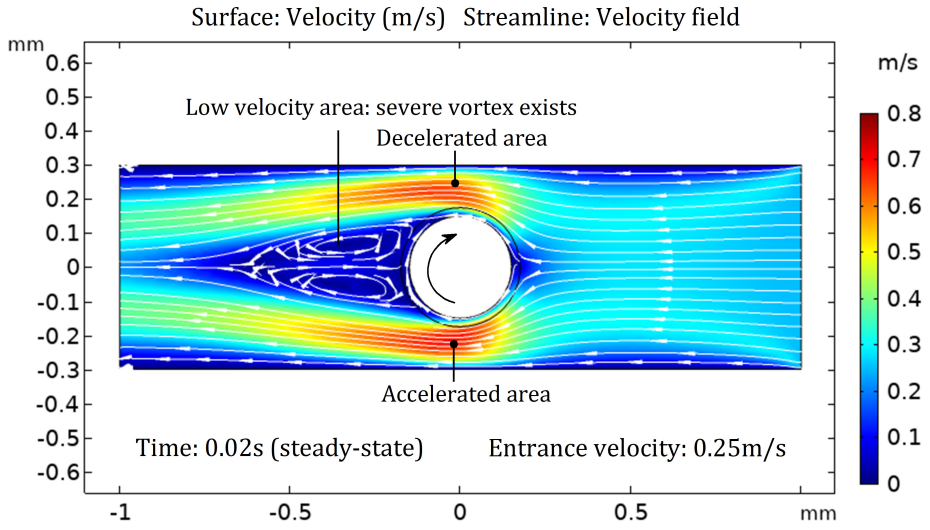

(c) Entrance velocity: 0.25m/s

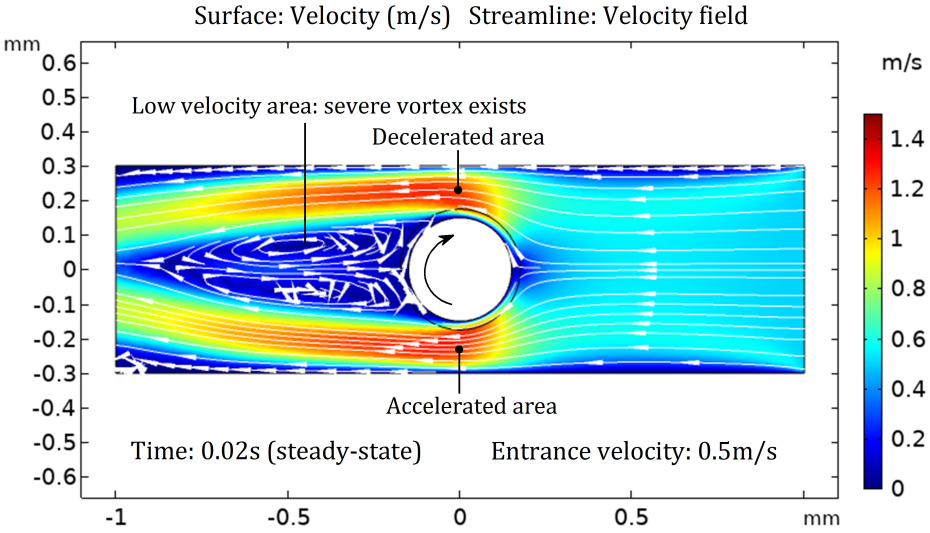

(d) Entrance velocity: 0.5m/s

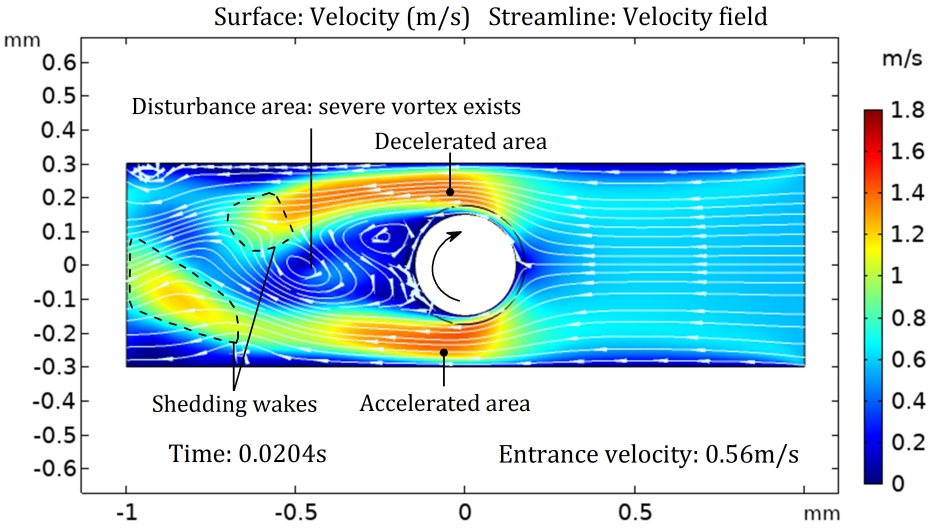

(e) Entrance velocity: 0.56m/s; Time: 0.0204s

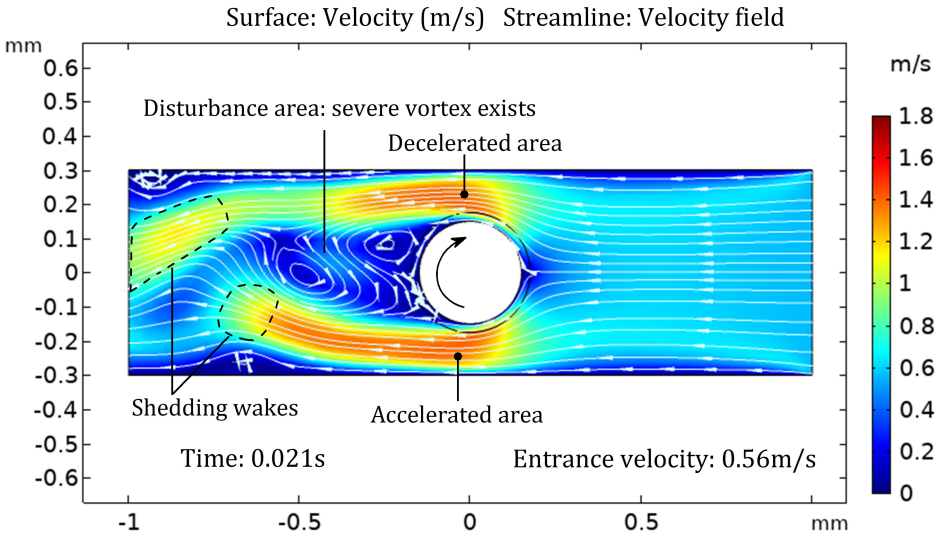

(f) Entrance velocity: 0.56m/s, Time: 0.021s

Fig. 4.8 Velocity fields at different entrance velocities

4.3.4 Influence of the workpiece thickness on the flow field

To obtain a blind hole in the sheet workpiece, the thickness of the workpiece should be larger than 0.5mm considering the installation error and width of the discharge gap. The distribution of the flow field was simulated in the workpiece with thicknesses of 0.6mm and 0.8mm and are shown in Fig. 4.9 respectively. The entrance velocity is set to 0.5m/s. The results show that the flow field in the thicker workpiece is enlarged but inclined to be more dispersed. The velocity of the flow field along two cut lines A and B are applied to estimate the changes of flow fields in the Y- and X- directions, which are shown in Fig. 4.10 respectively. It indicates that in the thicker workpiece, the flow field becomes more dispersed in the Y-direction; Meanwhile, the velocity decreases in the X-direction.

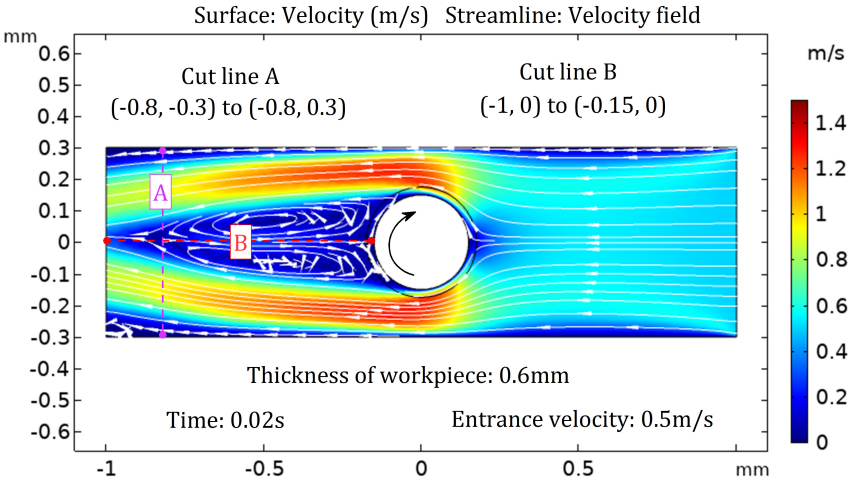

(a) In workpiece with thickness of 0.6mm

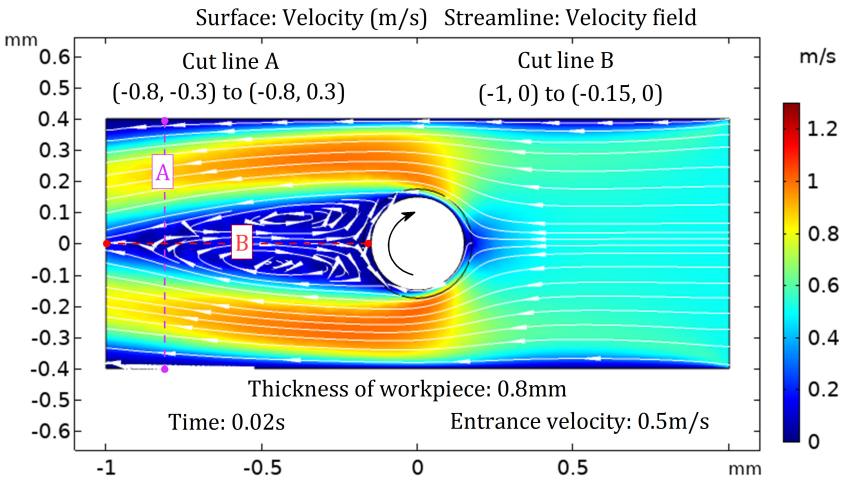

(b) In workpiece with thickness of 0.6mm

Fig. 4.9 Flow fields in 0.6mm and 0.8mm workpieces

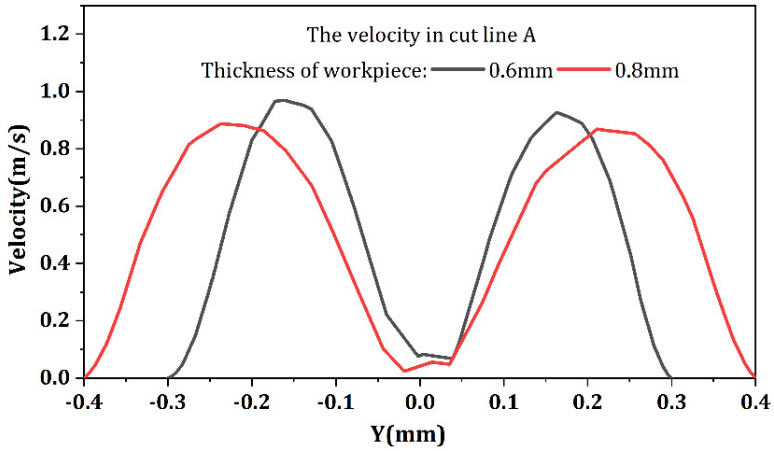

(a) Velocity along cut line A

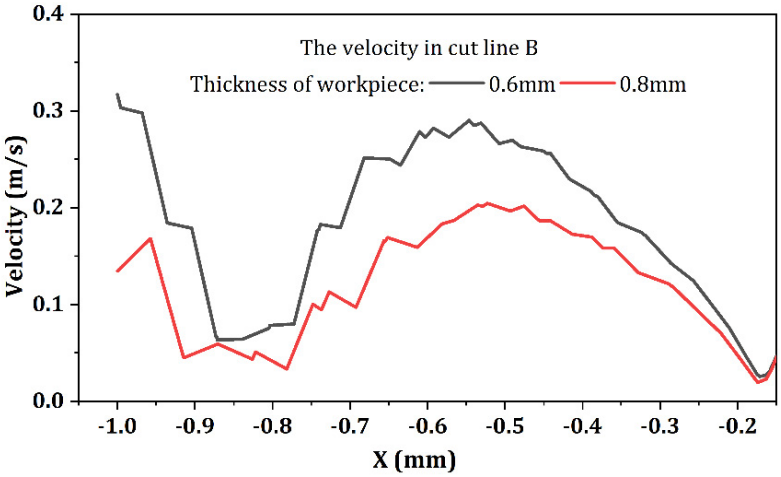

(a) Velocity along cut line B

Fig. 4.10 Velocities along cut line A and B

Bubbles in the dispersed flow field have a larger possibility to move out of the focus area, such as the defocused bubble in Fig. 4.5, which has been observed in Fig. 4.11. The

lower velocity in the X-direction may lead the bubble to move slowly in the low velocity zone and merge with other bubbles, as shown in Fig. 4.5, which is not convenient for the measurement. Therefore, in the experiment, the thickness of the workpiece should be as small as possible in the conditions that a blind hole can be guaranteed and the bubble can be flushed away effectively. In this research, the workpiece with the thickness of 0.6mm was used.

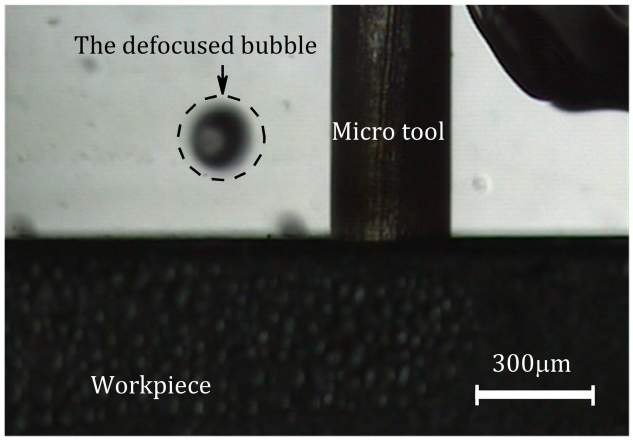

Fig. 4.11 Example of defocused bubble

In fact, in the machining, in order to create the constraint flowing area, the diameter of nozzle should be slightly larger than the width of the channel to make sure the stability of the water film. Thus, inevitably, a part of dielectric liquid leaks from the entrance of the channel. Therefore, the actual entrance velocity of the dielectric liquid may be slightly larger than 0.56m/s. In this research, the diameter of the nozzle was 0.72mm and the volume flowrate was 0.81ml/s.

Ultimately, the proper parameters for the flow field have been determined. Under these conditions, the bubbles escape from the micro hole one-by-one in the high-frame video and can be flushed away in an orderly manner, as observed in Fig. 4.12.

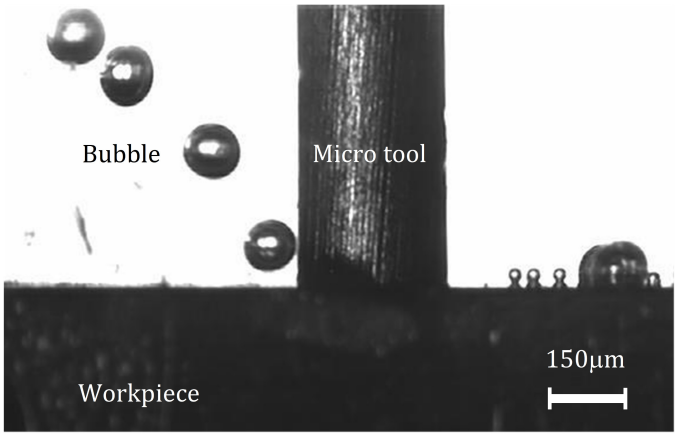

Fig. 4.12 Bubble escaping from micro hole in the feed depth of 1002μm

4.4 Measures adopted for data processing

In this section, a series of solutions for data processing are described to realize the quantitative measurement of the bubble behavior.

4.4.1 Match of video with discharge waveform

According to the reported studies, the bubble and debris are the byproducts of the discharge process. Therefore, the discharge state significantly influences the bubble behavior. In order to investigate the bubble behavior in the normal discharge state, it is necessary to match the video with the discharge signals in a chronological order.

Although the video and the voltage waveform are synchronously triggered by the same trigger signal, they are saved separately in the high-speed camera and the oscilloscope respectively. The high-speed camera records the image information by scanning the observation area line by line. During the period of one frame, an image of the observation area with redefined graphic resolution is scanned completely and saved in the internal storage. In the next frame, the current image information will be replaced by the new image information to form a new image. However, the moment that the high-speed camera receives the trigger signal, the recording of image information in current frame is interrupted and reset immediately. The sudden interruption of the recording by the trigger signal will lead to an incomplete frame, in which the image looks like to be torn and the period of the incomplete frame is obvious less than the period of a normal frame. The torn image near the trigger point (t=0) can be easily found from the video shown in Fig. 4.13 (b). In the other hand, since the frame signal is also input into the oscilloscope, triggered and recorded synchronously with the voltage waveform, the waveform of incomplete frame is also easily to be found near the trigger point. The period of incomplete frame, called 0 frame in our research, is obvious less than the period (25μs) of a normal frame in 40Kfps, as shown in Fig. 4.13 (a). Therefore, the video and discharge signals can be matched by the incomplete frame and tore image near the trigger point. After matching the torn image with the waveform of 0 frame, the whole discharge waveforms and images of video can be matched accurately in time order. The shutter speed is set to 10μs, which means that the shutter is open in 10μs and closed in the left 15μs.

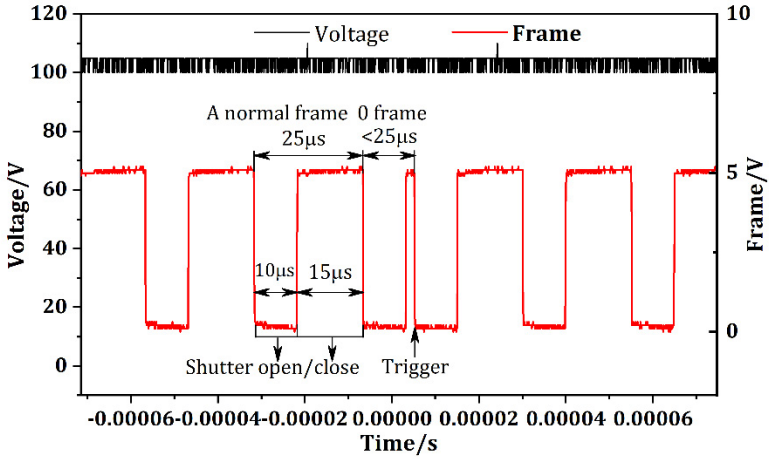

(a) Waveforms of voltage and frame

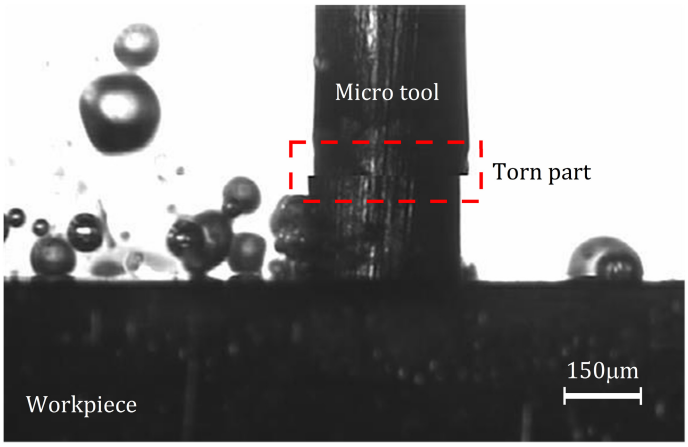

(b) Torn image

Fig. 4.13 Match of the discharge waveform with the video in blind hole drilling

4.4.2 Determination of the bubble sample set for the measurement

In the observation the camera lens is rightly faced the constraint flowing area and the schematic of vertical view of machining area is shown in Fig. 4.14. The ring gap area is distributed into four parts: α, β, γ_1 and γ_2. From the view of the camera lens, the area β is invisible due to the block of the micro tool. The stir caused by the rotation of the micro tool forces the dielectric liquid in the gap area to rotate towards the same direction, as the orange arrow in Fig. 4.14. The phenomenon also has been proved by the simulation in Fig. 4.7 (a). Moreover, according to the observation of the bubble in the constraint flowing area, it is also found that the spot where bubble escaping from the micro hole, called bubble escaping spot in our research, also changes with the flowing of the dielectric liquid in the constraint flowing area, which means the next bubble will definitely escape from the spot in the clockwise direction of the previous bubble escaping spot. In Fig. 4.14, the bubble A, B, C and D escape from the spot a, b, c and d respectively in chronological order,

which are actually observed and shown in Fig. 4.15 (Bubble D only represents the bubble escaping from part β). In area α, both the single bubble and bubble mergence shown in Fig. 4.14 and Fig. 4.16 can be observed clearly, while on the contrary in the area β neither of them can be observed. The bubble escaping from the area γ_1 and γ_2 is likely to be flushed into the area β due to the stir of the micro tool. Obviously, the bubbles escaping from the area α are the best samples for the measurement.

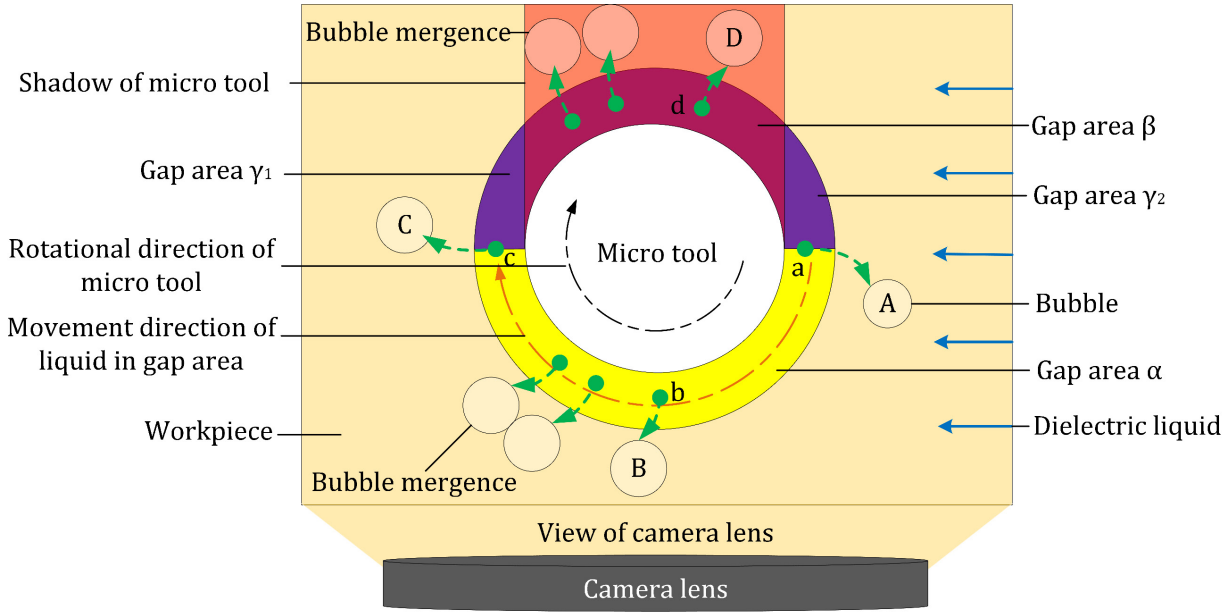

Fig. 4.14 Schematic of the vertical view of the machining area

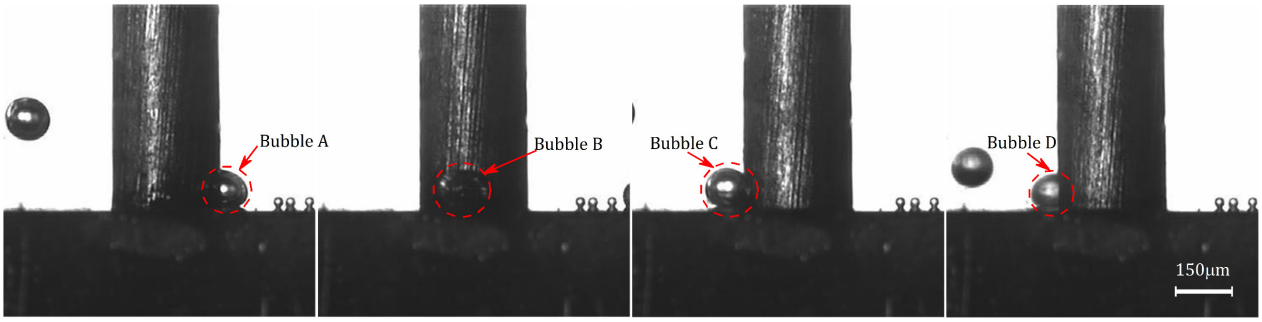

(a) Bubble A	(b) Bubble B	(c) Bubble C	(4) Bubble D
In N frame	In (N+260) frame	In (N+617) frame	In (N+934) frame

Fig. 4.15 Bubble escaping spots (N, a certain frame number)

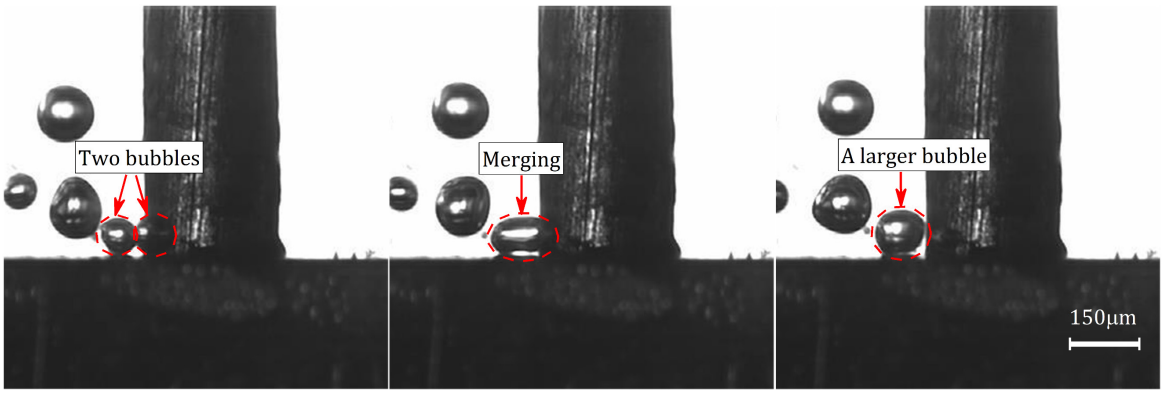

(a) In N frame (b) In (N+1) frame (c) In (N+2) Frame

Fig. 4.16 Mergence of bubble in area α (N, a certain frame number)

Above all, the bubble sample set for the measurement is determined in this period when bubble escaping spot is from a to c. All the bubbles in the bubble sample set are measured continuously in the data processing.

4.4.3 Simplification of 3D structure of bubble for measurement

It is difficult to accurately rebuild the 3D structure of the bubble due to its frequent deformation in the liquid. In most cases, the shape of bubble is generally thought to be ellipsoid [81]. The rebuilding of the 3D structure of the bubble by the method of the ellipsoid fitting at least needs the projections of the target bubble in two datum planes (XY, XZ or YZ) as shown in Fig. 4.17 (a). However, in the micro hole drilling with EDM, it is impossible to observe the bubble from two dimensions so far by using two high-speed cameras due to the limitation of the machine structure. In our research, one camera is used to observe the bubble as shown Fig. 4.14 so that actually only the projection of the bubble in XY plane can be by captured, which is not enough accurate to rebuild the bubble. Therefore, a simplified idea was put forward that the shape of the bubble was assumed to be a sphere as shown in Fig. 4.17 (b). In the machining, the bubble is always deforming due to the flushing of the flow field of dielectric liquid as shown in Fig. 4.18. In order to reduce the measurement error as much as possible, the measurement is carried out in the moment that the projection of bubble in XY plane is closest to a circle, for example, the bubble in Fig. 4.18 (d) is used in the measurement.

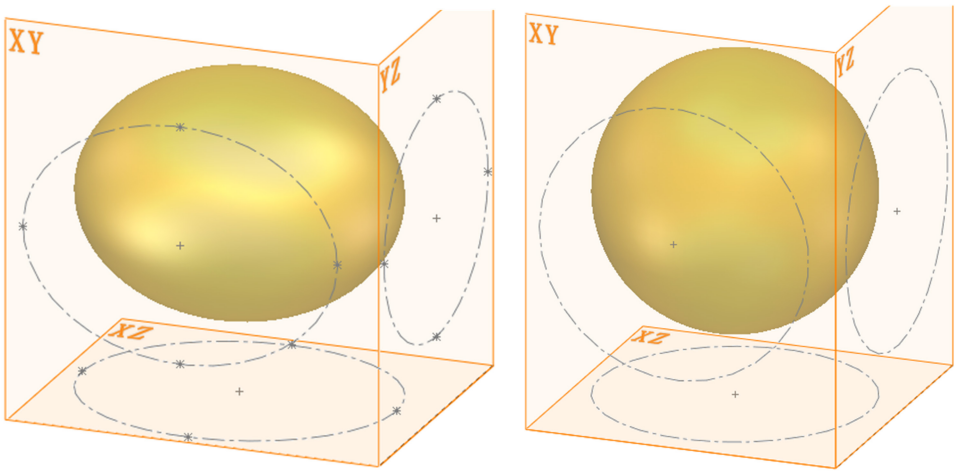

(a) Bubble rebuilt by ellipsoid fitting (b) Bubble thought to be a sphere

Fig. 4.17 3D structure of bubble

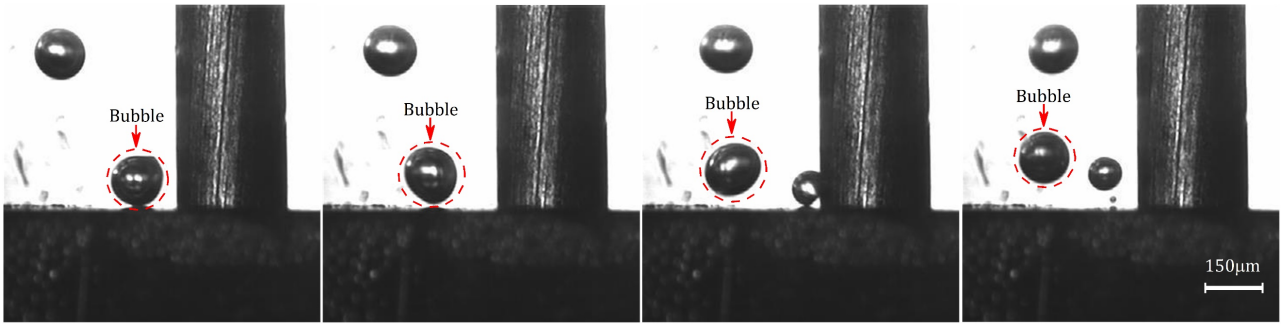

(a) In N frame (b) In (N+3) frame (c) In (N+7) frame (d) In (N+10) frame

Fig. 4.18 Deformation of bubble (N, a certain frame number)

4.4.4 Image segmentation method for extracting the target bubble

To accurately measure the size of the bubble, a method was put forward: Firstly, an image segmentation method was put forward based on the digital image processing in MATLAB to extract the bubble from the captured image and count the number of pixel patches occupied by the bubble; Secondly, the actual size of a pixel patch was calibrated, presented in the next section. Finally, the actual size of the bubble can be calculated.

The originally image in black and white captured by the high-speed camera is shown in Fig. 4.19. The observation is carried out under the strong light to ensure the high-definition of the observed video. Thus, there is the large difference between the bubble with the background in intensity. In the originally captured image the background is nearly white due to the strong illumination but the bubble is nearly black. In the digital image processing in the MATLAB, the light intensity of a black and white image is evaluated by a specific grayscale value. Therefore, the image can be segmented by an appropriate threshold and the bubble can be extracted by this method.

In the step 1, the captured image is input into the MATLAB and waited to be processed by the program. In the step 2, the image is segmented by a proper threshold value of the grayscale. After that, a circle with the red edge, slightly larger than the bubble, is used to mask the bubble in step 3. Then set the grayscale value of the mask area to 1 (pure white) and the inessential part to 0 (pure black) in step 4. The target bubble can be extracted in step 5 by performing the masking operation, which actually make a multiplication of grayscale vale between the mask area and image. However, due to the glistening of the bubble, usually the extracted bubble is incomplete. Thus, in the last step, the closing operation [82] is performed on the extracted bubble by using a disk structure element to repair the incomplete bubble. Eventually, the number of pixel patches occupied by the target bubble can be computed by counting the pixel patches in white (grayscale value is 1).

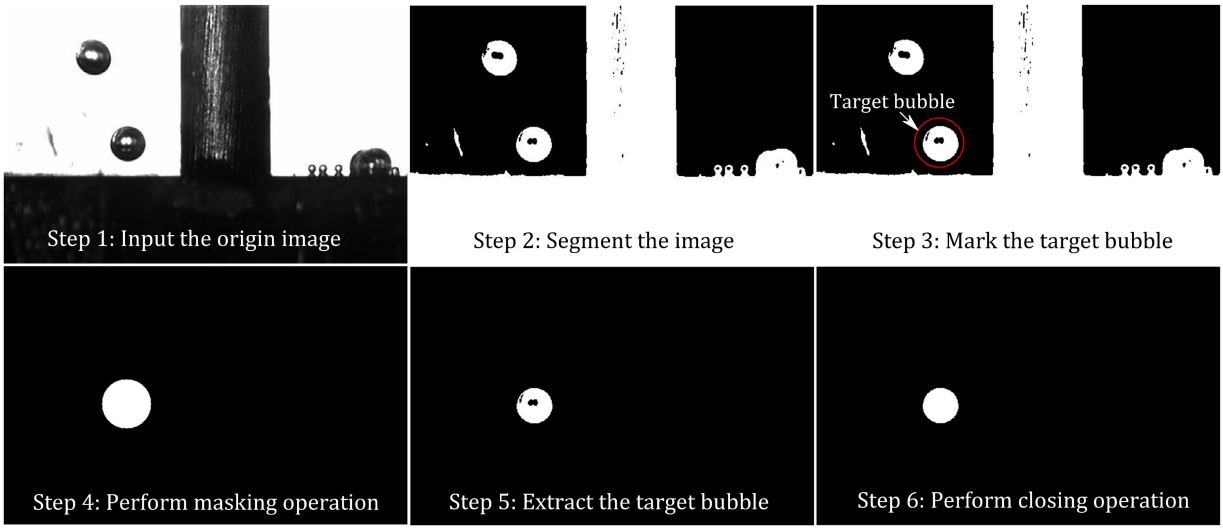

Fig. 4.19 Image segmentation method

The principle of making the closing operation to repair the incomplete bubble with the disk structure element can be simply described by the set operation:

$$A \bullet B = (A \oplus B) \ominus B \tag{1}$$

Where: A, the set of the incomplete bubble; B, the set of disk structure element with grayscale value 1 (pure white); •, the closing operation; ⊕, the dilating process; ⊖, the eroding process. The whole process mainly includes two steps: dilating and eroding.

The schematics of the dilating and eroding step are respectively shown in Fig. 4.20 and 21 respectively. The datum point of B is the center point. In the dilating step, the disk structure element B is used to scan the captured image C line by line and detect the pure white pixel patches according to the default image spatial frame in MATLAB. After

detecting the target pixel patches, the union operation is performed to dilate the bubble. Therefore, the bubble A is dilated from the boundary by the disk structure element B and becomes the dilated bubble D. The flaw area E in the incomplete bubble A has been repaired after the dilating step. In the eroding step, the same disk structure element B is used to detect the white pixel patches but the subtraction operation is performed. Therefore, the dilated bubble D is eroded from the boundary except the flaw area E because the flaw area E has been repaired and no boundary can be detected. After the eroding step, a complete bubble A' can be obtained.

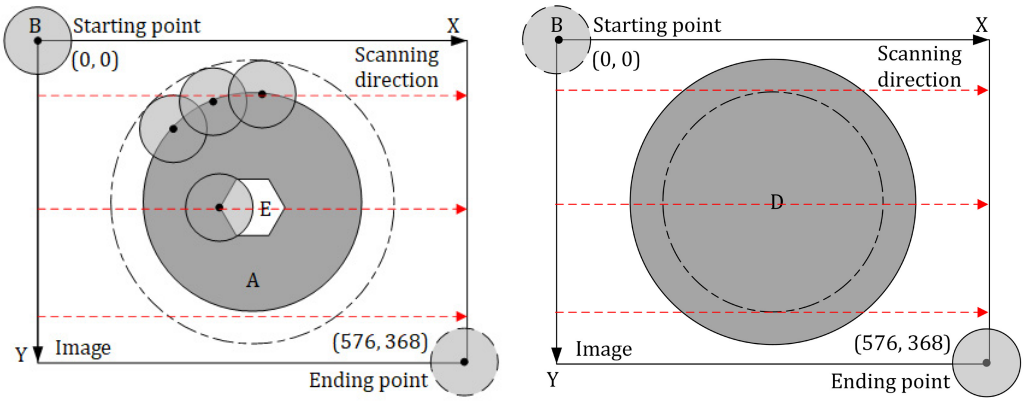

Fig. 4.20 Schematic of dilating step

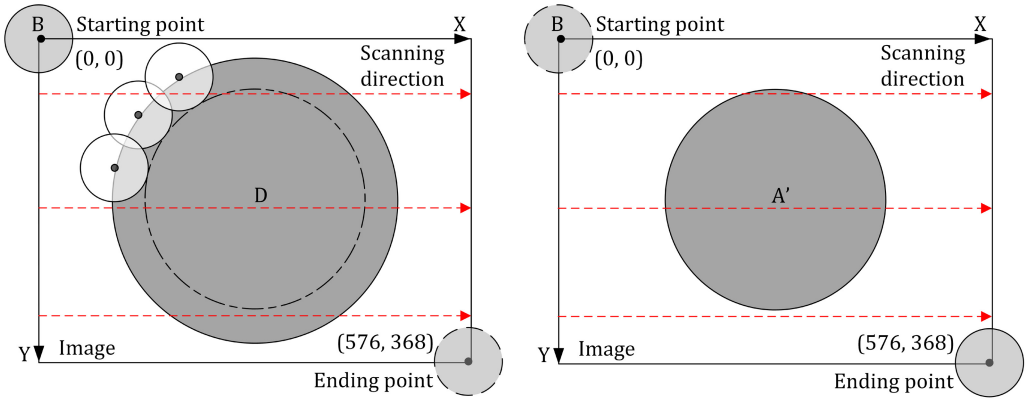

Fig. 4.21 Schematic of eroding step

The size of the disk structure element B almost has no effect on the bubble size because in one closing operation the same disk structure element B is used in both the dilating step and eroding step so that the dilated part has been eroded totally after the eroding step. Therefore, to different flaws of bubble, the size of the disk structure element can be chosen freely until the bubble is repaired.

4.4.5 Size calibration

After the number of pixel patches occupied by the bubble is counted, it needs to

calibrate the size of the single pixel patch to obtain the actual size of the bubble. The size calibration is based on the micro tool by contrasting its actual diameter with the number of pixel patches occupied by its diameter in the captured image because only the micro tool can be both observed during the observation by the high-speed camera and measured accurately after the experiment. The image after being segmented is shown in Fig. 4.22 (a). In MATLAB, a default image spatial frame is built for the digital image processing, where each pixel patch has a specific coordinate. The graphics resolution of image is 576×368 so that the coordinate of the last pixel patch is (576,368). To locate the position of the micro tool, 5 horizontal lines with proportional spacing of 50 pixel patches in Y-axis direction are created based on the 10 pixel patches in the boundary of the micro tool. It is found that the micro tool is nearly vertical to the X axis. Therefore, the number of pixel patches occupied by the diameter of the micro tool can be obtained by calculating the average length of 5 horizontal lines. On the other hand, the actual size of the micro tool after the experiment is measured by the optical microscope and shown in Fig. 4.22 (b). By contrasting the actual size of the dimeter with the pixel patches occupied by the diameter, the size of a single patch can be calibrated. In this research, the side length of a pixel patch is 2.3μm and the area of a pixel patch is 5.31μm^2. Finally, the real size of bubbles is obtained.

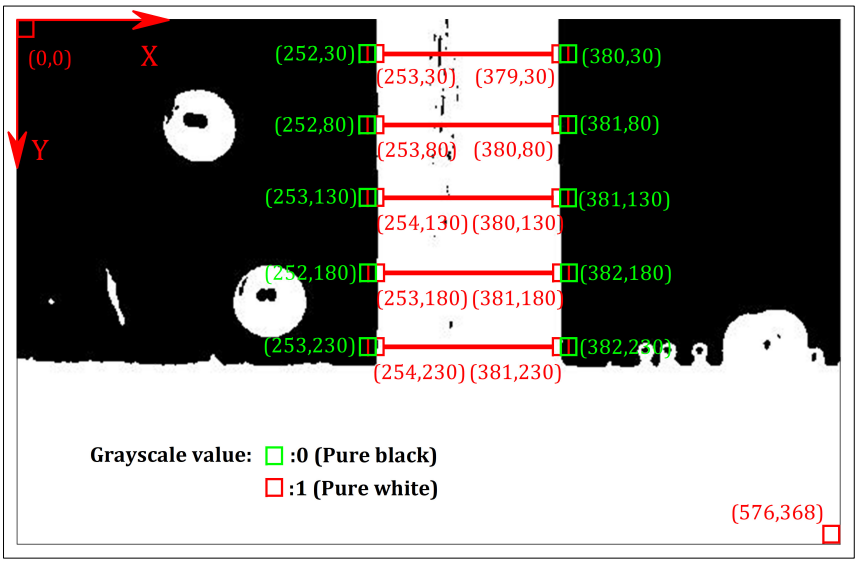

(a) Schematic of the image in the image spatial frame

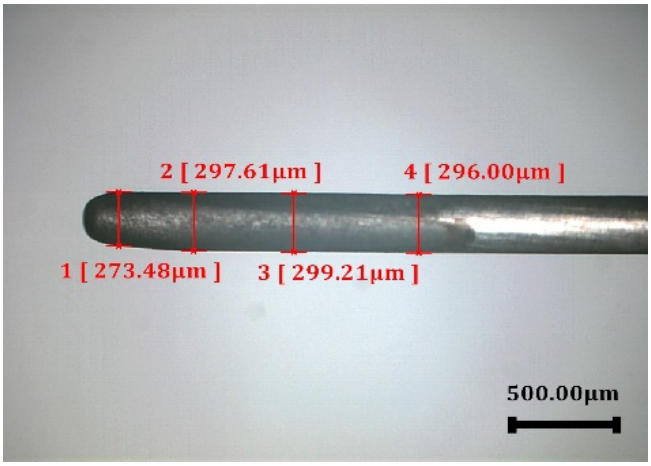

(b) Micro tool after machining

Fig. 4.22 Size calibration based on the micro tool

4.5 Conclusions

In the micro EDM drilling, the distribution of the bubbles near the entrance of the micro hole is totally irregular. The precondition of the quantitative estimation on the bubble behavior is to order the distribution of the bubbles escaping from the micro hole. Therefore, a method is put forward to make the irregular bubble distribution orderly by creating a constraint flowing area, which is also necessary for the stable observation of the high-speed camera. All the parameters influencing the flow field of the dielectric liquid have been considered and the determined depends on the simulation based on the COMSOL Multiphysics.

It is a great challenge to quantitatively evaluate the bubble behavior in the constraint flow area due to the complex environment in the constraint flowing area. Therefore, many solutions are put forward to solve the problem such as matching the discharge waveforms with the observed video, selection of the bubble sample set and accurate measurement on the bubble size with the image segmentation method.

Since the bubble behavior is strongly influenced by the discharge frequency, it is necessary to match the discharge signals with the high frame video and investigate the bubble behavior in the specific discharge frequency. Based on the specific recording of the high-speed camera in the trigger point, the high-frame video and the high-frequency discharge signals can be matched precisely. The string effect of the micro tool forces the dielectric liquid to flow towards the same direction. Therefor, the bubble also be flushed towards the same direction. In order to make sure the measurement reliable, the bubble

simple set is determined between two threshold points to ensure the all the bubbles in the simple set can be observed clearly. An image segmentation method based on the digital image processing in MATLAB is put forward to count the pixel patches occupied by the target bubble. Combined with the calibration of a single pixel patch based on the contrast of the size of the micro tool, the actual size of bubble can be calculated precisely.

The content presented in this chapter is the basis of the later quantitative estimation on the bubble behavior in blind micro drilling with EDM.

Chapter 5. Quantitative estimation on the behavior of the bubble and debris in micro EDM drilling

Based on the series of solutions presented in chapter 4, the quantitative estimation on the behavior of the bubble and debris will be performed in this chapter. Two kinds of experiments are planned to be carried out: observation of the single discharge by using a pair of the needle electrodes, observation of bubble escaping from micro hole in blind hole drilling.

The purpose of observing single discharge is to observe the breakdown process especially the generation of bubble and debris. Although it is well known that the bubble and debris, as the byproducts of EDM, are mainly generated in the discharge process, the details of generating process have never been reported because the significant short duration in the discharge process make it difficult to capture the details in low frame rate. On the other hand, in conventional micro EDM machining, the scale of the micro tool and workpiece is much larger than that of the discharge spot so that the formation of bubble and scattered debris cannot be observed so clearly due to the block of the micro tool and workpiece. In the case that needle electrodes are served as both the cathode and anode, if the diameter of the needle electrode is enough small, the single discharge occurring in the edge of the needle electrode can be totally captured by the high-speed camera with high frame rate.

The bubbles escaping from the micro blind hole was observed during micro hole drilling with EDM to investigate the bubble behavior. No matter how complex the bubble behavior inside the gap area, finally it escapes from the only exit of the gap area, the entrance of micro hole. Therefore, by observing the bubble escaping from the entrance of the micro hole in the constraint flowing area, recording the bubble number and size, and corresponding discharge waveforms at different hole depths, the relationships between the bubble behavior with the hole depth can be investigated quantitatively without any influence on the machining. The experimental conditions are shown in Table. 5.1.

Table. 5.1 Experimental conditions

Items	In single discharge	In blind hole drilling
Electrode diameter	38μm	300μm
Tool material	Tungsten	Tungsten
Tool feed rate	1μm/s	5μm/s

Open circuit voltage	110V	110V
Capacitance	1000pF	1000pF
Dielectric	Deionized water	Deionized water
Electrical conductivity	6×10^{-6}S/m	6×10^{-6}S/m
Frame rate	100000fps	40000fps
Exposure time	9.9μs	10μs
Graphics resolution	192×232	576×368

5.1 Observation on the single discharge

5.1.1 Setup of observing single discharge with needle electrodes

The schematic of observing the single discharge with a pair of needle electrodes is shown in Fig. 5.1. The cathode and anode with the same diameter of 38μm are sunk in the dielectric liquid. The cathode is aligned with the anode as much as possible by manual adjustment with the assist of the high-speed camera. The experimental conditions of machining and observing are shown in Table. 5.1. In order to observe the single discharge clearly, the frame rate is set to 100Kfps, which is nearly the limit of the high-speed camera considering the illumination in machining area and the graphics resolution of video. Even so it is not enough to capture the breakdown process because of the significantly short discharge duration in RC circuit, which is shown in Fig. 5.2.

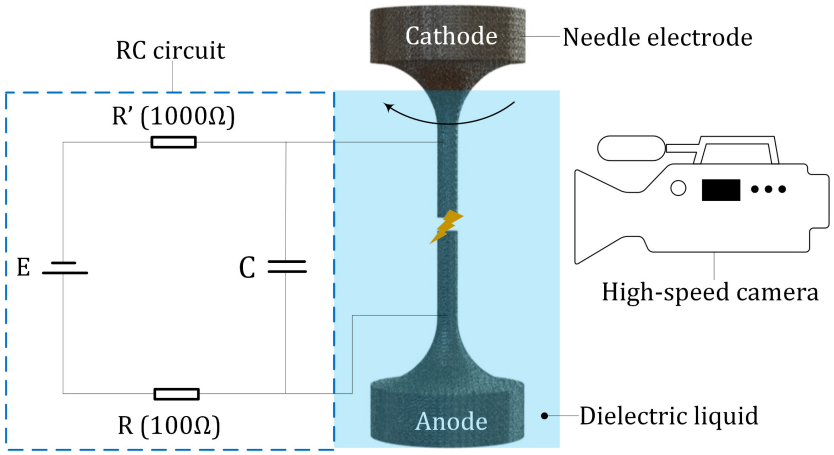

Fig. 5.1 Schematic of the single discharge observation

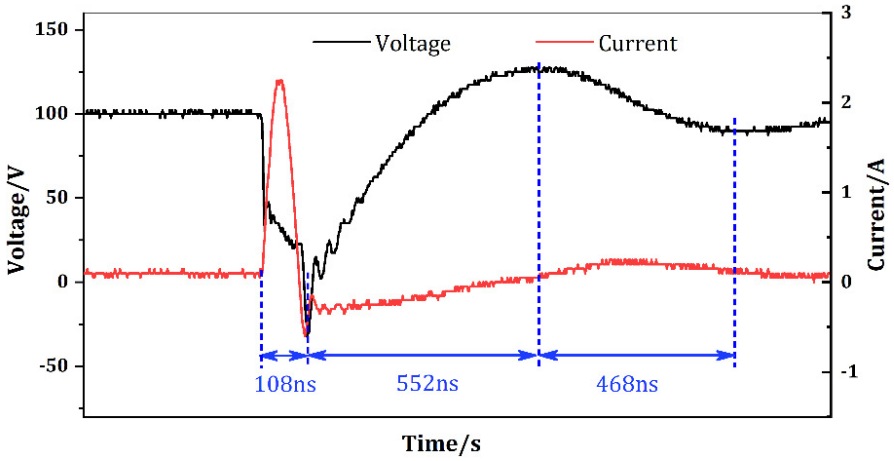

Fig. 5.2 Waveforms of a single discharge in RC circuit

It is found that under the conditions in Table 5.1 the discharge duration is about 100ns, which is much shorter than the period of one frame (10μs). However, generally, the discharge interval is much longer than 10μs as shown in Fig. 5.3. Therefore, the details of gap area after the breakdown can be captured clearly in this frame rate. In order to capture more images, the shutter is set in full open state and the exposure time is about 9.9μs except the shutter switching time, approximately 0.1μs.

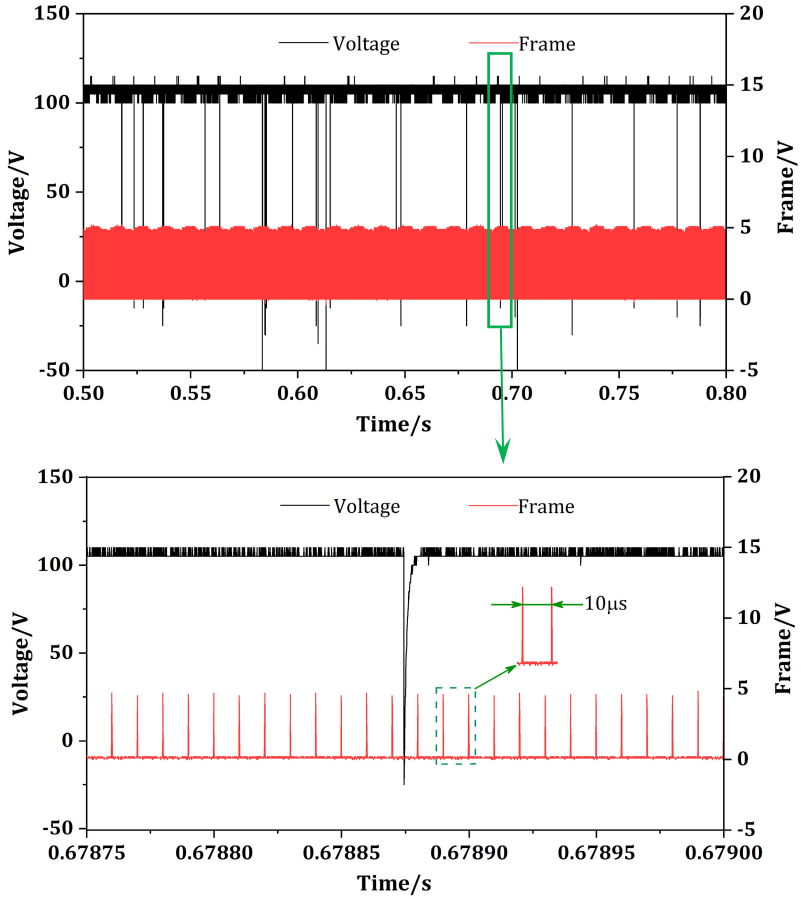

Fig. 5.3 Discharge in RC circuit

The match of the discharge signals with the video is same as that in micro hole drilling in Fig. 4.13. The 0 frame and torn image in observation of the single discharge with needle electrodes are shown in Fig. 5.4 (a) and (b). The only difference with the case in drilling blind hole is the frame rate. In this case, the frame rate is 100Kfps and the shutter is in full open in order to capture images as many as possible.

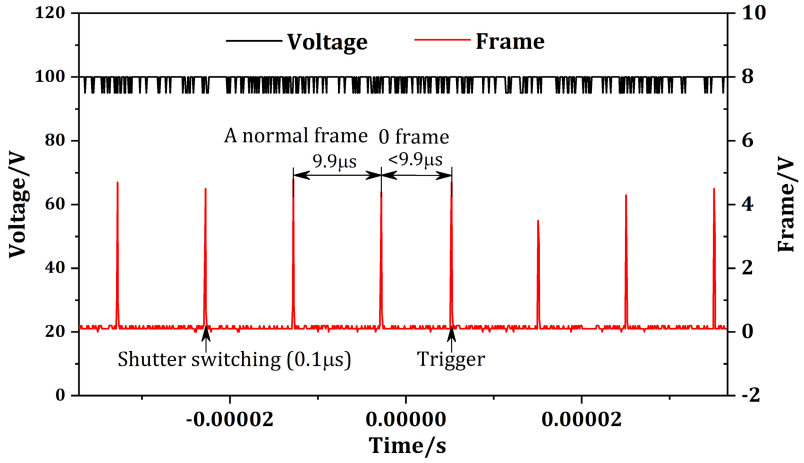

(a) Waveforms of voltage and frame

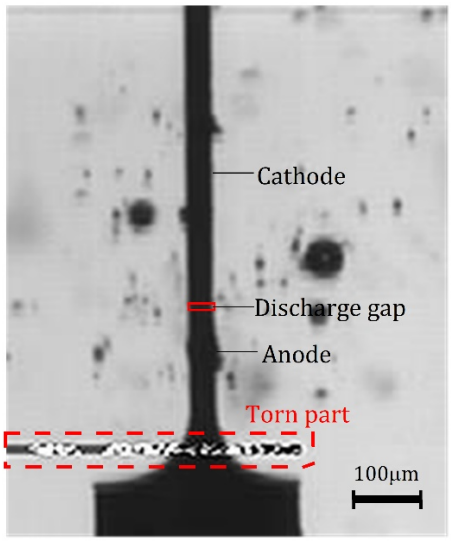

(b) Torn image

Fig. 5.4 Match of waveform with video in observation of single discharge

5.1.2 Results in observing the single discharge

With the proposed method and experimental conditions described above, the experiment of observing the single discharge has been carried out to investigate the generation of the bubble and debris. The waveforms of the voltage and frame are shown in Fig. 5.5 and the corresponding image in each frame is shown in Fig. 5.6.

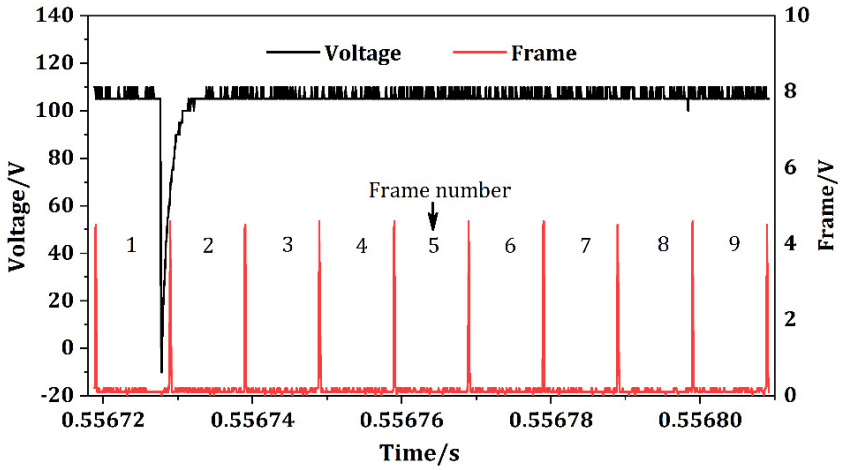

Fig. 5.5 Waveforms of the voltage and frame in observing the single discharge

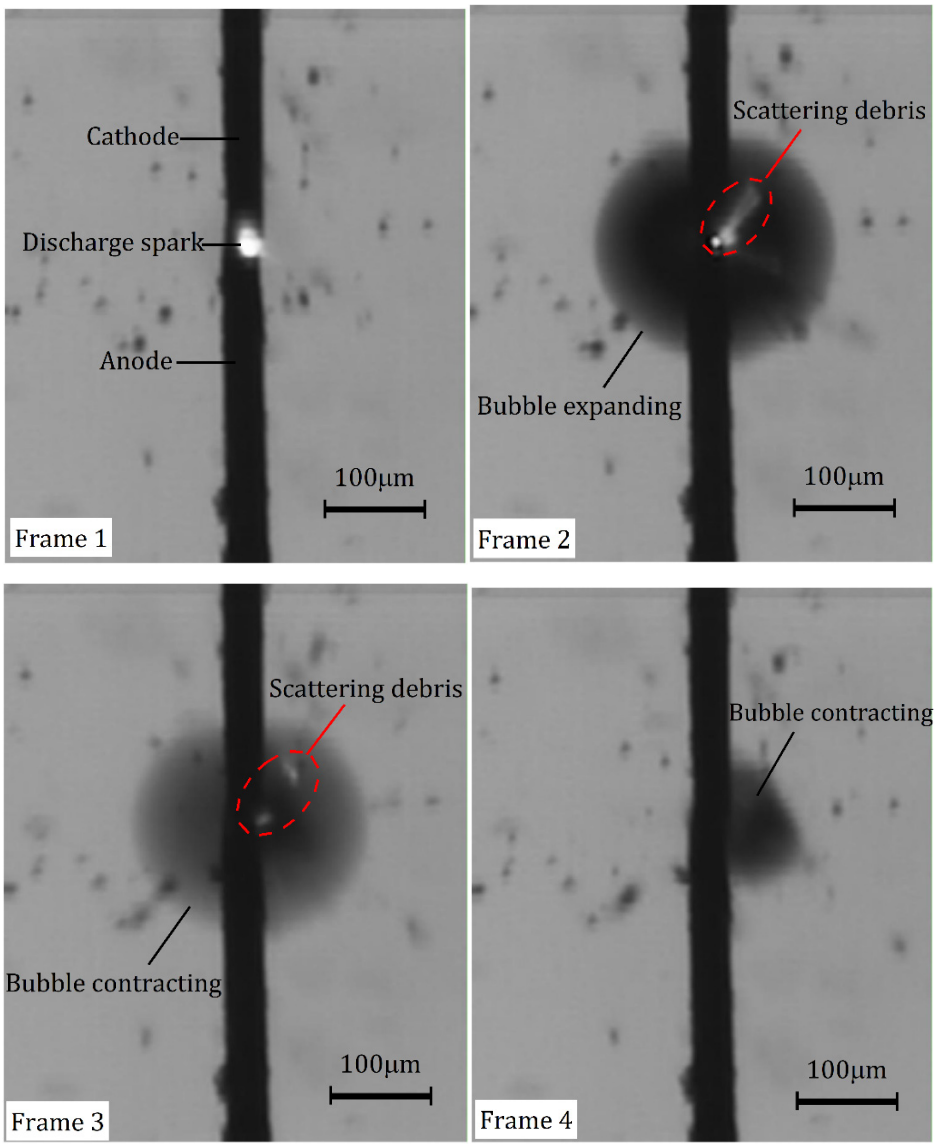

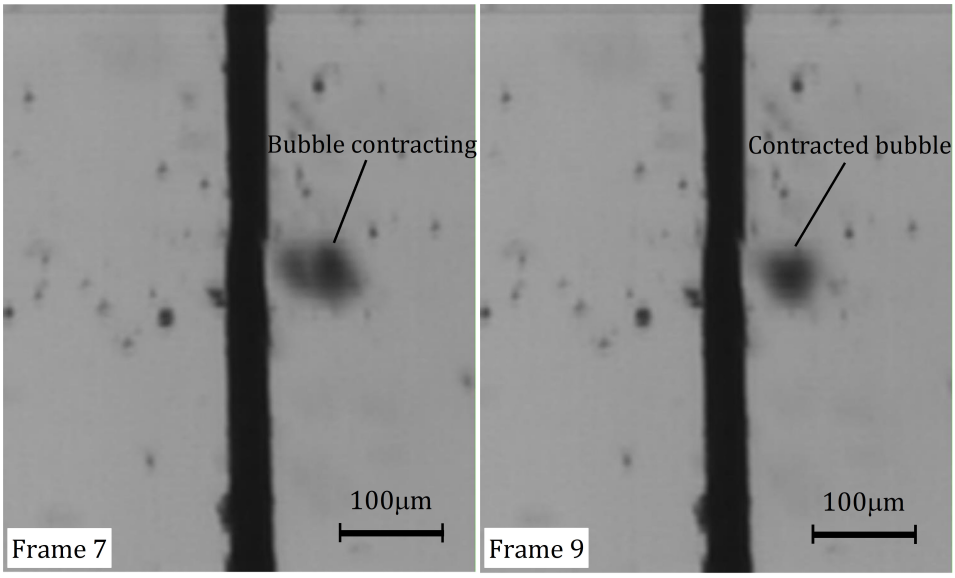

Fig. 5.6 Images in different frames

It is found that in the frame 1 during the breakdown stage, only the discharge spark occurs, no generation of bubble and debris is observed. In frame 2, the bubble is generated and expanded to the maximum in 10μs, while the melt material of workpiece is scattered into the dielectric to become the debris. It indicates that during the 10μs of frame 2 the discharge heat is releasing so that the bubble is generated from the evaporated dielectric liquid and kept expanding. At the same time, the material near the discharge spot is melt and becomes the scattering debris. The discharge heat stops releasing in the end of the frame 2 because the bubble has stopped expanding in frame 3 and begins to contract until the end of the frame 9. The debris scattering process lasts 20μs from frame 2 to 3 and the contracting process lasts 70μs from frame 3 to 9.

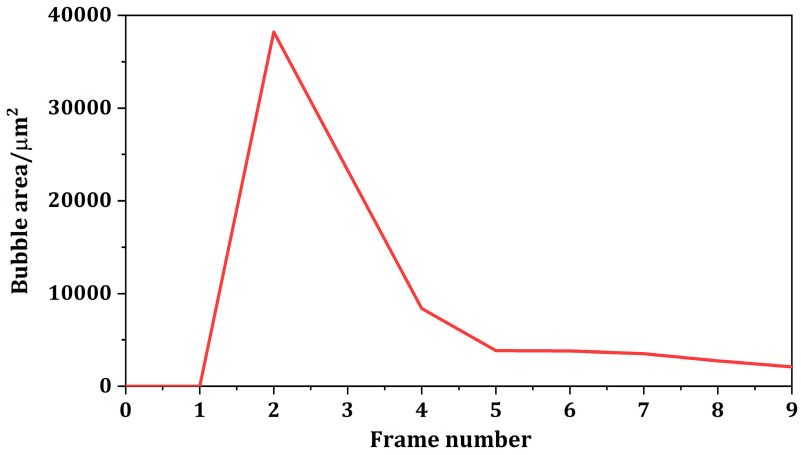

Fig. 5.7 Bubble area in different frames

The change of the bubble area is shown in Fig. 5.7. Results show that the bubble contraction mainly occurs in the frame 3 and 4 and spent 20μs, which is almost twice of

the bubble expansion time, approximately 10μs. It indicates the cooling of the discharge heat spends more time than the discharge heat releasing process. On the other hand, it has been observed that sometimes the expanded bubble can be separated into two or three little bubbles after the contraction process.

The time of the bubble expansion (10μs) and contraction (70μs) is much larger than the discharge duration (108ns) and insulation recovery time (552ns) shown in Fig. 5.2. A new discharge may occur during the bubble expanding or contracting of the previous discharge. The new discharge heat release before the finish of the cooling in the previous discharge may lead to the accumulation of discharge heat and an increase in the temperature of the discharge liquid. Therefore, it can be assumed that the discharge heat may accumulate in the gap area during the actual micro hole drilling and heat the dielectric liquid, which decreases the insulation strength of dielectric liquid and even causes the thermal breakdown in the gap area. This is also likely to be a reason for the deteriorated discharge environment.

As shown in Fig. 5.8 and 5.9, three single discharges occur in 40μs. The second discharge occurs during the bubble expanding stage of the first discharge. As the shown in the image of the frame 3, the releasing of the discharge heat in the second discharge breaks the expanding bubble in the first discharge. Then, the third discharge immediately occurs in frame 4. The mass discharge heat release even causes the secondary bubble expansion in Frame 5. It can be conjectured that in actual machining, the discharge heat accumulation in frequent discharges decreases the insulation strength of the dielectric liquid and even causes the thermal breakdown in the gap area. It may be a reason for the deteriorated discharge environment.

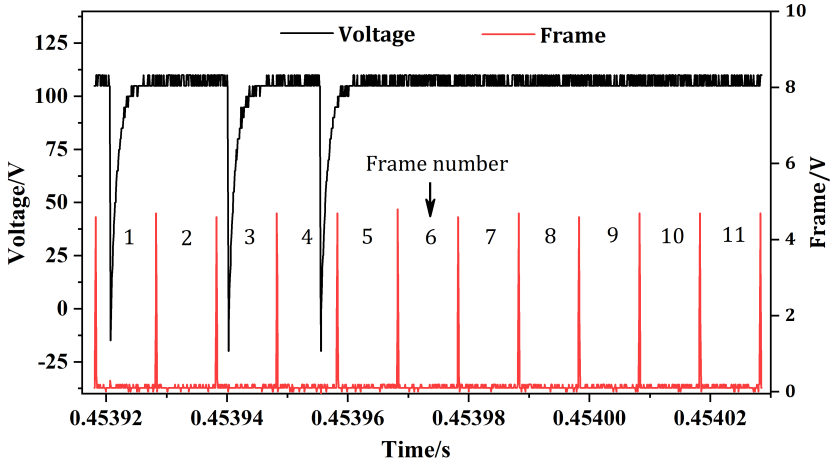

Fig. 5.8 Waveforms of the voltage and frame in three single discharges

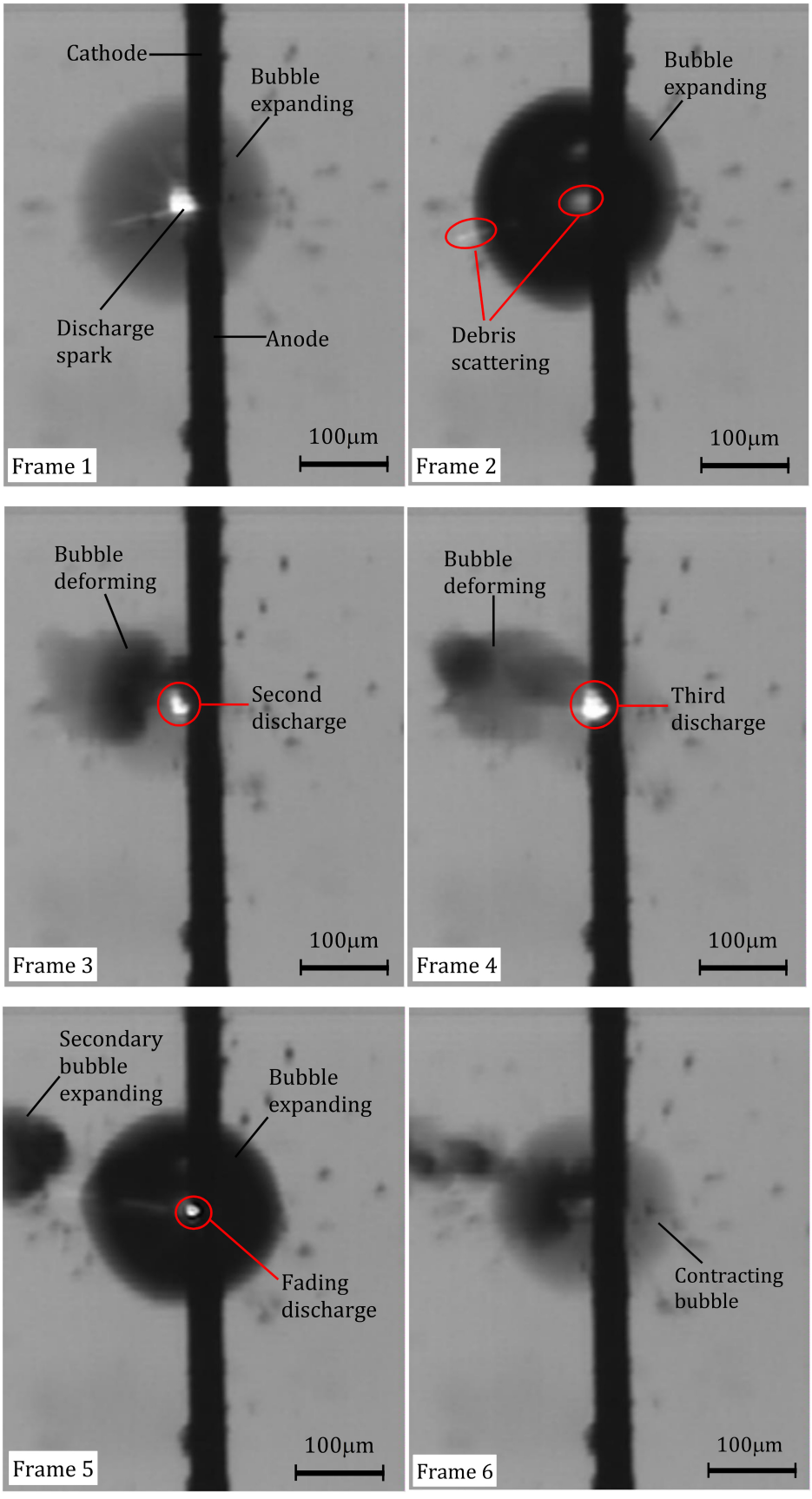
Cathode
Bubble expanding
Discharge spark
Anode
100μm
Frame 1
Bubble expanding
Debris scattering
100μm
Frame 2
Bubble deforming
Second discharge
100μm
Frame 3
Bubble deforming
Third discharge
100μm
Frame 4
Secondary bubble expanding
Bubble expanding
Fading discharge
100μm
Frame 5
Contracting bubble
100μm
Frame 6

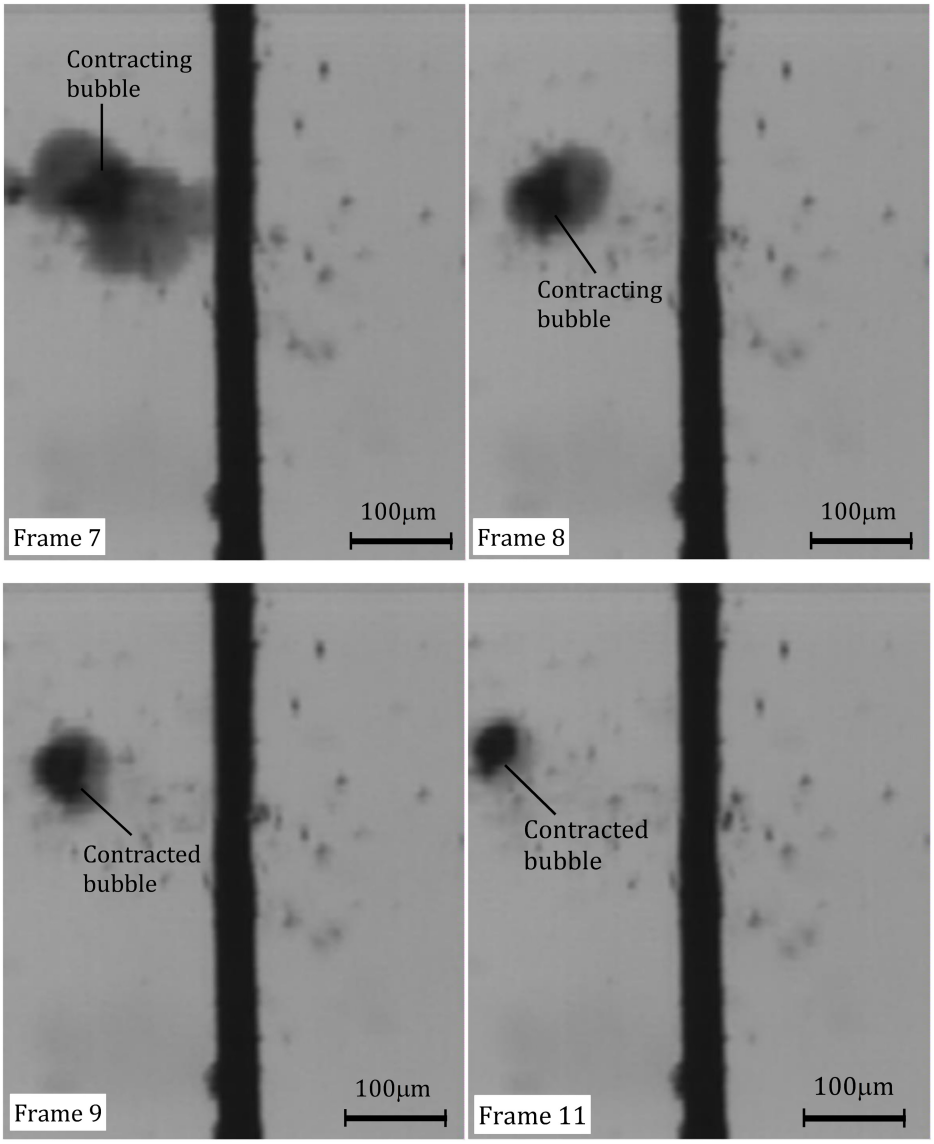

Fig. 5.9 Images in different frames

On the other hand, the diameter of the expanding bubble (about 200μm) is much larger than that of the micro tool (38μm), which means that in the actual micro hole drilling the bubble expansion and contraction may arouse a strong vibration of the dielectric liquid in the narrow gap area to improve the flow and exchange of dielectric liquid.

5.2 Quantitative estimation on bubble behavior in blind hole drilling with EDM

The observation on the bubble escaping from the micro hole has been performed based on the experiment of drilling blind hole with micro EDM. The feed curve is shown in Fig. 5.10. It is found that the machining speed decreased seriously with the increase of the hole depth. When the hole depth is larger than 1.5mm, the big retreat frequently occurs and the retreat distance even reach several hundred micro meters as shown in Fig. 5.10,

which is much larger than the width of the gap area, approximately about 10-20μm. According to the characteristic of the machining speed, the machining can be divided into three stages: the normal machining state, the large retreat state and the fluctuating state.

In the normal machining state, the machining speed is fast and the machining state is kept in a good state. In the large retreat state, the large retreat of the micro tool frequently occurs. In the fluctuating state, the machining speed decreases seriously and nearly become 0.

As discussed in the section 2.3.2 of the chapter 2, the proceed and retreat of the micro tool is controlled by the NC servo system based on the comparison of the quantity of electricity (integration of the short circuit current) during a certain period of time to the preset threshold value. Therefore, the larger retreat of the micro tool indicates that the consecutive short circuit continuously lasts during this period. The most likely thing is that the cathode and anode has been linked during the retreat process. Obviously, the consecutive short circuit occurs frequently in the deteriorated environment.

Therefore, in order to investigate the influence of the behavior of the bubble and debris on the machining speed, the behavior of the bubble and debris in the marked points are analyzed and discussed.

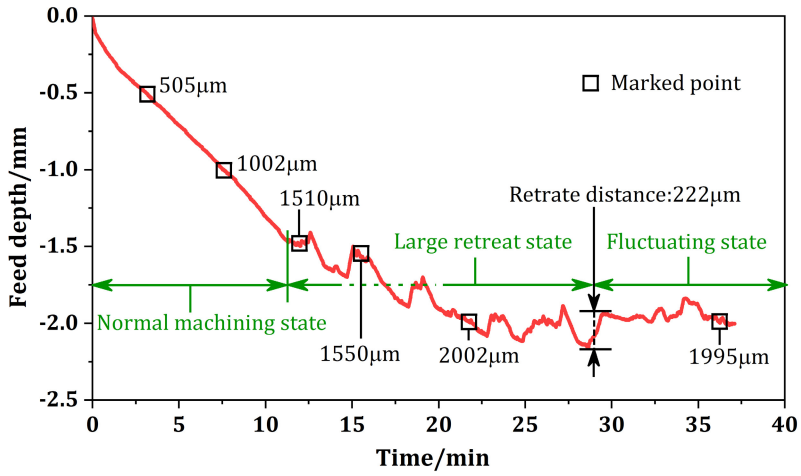

Fig. 5.10 The feed curve of micro hole drilling

5.2.1 Bubble behavior in normal discharge stage

With the proposed methods and optimized parameters for the flow field described in the chapter 4, the bubbles escaping from the micro hole at different feed depths were observed and the corresponding images are shown in Fig. 5.11. It is found that with increase of the feed depth, the number of the bubbles escaping from the micro hole decreases seriously, but the size of a single bubble has the trend to increase. When the

feed depth is less than 505μm, a mass of bubbles escape from the micro hole and even bubble clusters are formed near the entrance of the micro hole in the feed depth of 57μm and 111μm. When the feed depth is larger than 505μm, in the view of the high-speed camera, the bubbles seem to escape from the micro hole one-by-one, which can be observed very clearly and measured accurately. Therefore, the bubble behavior in feed depths of 505μm, 1002μm and 2002μm is quantitatively estimated respectively, as marked in the Fig. 5.10.

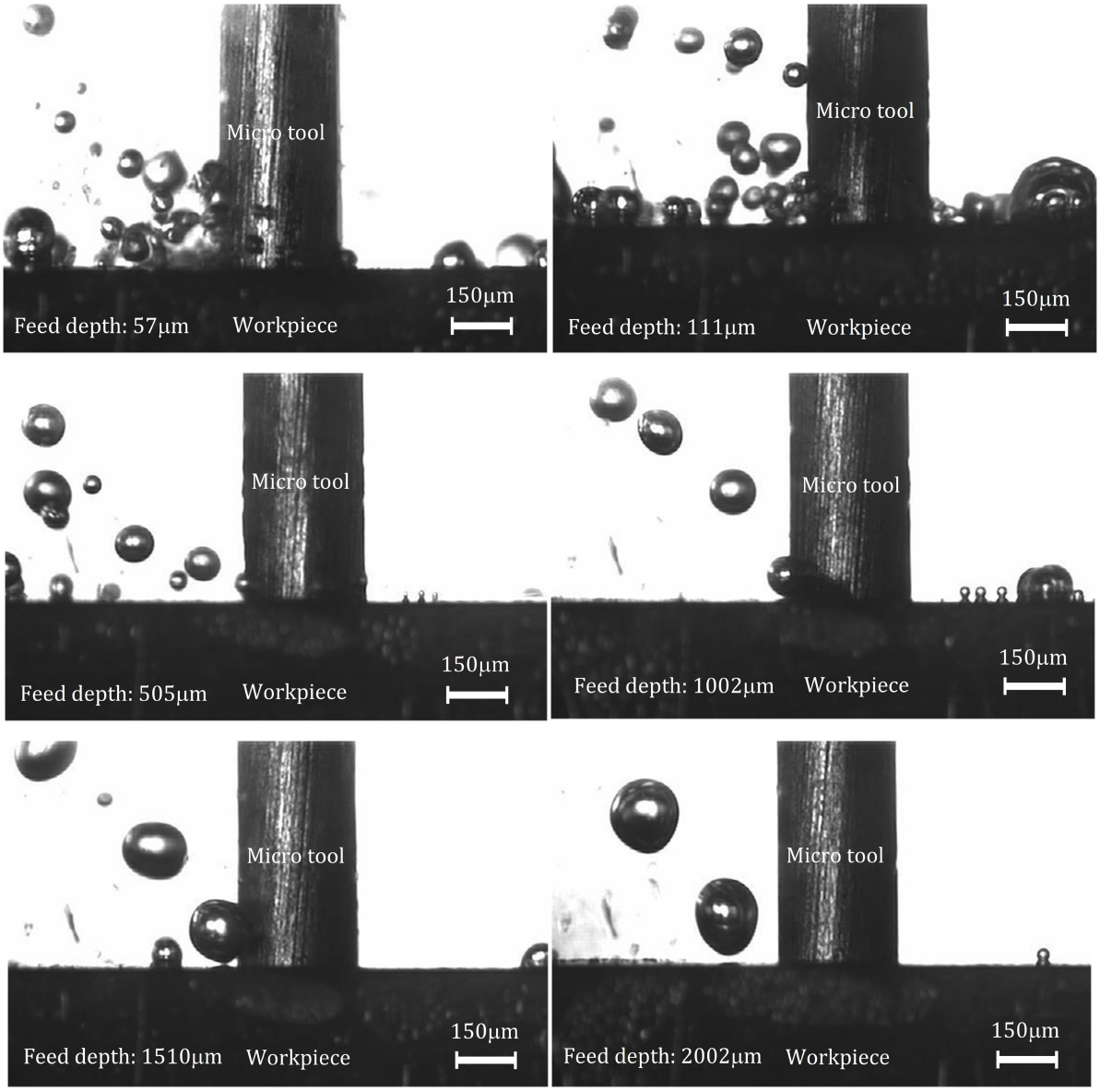

Fig. 5.11 Bubbles at different hole depths

5.2.2 Bubble escaping frequency at different feed depths

In order to investigate the bubble behavior in the normal discharge state, the bubble

sample sets in 505μm, 1002μm and 2002μm were selected as the method introduced in section 4.4.2 of the chapter 4 during the normal discharge stage. The voltage waveforms during the period of the bubble sample set are shown in Fig. 5.12. As the enlarged view of discharge waveforms showing, no short circuit occurs during the whole period of the bubble sample set. All the bubbles in the bubble sample set are continuously measured by using the image segmentation method introduced in section 4.4.4 of the chapter 4.

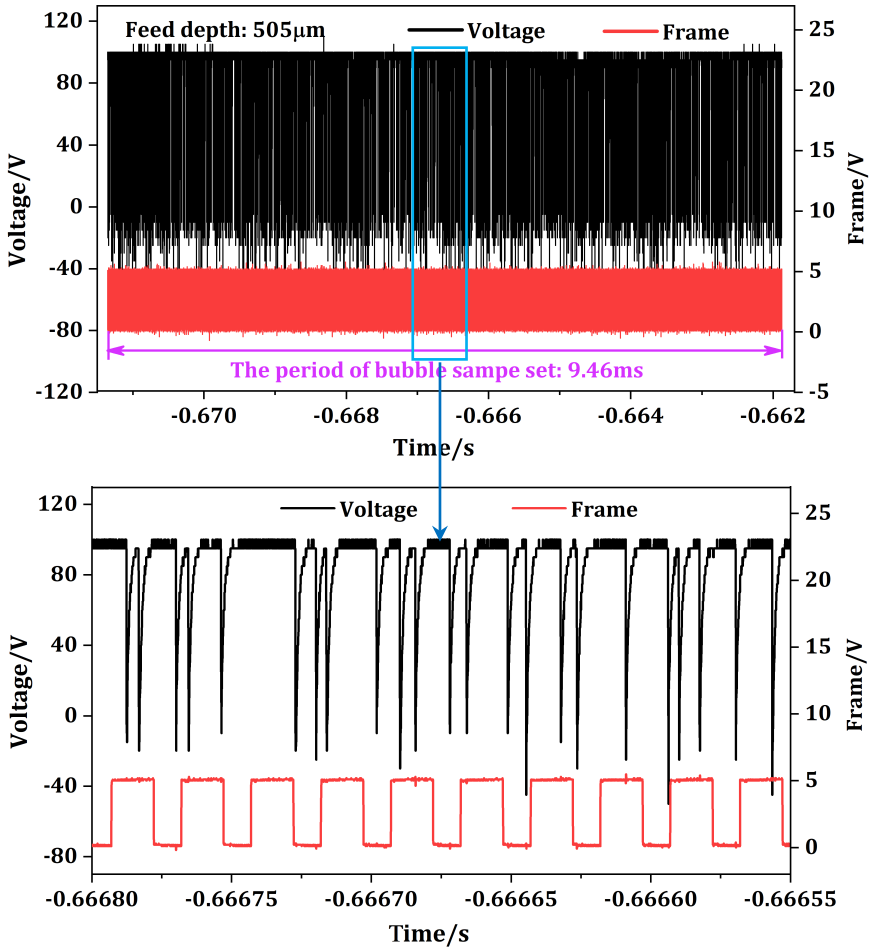

(a) In 505μm

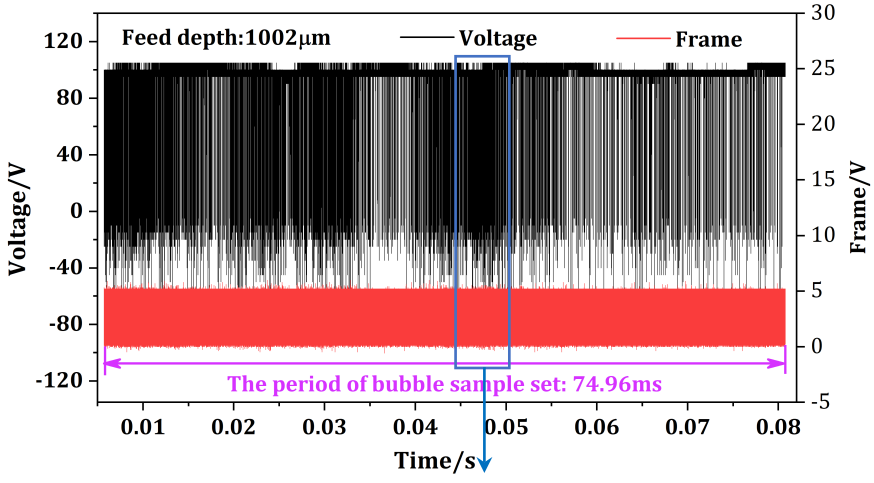

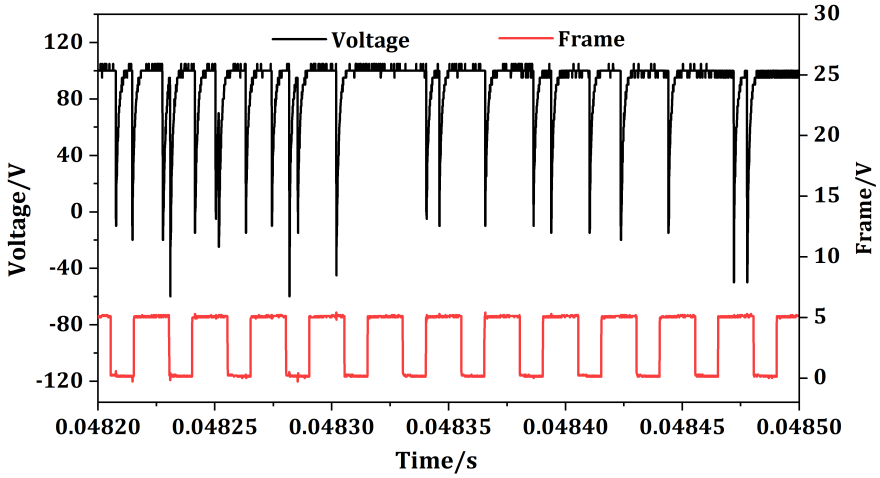

(b) In 1002μm

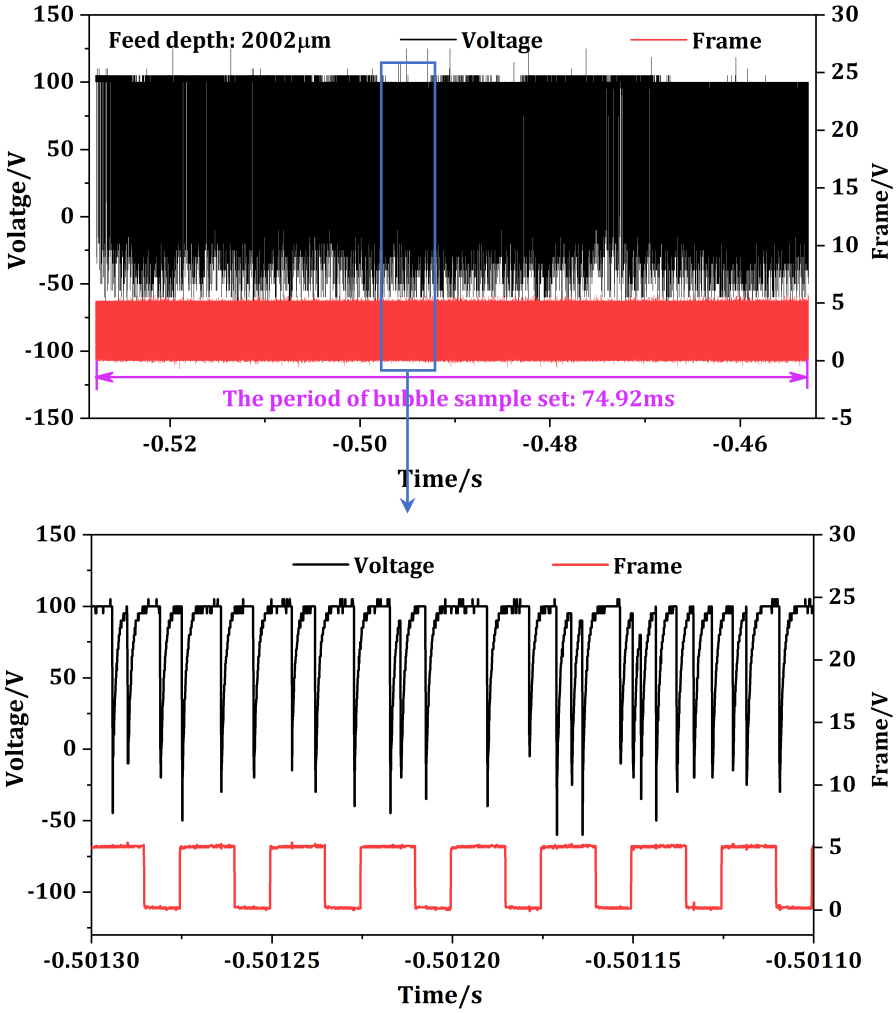

(c) In 2002μm

Fig. 5.12 Discharge waveforms in the bubble sample sets

The bubble escaping frequency is put forward to estimate the extent of the number of the bubbles escaping from the micro hole, which is defined as the ratio of the number of bubbles with the period of the bubble sample set. The bubble escaping frequency in the

feed depth of 505μm, 1002μm and 2002μm is measured respectively and shown in Fig. 5.13. Since in different feed depths, the number of bubbles among the bubble sample set and the period of the bubble sample set are both different, the bubble escaping frequency is an average in the corresponding bubble sample set to reflect the average number of bubbles escaping from the micro hole in the unit time.

It is found that the bubble escaping frequency decreases seriously with the increase of feed depth. In the feed depth of 505μm, nearly 10448 bubbles escape from the micro hole in a second but in 2002μm only left 1492. The bubble escaping frequency can reflect the extent of the dielectric liquid exchange. The large bubble escaping frequency indicates that the gap area can be flushed more frequently, thus the exchange of dielectric liquid and debris exhaustion is more quickly. Therefore, in the beginning of the machining, less debris accumulates in gap area resulting in a fast machining speed. However, in the deeper feed depth, mass debris is likely to accumulate in the gap area due to the weak bubble flushing effect, causing the frequent consecutive short circuits and eventually leading to the low machining speed.

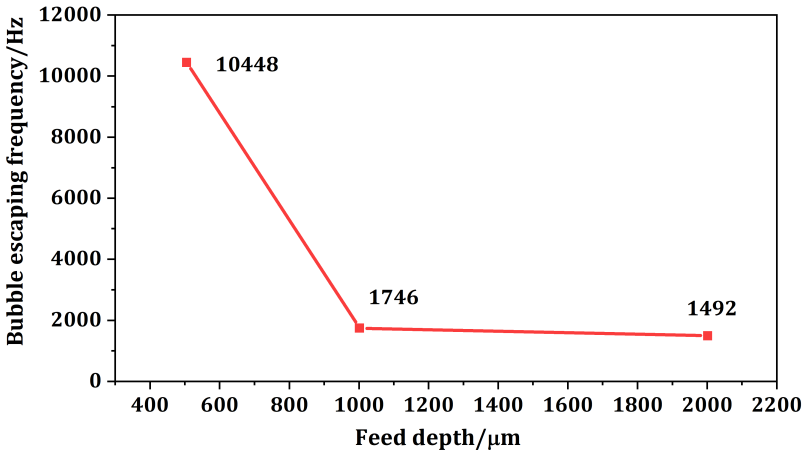

Fig. 5.13 Depth-dependent bubble escaping frequency

5.2.3 Bubble size at different hole depths

The size of bubbles in each bubble sample set and the corresponding different feed depths is measured after extracted by the image segmentation method. The scatter plot of the bubble diameter is shown in Fig. 5.14 (a), in which the bubble is arranged depending on the bubble diameter and X axis is the number of the bubbles. It is found that with the increase of the hole depth, the diameter of the single bubble has the trend to become larger. In order to investigate the distribution of the bubble size, the normal distribution in each case is made and shown in Fig. 5.14 (b).

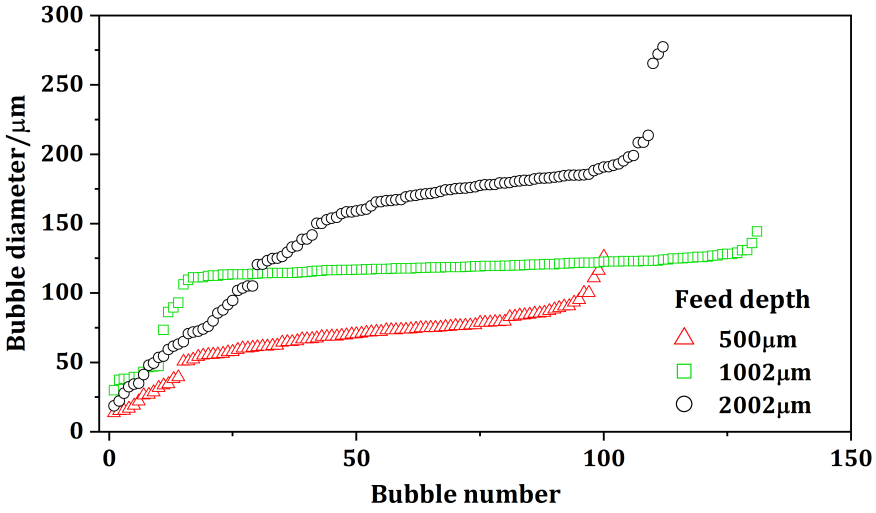

(a) Scatter plot

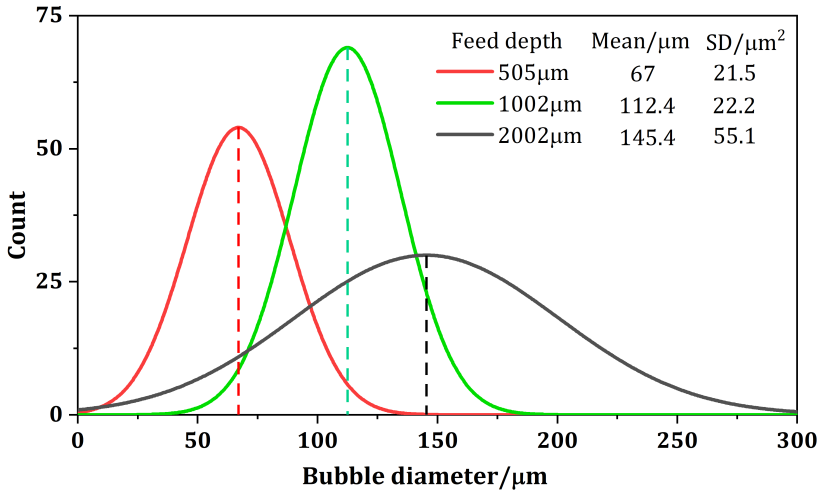

(b) Normal distribution

Fig. 5.14 Distribution of bubble size at different feed depths

From the feed depth of 505μm to 2002μm, the increase of the mean value shows that the size of the single bubble has the trend to become larger with the increase of the feed depth. The SD (Stand Deviation) reflects the amount of variation of the bubble size. In the feed depth of 505μm and 1002μm, the low SD means that the size of most bubbles are close to the mean value, which indicates the generation and exhaust of bubble has a good balance. At the feed depth of 2002μm, the large SD implies that the bubbles spread out over a wide range although more larger bubbles escape from the micro hole. It indicates that the continuous exhaust of the large bubble is unstable, which may be because the generation of the large bubble cannot catch up with the exhaust of the large bubble.

5.2.4 Bubble escaping volume at different hole depth

In order to evaluate the extent of the volume of bubble escaping from the micro hole,

the flowrate of bubble escaping volume is put forward, which is defined as the average of volume of bubbles escaping from the micro hole in the unit time. As discussed in part 4.4.3, the bubble is thought to be the sphere in our research. By using the image segmentation method, the equivalent spherical diameter of the bubble can be obtained so as that the volume of bubble can be calculated. The curve of the flowrate of bubble escaping volume at different hole depth is shown in Fig. 5.15. It is found that with the increase of feed depth, the flowrate of bubble escaping volume decreases firstly than increased, which is totally different with the empirical understanding of the bubble behavior. The flowrate of bubble escaping volume is related to the bubble escaping frequency and the size of single bubble. The reason can be attributed to the increase of the single bubble size. Although the bubble escaping frequency decreases seriously, the increase of the single bubble size in Fig. 5.14 leads to the larger flowrate of bubble escaping frequency. The flowrate of bubble escaping frequency in a certain extent can reflect the dielectric exchange volume because the left space after the bubble escaping will be occupied by other bubbles or dielectric liquid, which can improve the flowing and exchange of the dielectric liquid in the gap area. However, the continuously decreasing machining speed with the increase of feed depth in Fig. 5.10 exhibits the different trend with the flowrate of bubble escaping frequency, which indicates that the large flowrate of bubble escaping volume is almost no effect on improving machining speed in the feed depth of 2002μm. It is maybe because compared to the flowrate of bubble escaping volume, the bubble escaping frequency has more influence on the debris exhaust so as that the debris exhaust in the large flowrate of bubble escaping volume can't catch up with the debris accumulation in the low bubble escaping frequency. Therefore, even the increase of the flowrate of bubble escaping volume in the feed depth of 2002μm can't prevent the deterioration of environment.

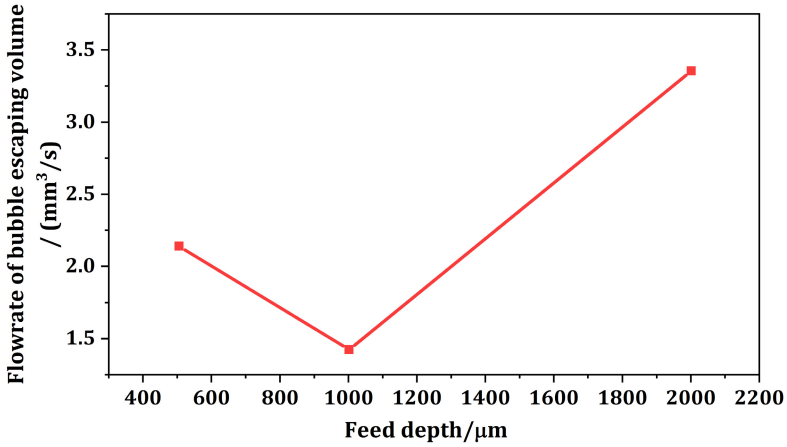

Fig. 5.15 Flowrate of bubble escaping volume

5.2.5 Discharge frequency in different feed depth

The discharge wave in 505μm, 1002μm and 2002μm is respectively shown in Fig. 5.12 respectively. As the enlarged view showing, in the normal discharge state, the discharge occurs from the full open voltage and no short circuits exist. The discharge frequency is put forward to evaluate the extent of discharge number in the unit time, which is defined as the ratio of the totally number of discharges during the bubble sample set with the period of bubble sample set. The discharge frequency is an average of the discharge number in a second because the discharge interval was uncertain and mainly dominated by the state of gap area in RC circuit. The curve of discharge frequency is shown in Fig. 5.16. The discharge frequency can be used to estimate the state of gap area in a certain depth. It is found that with the increase of feed depth the discharge frequency decreases firstly then increases. It can be explained that in the beginning of machining the discharge occurs in the good environment. With the increase of feed depth, the gradually deteriorated environment of gap area, for instance, the irregular gap width caused by the tool wear and the short circuit, lead to the larger possibility for the retreat of micro tool and finally decreases the discharge frequency. In deeper hole depth, the further deteriorated environment of gap area due to the debris accumulation and low bubble escaping frequency decreases the insulation strength of dielectric seriously so as that the breakdown can occur more easily. Thus, the discharge frequency become larger. During this period, a quite number of discharges is likely to be arc discharge in the weak insulation strength of gap area. Generally, the arc discharges cannot be treated as the normal discharge state but it is inevitable in the actual machining because the actual gap width controlled by the regulation of NC servo control system always fluctuates around the threshold breakdown width. On the other hand, the distinguish between the normal discharge with the arc discharge is difficult in the RC circuit without the pulse-off time. Therefore, in our research, the arc discharge is not clearly distinguished and analyzed together with the normal discharge. According to the depth-dependence characteristics of discharge frequency, the weakened insulation strength of gap area can be exhibited. It is obviously found from Fig. 5.10 that the average discharge duration in the feed depth of 2002μm is much shorter than that in 505μm.

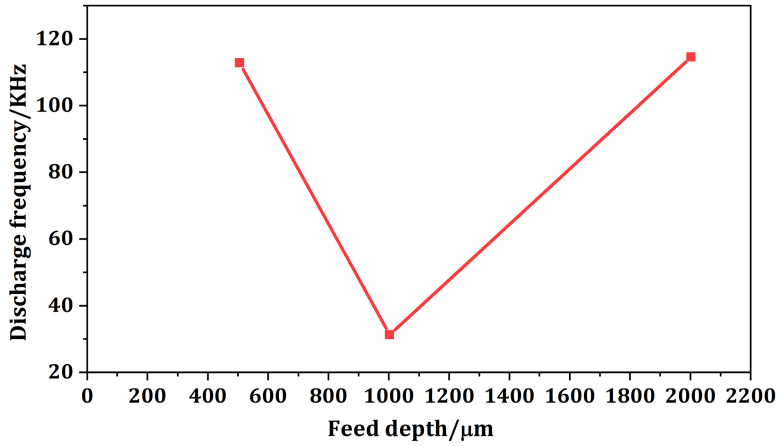

Fig. 5.16 Discharge frequency

5.2.6 Influence of discharge frequency on bubble behavior in normal discharge state

Since in the micro EDM the bubble is mainly generated from the evaporation of the dielectric liquid during the discharging process as shown in Fig. 5.6. Therefore, the discharge frequency has significant influence on the bubble behavior. Although the influence has not be clarified clearly due to unknown to the mechanism of breakdown process, it can be roughly estimated depending on the bubble number and volume in the specific discharge frequency.

The previously proposed two parameters, the bubble escaping frequency and the flowrate of bubble escaping volume, are not considered the relation of discharge frequency. In this section, two parameters, the bubble frequency efficiency and the bubble flowrate efficiency, are put forward to quantitatively evaluate the influence of discharge frequency on the bubble behavior. The bubble frequency efficiency is defined to be the bubble escaping frequency in the unit discharge process, which is equal to the bubble escaping frequency divides the total number of discharges in the corresponding bubble sample set. The bubble flowrate efficiency is defined to be the flowrate of bubble escaping volume in the unit discharge process, which is equal to the flowrate of bubble escaping volume divides the total number of discharges in this period. These two parameters consider the relation of discharge frequency on the bubble escaping frequency and flowrate of volume, which can be used to estimate the bubble escaping frequency and flowrate in the unit discharge process and comprehensively reflect the influence of discharge efficiency on the bubble behavior. The curve of bubble escaping frequency and bubble flowrate efficiency is shown in Fig. 5.17 and 5.18 respectively.

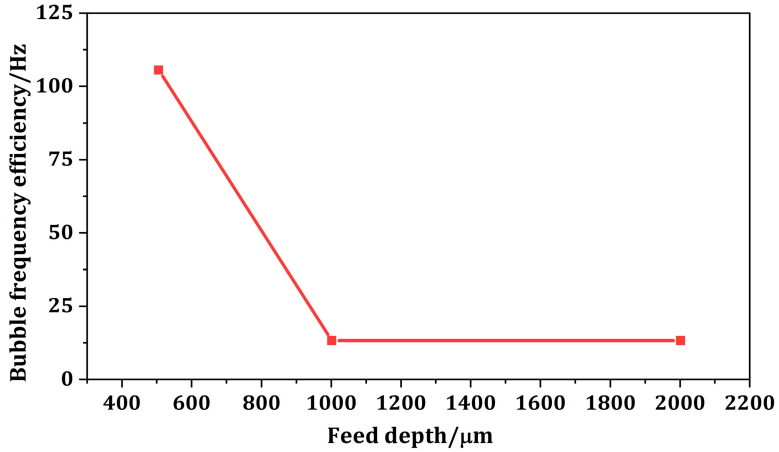

Fig. 5.17 Bubble frequency efficiency

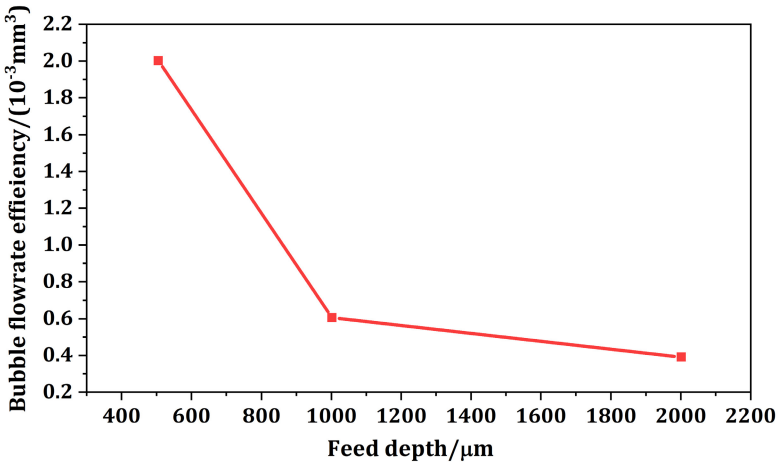

Fig. 5.18 Bubble flowrate efficiency

It is found that with the increase of feed depth both the bubble frequency efficiency and bubble flowrate efficiency decrease seriously, which indicates that in the deeper feed depth, the discharge efficiency has been lowered seriously. Less bubbles escape from the micro hole and the lower exchange of media due to the smaller flowrate of bubble. It is attributed to the deteriorated environment, which decrease the possibility for the normal discharges and cause the more abnormal discharges.

On the other hand, the trend of bubble frequency efficiency and bubble flowrate efficiency seems not consistent with trend of machining speed. As shown in Fig. 5.10, the machining speed in 505μm and 1002μm is nearly same, but there is huge distinguish for two terms in the feed depth of two situations, which also exist in the terms of bubble escaping frequency. It implies that in the assumption that the exchange of dielectric liquid is determined by the bubble escaping frequency and bubble flowrate efficiency, the debris exhaust is not simply proportional to the extent of dielectric liquid exchange although it is certain that the frequent dielectric exchange can improve the debris exhaust. The

reason is maybe that the debris is not freely distributed in the gap area, which is likely to be influenced by the electric field or other factors.

5.3 Bubble behavior in consecutive short circuit

The short circuit is inevitable in the micro EDM. But the consecutive short circuit, as a kind of abnormal discharges, should be avoided. Since the bubble is mainly generated in the discharge process, it can be assumed that no bubble should be generated during the consecutive short circuit. In the other hand, according to the experience in micro EDM, the gravity and buoyancy is nearly no effect on the movement of bubbles due to strong viscous effect in the narrow gap area. Thus, it can be inferred that there should be almost no bubble escaping from the micro hole during the consecutive short circuit.

In this section the bubble behavior during the consecutive short circuit is investigated. The voltage waveforms in the target consecutive short circuit is shown in Fig. 5.19 in the feed depth of 505μm. It is found that during a period t_D, about 8.17ms, there only exists the consecutive short circuit, the voltage difference between the cathode and anode nearly becomes 0 and no discharge occurs.

The waveform in the beginning of the consecutive short circuit is enlarged and shown in Fig. 5.19 (b). The F_D is the last frame of the discharge stage and F_S is the first frame of the consecutive short circuit. The image of F_D and F_S is shown in Fig. 5.20 respectively. It is found that during the whole consecutive short circuit, only in F_D, a bubble escapes from the micro hole and merges with the bubble nearby to become a big bubble in F_S. From F_S the consecutive short circuit stage starts. By observing the bubble behavior during this period, it is found when the consecutive short circuit starts, the process of bubble escaping from micro hole stops immediately. It shows that there is nearly no bubble escaping from the micro hole in the consecutive short circuit, which is consistent with the assumption discussed in the beginning of this section.

Moreover, it is observed that the debris piece or debris cluster is flushed out of the micro hole. The phenomenon is not only found in 505μm, but also in 307μm, 1510μm and 2002μm as shown Fig. 5.20. Obviously, the debris piece with a shape of cambered surface seems to peel off from the surface of micro tool or the inner surface of micro hole. It implies that the debris is not freely distributed in the gap area, it will be absorbed onto the surface of micro tool or inner surface of micro hole. It can be confirmed that the debris in micro scale can form the big debris piece as shown in Fig. 5.21. Obviously, the size of

debris piece is enough large to link the cathode with anode. Therefore, the consecutive short circuit in micro hole drilling with EDM is caused by the debris piece.

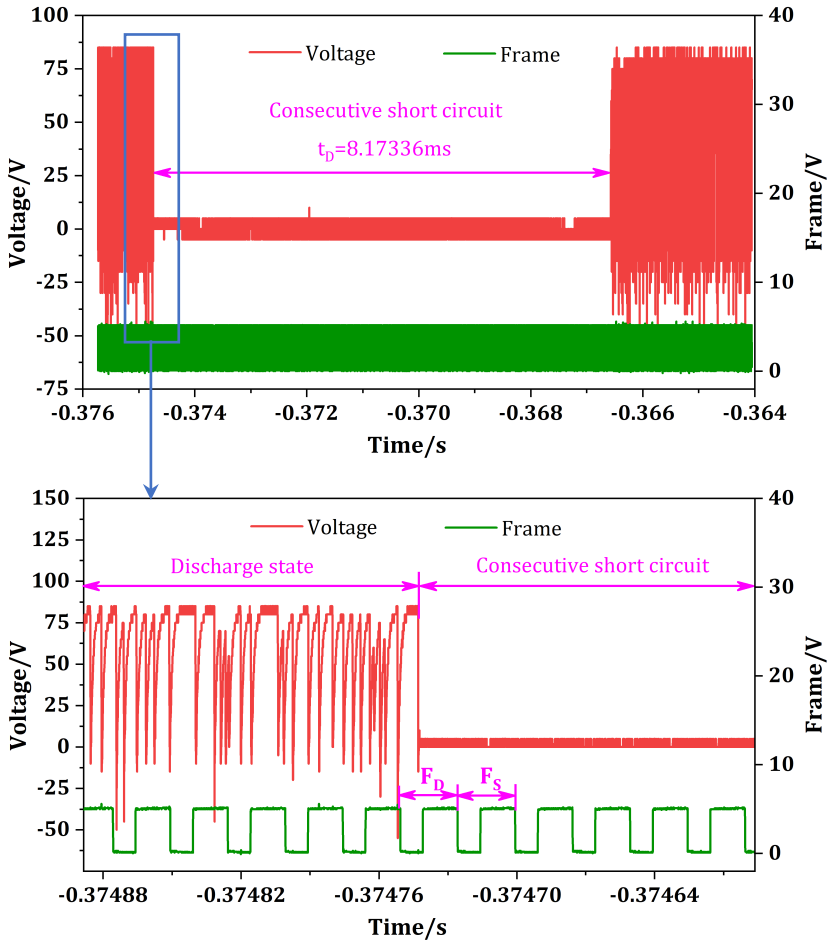

Fig. 5.19 Waveforms of the consecutive short circuit in the feed depth of 505μm

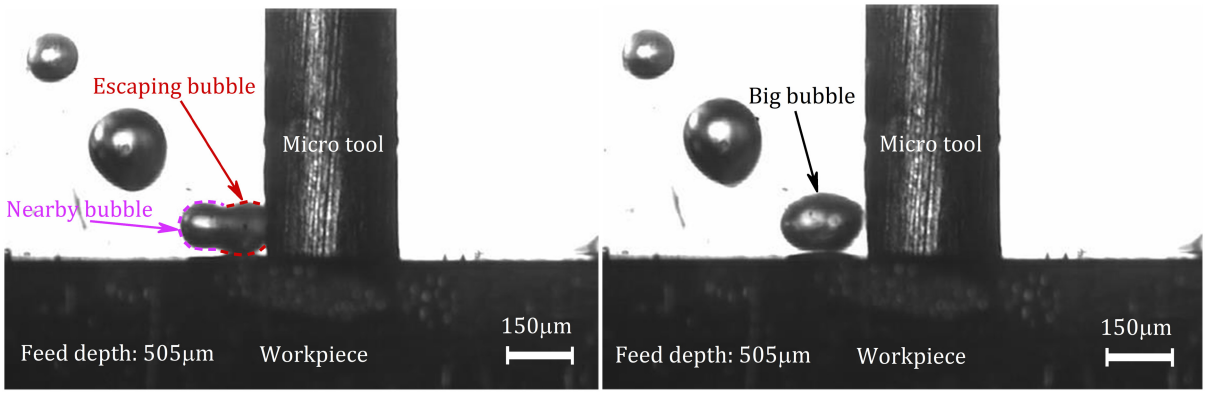

(a) Image in F_D (b) Image in F_C

Fig. 5.20 Images in F_D and F_C

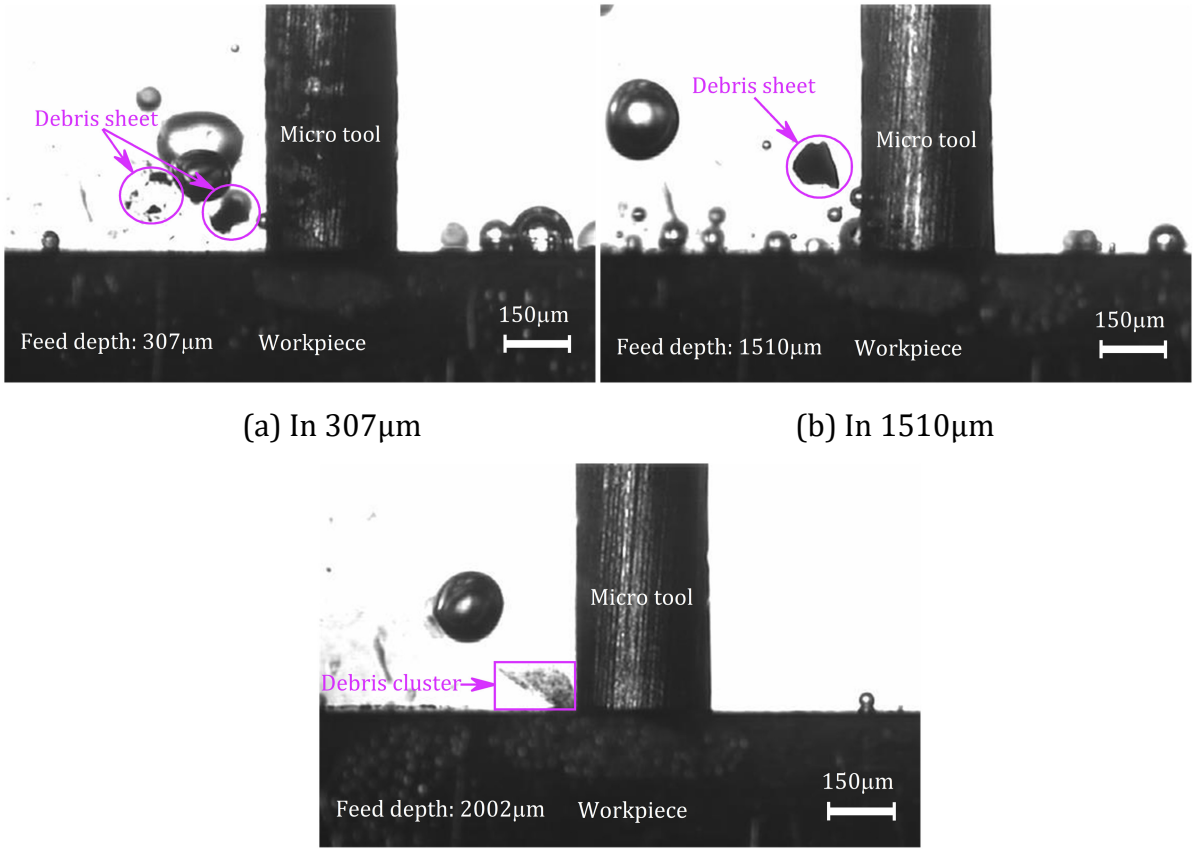

(a) In 307μm (b) In 1510μm

(c) In 2002μm

Fig. 5.21 Debris sheet and cluster in the consecutive short circuit

Actually, the environment of gap area in micro EDM can be treated as a complex dispersion system, including the debris, bubbles, dielectric liquid and the electric field. Although the characteristic of the dispersion system is rarely reported, it has significant influence on the behavior of bubble and debris and the breakdown process. The debris in the gap ranges from several nanometers to tens of micro meters [95]. Those debris particles in sub-micro scale and micro scale can form the colloids according to colloidal chemistry [96]. The debris colloids can absorb the ions in the dielectric and become the charged debris colloids. Therefore, it can be inferred that the electrophoresis action can also occur in the gap area.

The schematic of the electrophoresis action is shown in Fig. 5.22. The charged debris colloids will move in the dielectric and stick on the surface of micro tool and workpiece under the influence of the electric field to form the debris film. After the debris film peels off from the surface of micro tool or the inner surface of micro hole in the influence of the centrifugal effect or the discharge, the big debris piece is formed as observed in Fig. 5.21, which will cause the consecutive short circuit. Also, by using the colloidal chemistry to explain the behavior of debris in the gap area, the discharge occurs in debris can be easily

understood [27].

On the other hand, the electric field in the narrow gap is not uniform due to the tip effect or tool wear. More debris colloids are inclined to concentrate in the spots with intenser electric field and build the electric bridge, lowering the insulation strength of gap and causing the discharge under lower open voltage, which will be analyzed in the next section.

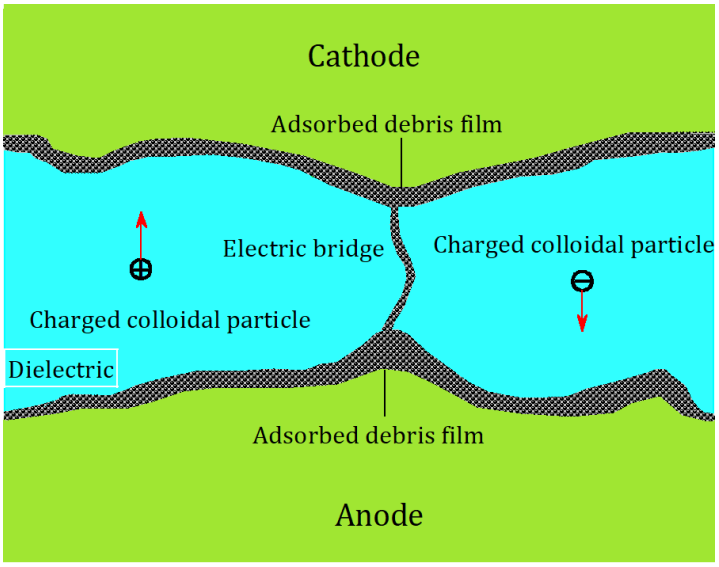

Fig. 5.22 Schematic of electrophoresis

5.4 Bubble behavior in discharge occurred in low open voltage

As one of abnormal discharges, the discharge in low open voltage frequently occurs in micro EDM, which is also found in the feed depth of 1510μm in the experiment. The bubble behavior has been investigated in this discharge state during the duration of bubble sample set of 51.4ms. The waveforms of the voltage and frame of video are shown in Fig. 5.23. It is found that all the discharges during this period occur in about 75V, obviously lower than the full open voltage of 110V. The observed behavior of the bubble and debris are shown in Fig. 5.24.

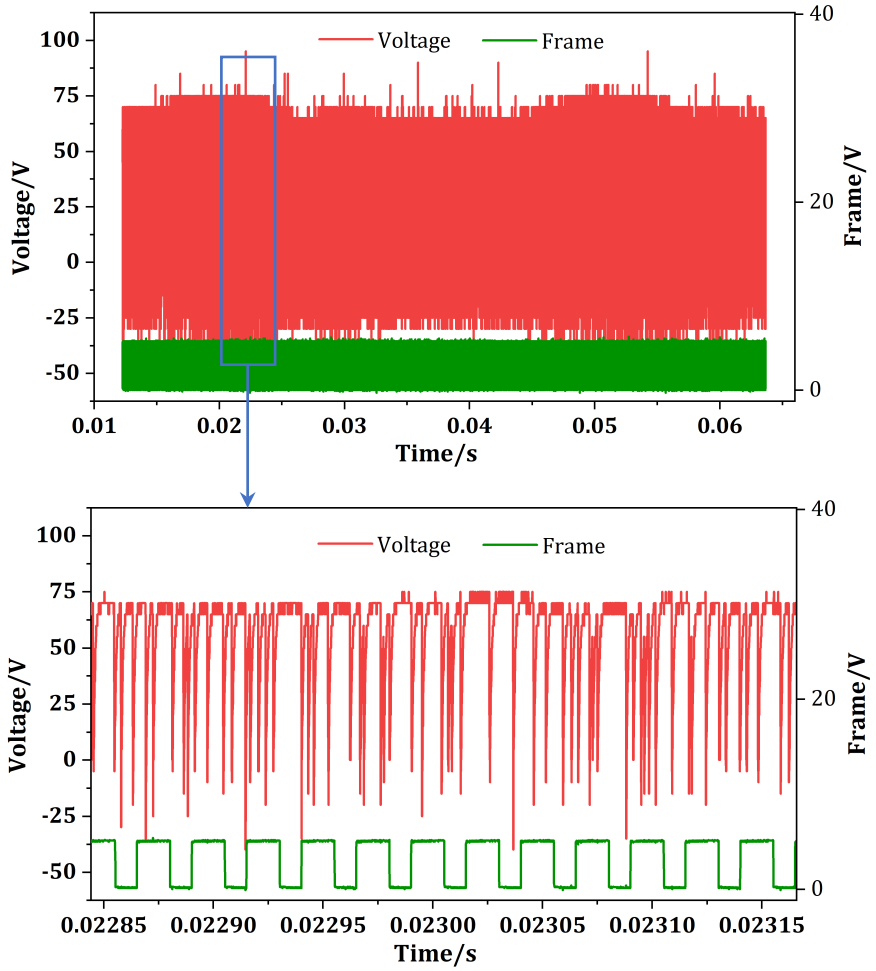

Fig. 5.23 The voltage and frame wave forms in discharges occurred in low open voltage in the feed depth of 1510μm

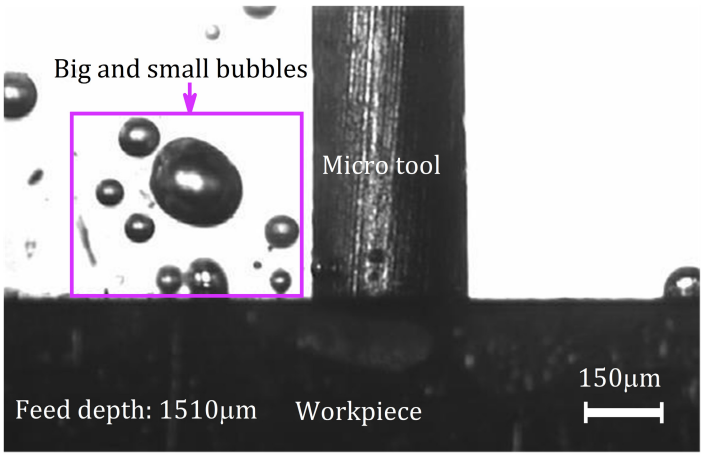

(a) Bubble

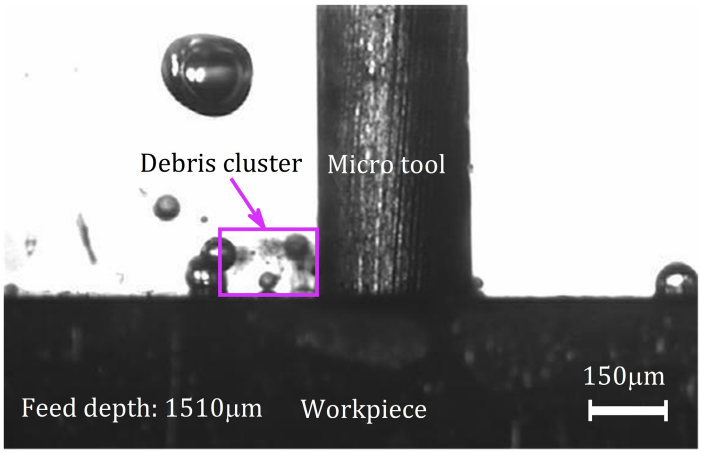

(b) Debris cluster

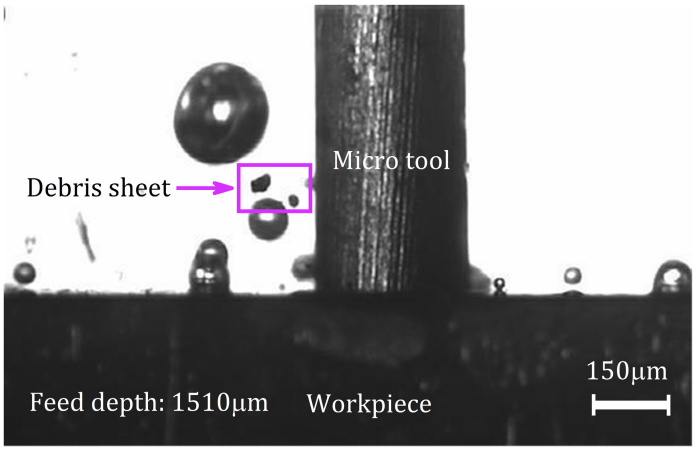

(c) Debris sheet

Fig. 5.24 Bubble and debris in low open voltage in the feed depth of 1510μm

It is found that in the discharge with low open circuit voltage both big and small bubbles escape from the micro hole. Moreover, the debris cluster or sheet is found in the low open voltage state as shown in Fig. 5.24 (b) and (c), which is only discovered in consecutive short circuit state.

In order to compare the bubble behavior in the state of low open circuit with those in the normal discharge state, the contrast analyzations have been done in the following part to investigate the characteristics of behavior of bubble in low open circuit state.

5.4.1 Bubble distribution

The curve of distribution of the single bubble size is shown in Fig. 5.25. In Fig. 5.25 (a), the scatter plot shows that in the low open voltage state, both many small and big bubbles escape from the micro hole. The diameter of most small bubbles is less than 70μm and the diameter of most big bubbles is larger than 150μm. There are only 23 bubbles in the range from 70μm to 150μm, which is only occupied about 9.3% of the total number of

bubbles. Thus, in order to describe the distribution of bubble size more accurately, the normal distribution is divided into two parts depending on the concentration extent of the bubble single size from the 110μm. The first part is used to describe the distribution of small bubbles and the second part is for the big bubble.

It is found that the distribution of bubble in the low open circuit state has two wave crests. The first crest indicates that the size of most small bubbles is close to 50μm, which is even smaller than that in the feed depth 1002μm. It implies that these small bubbles may be generated in the feed depth less than 505μm. According to the analyzation on the bubble behavior in section 5.2.3, the conclusion can be draw that the size of single bubble will definitely become larger with the increase of feed depth because the bubbles generated in the bottom of micro hole cannot escape from the immediately. Therefore, it can be inferred that these small bubbles are generated near the entrance of micro hole.

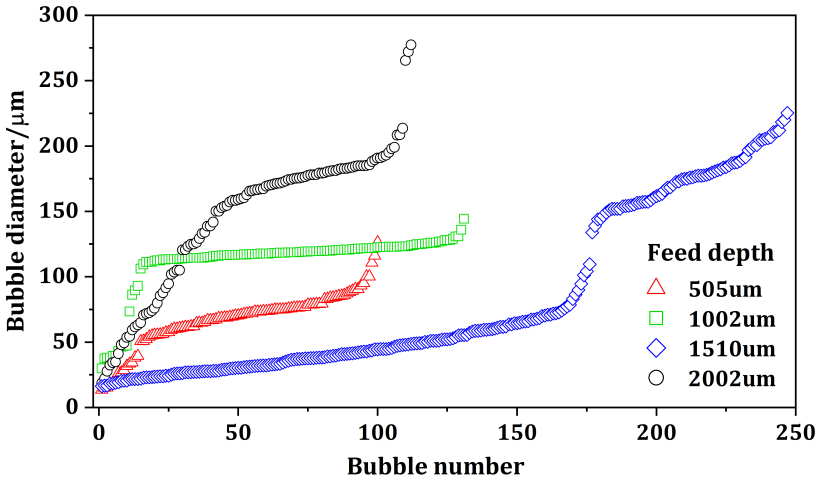

(a) Scatter plot

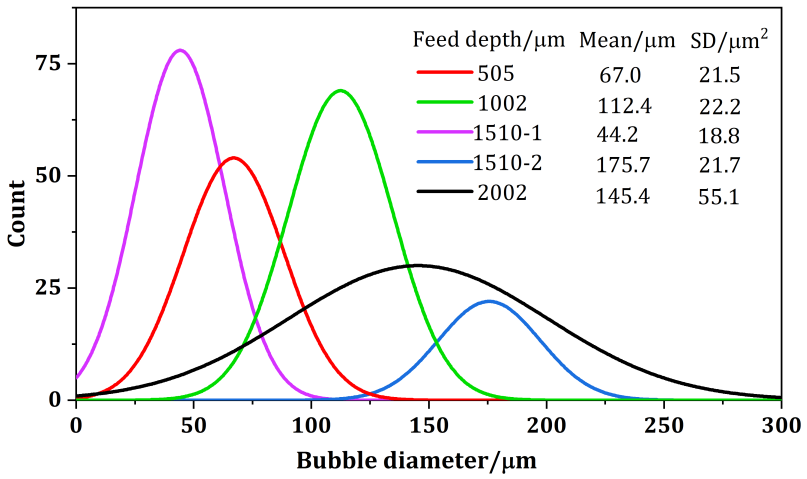

(b) Normal distribution

Fig. 5.25 Distribution of the single bubble

The normal distribution in the second part shows that the average diameter of the big bubble in the low open circuit voltage is even larger than that in the feed depth of 2002μm. It indicates that there are still many bubbles are generated in the bottom of micro hole. When these large bubbles approaching the discharge spot near the entrance of micro hole, they might merge with the small bubbles to become the bigger bubble.

The debris cluster observed in the low open circuit voltage state shows that many debris exist near the entrance of micro hole, which might come from the bottom of micro hole. In the normal machining state, from the beginning of machining to 1510μm, debris slowly accumulates in the gap area. In 1510μm, it reaches a certain value, influences the normal discharge and leads to the low machining speed. The debris is flushed towards the entrance of micro hole by the movement of bubble. The debris near the entrance of micro hole decreases the insultation strength of dielectric, builds the electric bridge between micro tool and workpiece, decreases the discharge voltage and finally leads to the discharges occur near the entrance of micro hole. Therefore, mass small bubbles are generated and escape out of the micro hole as the scatter plot shown in Fig. 5.25 (a).

5.4.2 Bubble escaping frequency

The comparison curve of the bubble escaping frequency is shown in Fig. 5.26. It shows that compared to the decreasing trend of bubble escaping frequency in the normal discharge state, more bubbles escaps from gap area in the low open voltage with feed depth of 1510μm. The sudden rise in 1510μm is attributed to the many little bubbles generated in the discharge spots near the entrance of micro hole.

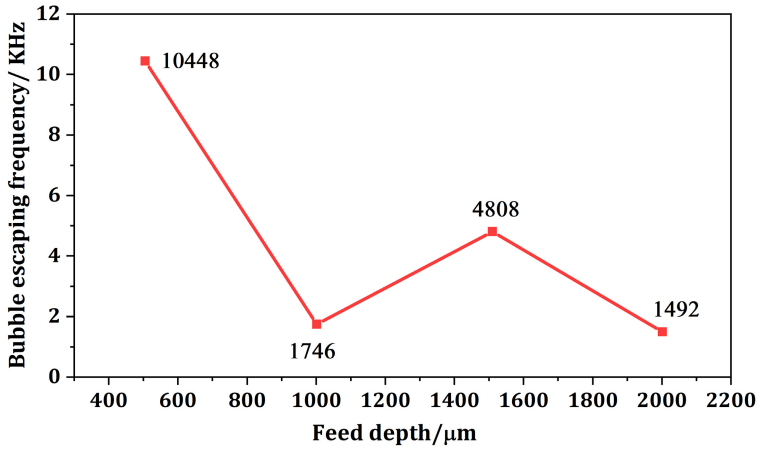

Fig. 5.26 Bubble escaping frequency

5.4.3 Flowrate of bubble escaping volume and discharge frequency

The curve of flowrate of bubble escaping volume is shown in Fig. 5.27. Lots of bubbles escaping from the micro hole lead to the sudden increase of flowrate of bubble escaping volume in 1510μm. It shows that the flowrate in the low discharge state is even large than that in the feed depth of 2002μm, which indicates that the speed of dielectric exchange is very fast.

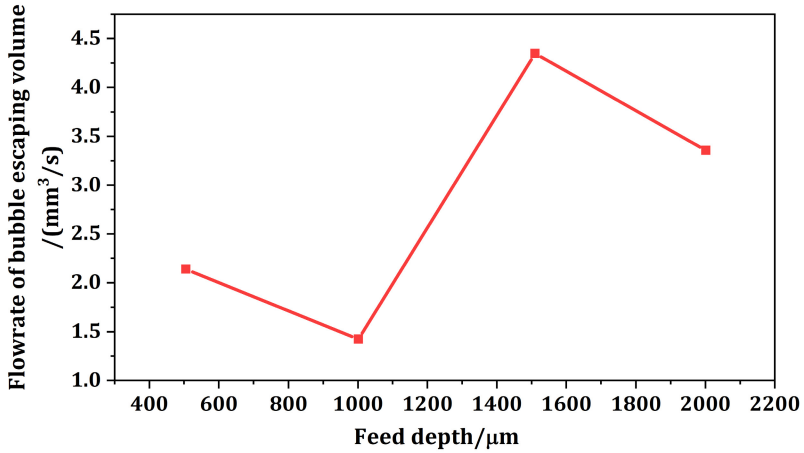

Fig. 5.27 Flowrate of bubble escaping volume

The curve of the discharge frequency is shown in Fig. 5.28. Due to the weak insulation strength near the entrance of the micro hole, the discharge frequency is very high in low open voltage. It can be inferred that the low insulation strength of gap area even supports the discharge in low open circuit. Most of the discharges might be the arc discharges.

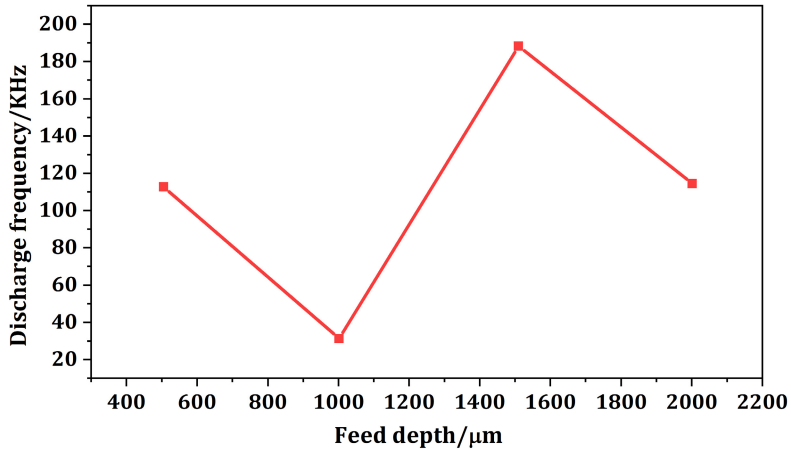

Fig. 5.28 Discharge frequency

5.4.4 Influence of discharge frequency on bubble behavior

The two parameters, bubble frequency efficiency and bubble flowrate efficiency, are also be calculated in the low open circuit state to investigate the influence of the discharge frequency on the bubble behavior as that in the normal discharge state. The curve of the bubble frequency efficiency and bubble flowrate efficiency are respectively shown in Fig.

5.29 and 5.30.

It can be seen that with the increase of feed depth, the discharge efficiency decreases seriously. Although the bubble frequency efficiency has a little increase in 1510μm compared to 1005μm and 2002μm, it is still far less than that in 505μm. It indicates in the discharge with low open voltage state, the bubble frequency and flowrate increase but the influence of discharge frequency on the bubble behavior is similar to that in normal discharge state, which the discharge efficiency decreases seriously with increase of hole depth.

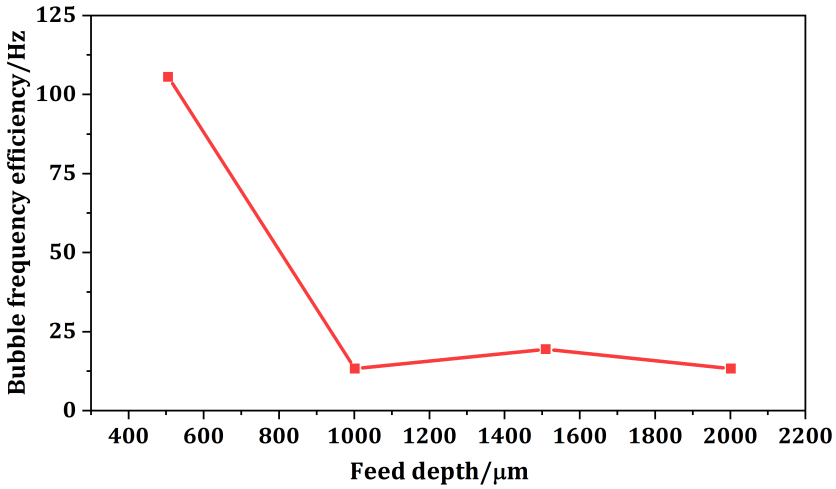

Fig. 5.29 The curve of bubble frequency efficiency in 1510μm

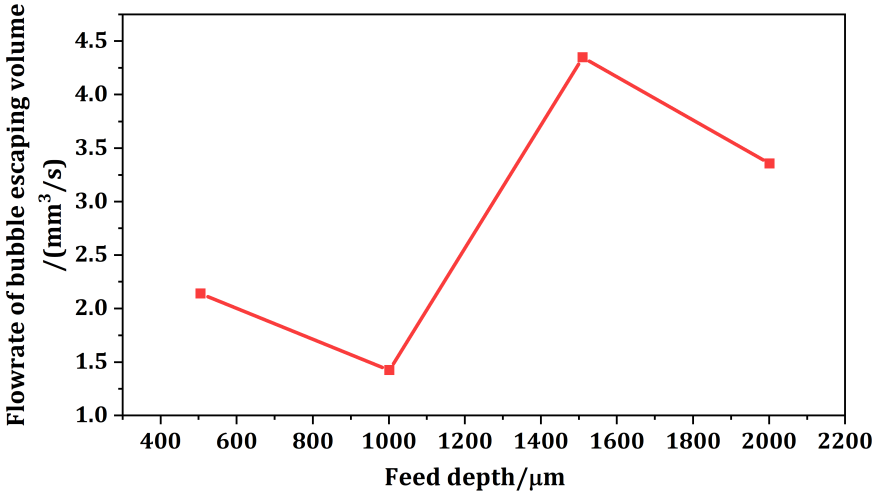

Fig. 5.30 The curve of bubble flowrate efficiency in 1510μm

This result reflects that the deteriorated environment seems inevitable with the increase of the feed depth.

5.5 Conclusions

In this chapter, the behavior of bubble and debris are quantitatively estimated in the

micro EDM. Firstly, in order to clearly investigate the generation of the bubble and debris in the single discharge process. A method by using the needle electrode is put forward to observe the details in the discharge process to avoid the block of micro tool or workpiece on the discharge spot. Secondly, the behavior of the bubble and debris in micro hole drilling has been observed and quantitatively estimated depending on a series of solutions put forward, such as, the method to order the distribution of bubbles escaping from the micro hole, investigate the flow field in the constraint flowing area to ensure the effectively flushing on the bubbles, match the high-frame rate of video with the high-frequency discharge waveforms, selection of the proper bubble sample set and extract the bubble accurately by the image segmentation method. Relying on these solutions, the quantitative estimation on the bubble behavior is reliable, which reveals many new insights in the recognition of the mechanism of the micro EDM.

The bubble and debris are mainly generated in discharge process. In the breakdown stage of the voltage drop, only the discharge spark occurs and no generation of bubble and debris. In the following 10μs, the discharge heat starts to be released so as that the bubble is generated from the evaporation of dielectric liquid and expands to the maximum, and the material of the workpiece are melted and scattered into gap area to become the debris. The discharge heat release can be completed in 10μs. Then the cooling of the discharge heat begins. The expansion and contraction of bubble indicate the change of discharge heat near the discharge spot. The phenomenon that bubble contraction is spent more time than the expansion indicates that the discharge heat cooling takes more time than the discharge heat releasing in the single discharge process. It is possible for the accumulation of heat in gap area in long time machining, which may be a reason for the weaken the insulation strength of dielectric. Moreover, the time for discharge heat cooling is so long that a new discharge can occur during the cooling of discharge heat in the previous single discharge process. The observed phenomena, the later discharge process breaks the bubble expansion in the previous discharge process and the secondary bubble expansion, indicate that it is possible for the accumulation of discharge heat during the frequent discharges in the actual machining.

In the normal discharge state of blind hole drilling, with the increase of the feed depth, the bubble escaping frequency decreases seriously, which indicates that number of bubble escaping from micro hole decreases seriously. It is inevitable and easily to be understood that in deeper hole depth, the bubble generated in the bottom of micro hole

is impossible to escape from the micro hole because it needs to go through the micro hole and reach the entrance of micro hole. However, the increase of the single bubble size according to the normal distribution of diameter of the single bubble leads to the flowrate of bubble escaping volume decreases firstly then increases, which is different with the empirical understanding of the bubble behavior. It means that the average of bubble flowrate increases in deeper hole depth. The change of discharge frequency, firstly decreasing then increasing, shows the characteristic of deteriorated environment. With the increase of feed depth, the debris accumulation and non-uniform gap width definitely will cause the more and more short circuits and decrease the number of normal discharges. Then in deeper feed depth, the environment will be further deteriorated, exhibiting in the frequent large retreat of micro tool and discharges in low open circuit. Thus, the insulation strength of gap area is weakened seriously so as that the gap area can be breakdown more easily, eventually leading to the rise of discharge frequency.

The debris cluster and piece observed in consecutive short circuit and low open voltage state indicates the debris is not freely distributed in gap area. It has the complex behavior in the gap area, for instance, it can be adsorbed onto the surface of micro hole to form the debris film, link the cathode and anode directly to cause the consecutive short circuit or build the electric bridge to decrease the open circuit voltage between the cathode and anode. The debris cluster or sheet, only observed in abnormal discharge state, indicates the debris behavior has a close relation with the short circuit and abnormal discharge state. By using the theory of colloidal chemistry, the behavior of debris seems can be well explained. The debris particles in sub-micro scale and micro scale can form the colloids. The debris colloids can absorb the ions in the dielectric, become the charged debris colloids and absorb onto the surface of micro tool or the inner surface of micro hole. Then the formation of debris piece and discharge in debris can be easily understood.

With the increase of feed depth, the discharge efficiency decreases seriously no matter in normal discharge state or the low open circuit discharge state. It reflects the influence of deteriorated environment on the discharge. However, the trend of bubble frequency efficiency and bubble flowrate efficiency is not totally consistent with the trend of the machining speed. The reason is because in deeper feed depth the debris is become more complex so as that the efficiency of bubble flushing on the gap area is not totally consistent with the efficiency of debris exhaust.

The methods proposed in this paper can be the foundation for the quantitative

investigation on the more complex phenomena in the gap area of micro EDM in further research, such as the quantitative estimation of the influence of bubble behavior on the exchange of dielectric liquid and debris exhaust or the effects of bubble behavior on weakening the insulation strength of the dielectric liquid.

Chapter 6. Mist jet to improve the machining speed and accuracy in micro EDM

6.1 Introduction

In EDM process, the material is removed by the discharge heat released after break-downing the narrow gap. The dielectric medium has a decisive role in EDM. Firstly, the high accuracy of EDM depends on the occurrence of discharge in a significantly narrow gap area. Under a certain open voltage, the breakdown of gap is dominated by the insulation strength of dielectric medium. Secondly, the dielectric medium cools down the gap area to maintain the stability of machining. Thirdly, the dielectric medium, circulated between electrode and workpiece, flushes away the discharge byproduct. These three basic functions of dielectric medium [83] make it essential in EDM process: insulation, cooling, exhaust of byproduct. Therefore, the development of EDM also accompanies the development of dielectric medium [28].

Since the critical role of dielectric medium has been discovered by Boris and Natalie I. Lazarenko [12], many kinds of dielectric media have been used in different machining depended on their special characteristics [83]. The dielectric media can be distributed into three types depended on the state of matter: liquid media, gas media and special media such as the plasma jet. The liquid media is most widely used in varieties of EDM processes such as the wire EDM [84] and sinking EDM [85], mainly including the oil-based media and water-based media. The oil-based dielectric media includes kerosene, mineral oil and transformer oil. The kerosene is the most common choice in the conventional EDM machining with high machining accuracy due to its low viscosity [12]. However, the disadvantages of air pollution, adhesion of carbon particles and potential fire hazard limit its application in the trend of green manufacture [29]. Water-based media mainly includes the tap water, deionized water and distilled water. Compared to the oil media, higher insulation strength and higher thermal stability provide a narrower gap width and higher material removal rate in water media [8]. Tap water is commonly used in the wire EDM with low cost and free from contamination. Less micro cracks in the white layer [86] promotes the application of deionized water in sinking EDM and micro hole drilling than the distilled water. The gas-based dielectric media, mainly pointing to the air, have a great virtue that the tool wear is nearly zero due to the adhesion of removal debris to the tool [31]. Compared to the liquid media, gas media has lower viscosity and flushs away the

debris more effectively to decrease the debris accumulation and abnormal discharges. However, the narrower gap width in gas media causes the frequent short circuits [31]. The requirement of more precise control system for tool movement is a big obstacle before its commercial use. In order to improve the quality of finish surface, many researchers added powders or particles into the liquid media to improve the machining accuracy. The prosperities of powder significantly affect the performance of EDM processes [87]. For example, conductive powders can decrease the insulation strength of dielectric and disperse the discharge energy, resulting in the removal of material with lower energy [88]. Some researchers also applied the compound emulsion, which is mixture of two kinds dielectric in special conditions such as the mixture of oil and distilled water to the EDM machining. A smoother edge of discharge crater can be obtained in this method [89]. The novel gas medium, nitrogen plasma jet, was attempted in micro EDM. The comparisons with other dielectric media reveal its improvements in machining efficiency and surface quality [33].

It is evident that both the liquid and gas media have outstanding advantages and inevitable disadvantages. In the liquid media, the deteriorated environment is a big obstacle in EDM especially in micro hole drilling due to the debris accumulation [27]. The large viscosity of liquid medium makes the debris exhaust and dielectric exchange difficult. In the gas media, extremely frequent short circuits give a great challenge for the control system [31]. Based on these problems, the mist medium has put forward to combine the liquid medium with gas medium. The thought is to create a medium, which has the advantages of both liquid and gas media while overcome their disadvantages. The reported research has presented its improvements: higher material removal rate and less debris deposition compared to gas media; higher material removal rate at lower discharge energy and narrower gap width compared to the liquid media [90]. The aerosol, a mixture of by oxygen and water, was used in the deep hole drilling with EDM and the excellent surface quality and high machining accuracy were obtained [91]. The mist medium with EDM jetting was also applied to dress metal-bonded super-abrasive wheels [92]. However, the mechanism of mist dielectric has not been analyzed, since these researches about mist medium mostly focus on the application on EDM field. These mentioned researches indicate the potential of mist medium in EDM. It is necessary to clarify its mechanism, present its advantages and broaden its applications.

In the previous chapters, the deteriorated environment attributed to the debris

accumulation and decreasing bubble escaping frequency in micro EDM has been investigated and quantitatively estimated. The complex debris behavior makes it difficult to be exhausted and leads to the inevitably deteriorated environment of gap area with increase of hole depth in micro EDM.

In this chapter, the performance of the mist deionized water jet in micro hole drilling with EDM was investigated. Firstly, the advantages of mist jet in suppression of electrolysis action, disturbing electrophoresis action and improving the debris exhaust has been analyzed; Secondly, an originally designed mist device has been fabricated and used in two projects of drilling experiments to verify the performance of mist jet in micro hole drilling with EDM. Thirdly, a method was put forward to directly observe the interelectrode gap area based on the original sandwich workpiece put forward in section 3.3 of chapter 3 to clarify the improvement of mist deionized water jet on the machining speed and accuracy. Finally, the results are analyzed and discussed.

6.2 Principle of micro EDM drilling by using mist jet

6.2.1 Problems in micro EDM drilling with deionized water

The deionized water is widely used in the micro hole drilling and sinking EDM since the high accuracy and material removal rate. However, the following three problems still exist: the electrolysis action, electrophoresis action and gradually deteriorated gap environment.

In micro EDM, although the deionized water has high insulation strength and contains few ions, the electrolysis can still occur and leads to the low machining speed and poor surface quality of workpiece near the entrance of micro hole [93]. The reasons are as follows: Generally, the deionized water is weak acidic, because it is generated from the tap water after being filtered by acidic cation exchange resin. In the weak acidic condition, the hydrogen evolution reaction occurs in the vicinity of the cathode as shown in equation (1) and (2), while the oxidation reaction takes place in the anode resulting in the dissolution of the metal ions such as the iron from the stainless steel as shown in equation (3). Moreover, in the narrow gap area, the hydrone will be ionized in the strong electric field as shown in equation (4). Therefore, the electrolysis action always occurs in micro EDM and leads to the poor machining accuracy especially in the long-time drilling [94]. The schematic of electrolysis action is shown in Fig. 6.1.

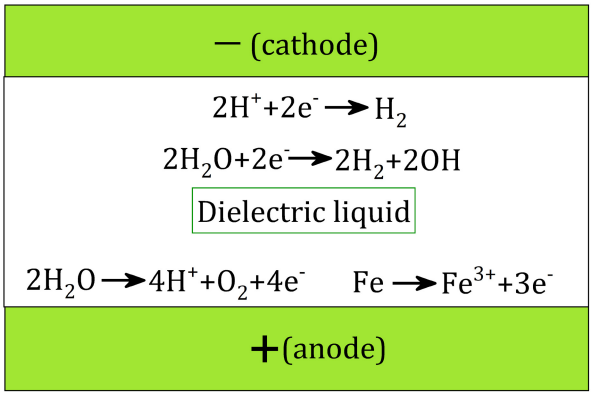

Fig. 6.1 Schematic of electrolysis action

$$2H^+ + 2e^- \rightarrow H_2 \quad (1)$$

$$2H_2O + 2e^- \rightarrow 2H_2 + 2OH^- \quad (2)$$

$$Fe \rightarrow Fe^{3+} + 3e^- \quad (3)$$

$$2H_2O \rightarrow 4H^+ + O_2 + 4e^- \quad (4)$$

The dispersion system in the gap area of micro EDM including dielectric liquid and erosion products such as debris and bubble is complex and rarely reported, but it significantly influences the breakdown of gap area. The debris in the gap ranges from several nanometers to tens of micro meters [95]. Those debris particles in sub-micro scale can form the colloids according to colloidal chemistry [96]. The debris colloids can absorb the ions in the dielectric and become the charged debris colloids. Therefore, it can be inferred that the electrophoresis action can also occur in the gap area. The schematic of electrophoresis is shown in Fig. 6.2. The charged debris colloids will move in the dielectric and stick on the surface of micro hole and inner surface of micro hole under the influence of the electric field. The absorbed debris film is always observed on the surface of micro tool after machining. Moreover, the discharge even occurs in debris. On the other hand, the electric field in the narrow gap is not uniform due to the tip effect. More debris colloids are inclined to concentrate in the locations with the stronger electric field and build the electric bridge, lowering the insulation strength of gap and causing the discharge under lower open voltage.

In the micro hole drilling, the exchange of dielectric and debris exhaust are big obstacles in the narrow gap. The gap-contamination caused by debris accumulation results in the lower insulation strength and abnormal discharges, which has been clearly analyzed and quantitatively estimated in previous chapters. Many methods have been put forward to improve the exchange of dielectric and debris exhaust such as the ultrasonic vibration [97, 64], planetary movement [64] and using the tube electrode [69]. The mist

jet is also a solution for the problem.

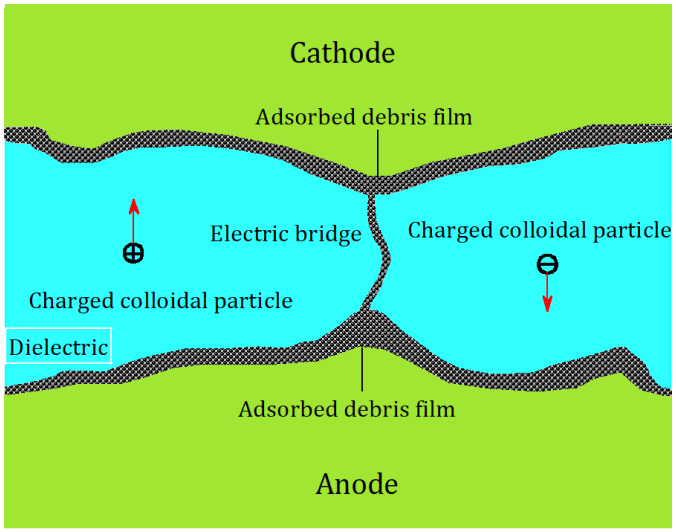

Fig. 6.2 Schematic of electrophoresis

6.2.2 Principle and advantages of the mist jet

In our research, the mist jet is generated from the deionized water crushed by the violent collision of the compressed air. The schematic is shown in Fig. 6.3. The misted deionized water is jetted towards the workpiece coaxially with the rod electrode to assure the tiny mist drops can impact the gap area rightly. Since the mist drops have the large momentum, the dielectric liquid in the vicinity of the entrance of the micro hole can be blown off immediately. The electrolysis action in the area near the entrance of micro hole can be prevented compared to the conventional supply of the dielectric liquid. Therefore, the smaller entrance size and gap width is expected in the drilling micro hole with the mist jet.

In the micro drilling, the surface tension on the interfaces of solid-liquid (workpiece and electrode-dielectric liquid) and liquid-gas (dielectric-bubble) causes the surface adsorption and capillary action, resulting in the low moving speed of bubbles and dielectric. It has been reported that by using the high-pressure dielectric liquid the machining speed can be significantly improved [98]. The mechanism is similar to the mist jet that the impact of mass mist drops on the dielectric liquid can bring the surge to the gap area. Under the impact of mist drop, the dielectric liquid is forced to move. On the other hand, it has been presented in chapter 3 that the large bubble exists in the gap of micro hole drilling especially in the deeper feed depth. Since the surge of dielectric can improve the movement of bubble, the bubble can escape from the gap area more quickly. Moreover, in the surging dielectric liquid, the debris colloids are hard to concentrate

together to build the electric bridge and cause abnormal discharges, and the exhaust of debris is easier. Therefore, it can be expected that less debris will accumulate in the gap area by using the mist jet.

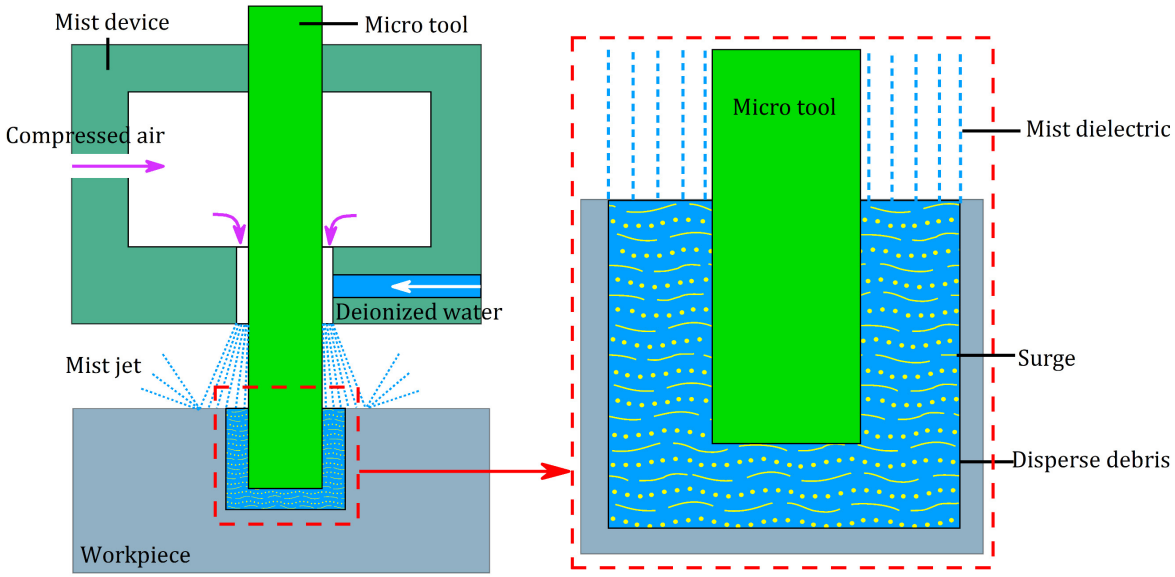

Fig. 6.3 Principle of mist jet

6.3 Experimental design, equipment and conditions

6.3.1 Experimental design

In our research, a mist device has been designed and fabricated to generate the mist jet. Three experimental projects have been designed. In project 1, in order to investigate the influence of electrolysis action on the micro EDM, the shallow micro hole drilling is conducted in mist deionized water jet and conventional deionized water jet to compare the size of entrance of micro hole. The proposed and conventional methods for dielectric supply are schematically shown in Fig. 6.4. In project 2, the experiment of drilling deep micro hole in stainless steel is conducted by using the device to investigate performance of mist jet. In project 3, to investigate the debris accumulation and the bubble in the gap, the method put forward in section 3.3 of the chapter 3 is used to directly observe interelectrode area of micro hole from the side wall by a high-speed camera with an originally made sandwich workpiece. Two kinds of sandwich workpieces based on the transparent SiC and stainless steel SUS304 have been applied in the observation conducted in mist jet and conventional water jet to compare the debris accumulation and bubble in the interelectrode gap area.

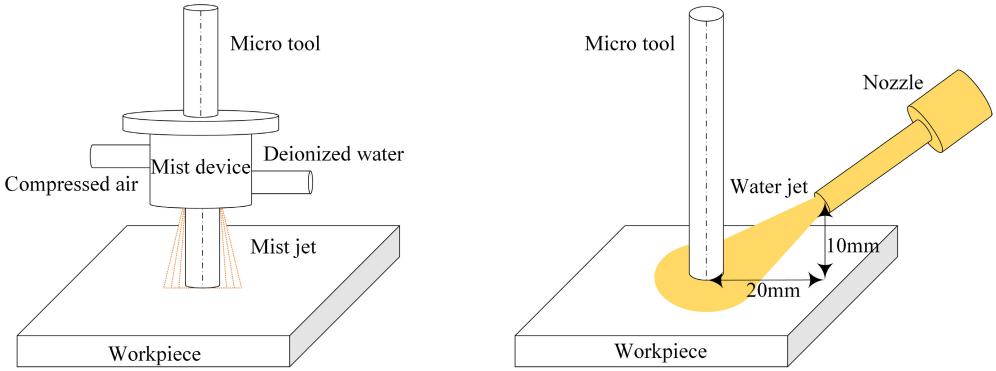

(a) Mist jet (b) Conventional water jet

Fig. 6.4 Supply of mist jet and water jet

6.3.2 Setup for drilling micro hole with mist device

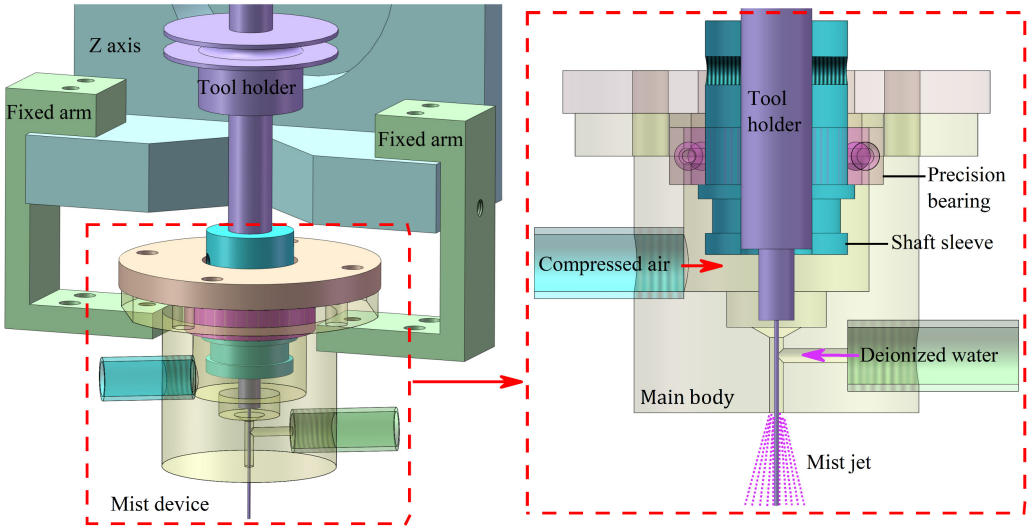

Fig. 6.5 Originally designed and fabricated mist device

The mist device designed and fabricated for micro hole drilling is shown in Fig. 6.5. Two channels are designed in the side wall of device for the supply of compressed air and deionized water. After being crushed by the compressed air, the mist deionized water jet is spouted coaxially with the micro tool from the nozzle in the bottom of the device. The whole device is suspended on the Z axis and fixed by two fixed arms to avoid the shake of main body after the compressed air is injected. A tiny precision bearing is installed between the shaft sleeve with tool holder to support the rotation of the micro tool.

The experiment is carried out in the micro EDM machining (MG-ED71, Panasonic) with the RC circuit. The micro tool feeds at a desired feeding speed set in the control program and retreats when the quantity of electricity (integration of short circuit current) reaches the threshold value during a certain period of time. A laser sensor (LK-G80, Keyence) is used for detecting the position of Z axis and recording the feed depth of the micro tool.

In project 1, in order to investigate the influence of electrolysis action on micro EDM, the shallow micro hole drilling is designed. The feed amount of micro hole is set to 500μm to avoid the influence of debris accumulation in the deeper hole depth. Meanwhile, the micro tool does not rotate to avoid the tool vibration caused by the centrifugal effort. In project 2, the tool rotates since the rotation of micro hole is essential to disperse the discharge spot, uniform tool wear and improve machining speed in deep micro hole drilling. First, the micro hole drillings are conducted with the mist jet and water jet in the stainless steel SUS304 workpiece with thickness of 5mm to verify the performance of the mist jet. Second, a deeper hole is drilled in stainless steel SUS304 workpiece with thickness of 15mm to investigate the limitation of mist jet in the micro hole drilling. The feed amount is set to 13.8mm, which is the largest feed amount of the micro tool due to the limitation of the mist device. The other experimental parameters are shown in Table 6.1.

Table 6.1 Experimental conditions

Items	Project 1	Project 2 and 3
Tool electrode	Φ60μm Tungsten	Φ300μm Tungsten
Tool feed rate	3μm/s	5μm/s
Open circuit voltage	100V	110V
Capacitance	220pF	1000pF

6.3.3 Setup for observing the gap area

In project 3, a high-speed camera (VW9000, Keyence) and a high magnification lens with long working distance (VH-Z50L) are applied to observe the interelectrode gap area of the micro hole. This lens of long working distance can assure the position of lens out of the rang of mist jet to obtain clear image of observation area. The schematic of setup is shown in Fig. 6.6. The control computer controls the machining and displays the feed depth and observation video real-timely after accepting signals from the laser displacement sensor and high-speed camera.

An original sandwich workpiece realizes the observation of interelectrode gap area, which is made of a sheet workpiece (stainless steel SUS304 or SiC) glued from both side with two pieces of glass plates by transparent resin adhesive as shown in Fig. 6.7 (a). The thickness of workpiece is equal to the diameter of micro tool so as that the material in the

gap is totally removed. A widow A in the side wall of micro hole is then created, through which the interelectrode gap area can be observed directly by the high-speed camera. The top view of sandwich workpiece and window A are shown in Fig. 6.7 (b) and (c) respectively.

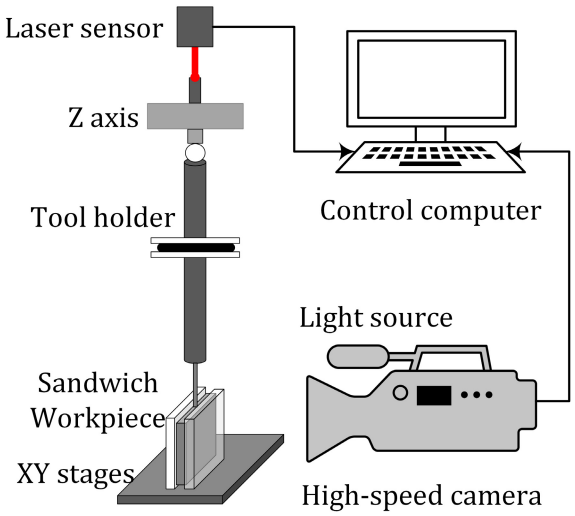

Fig. 6.6 Experimental equipment

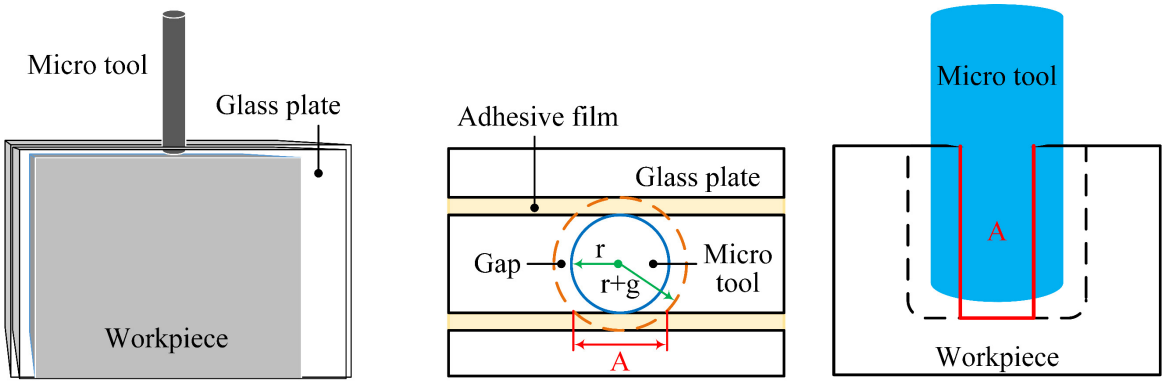

(a) Sandwich workpiece (b) Top view (c) Window A for observation

Fig. 6.7 Sandwich workpiece applied in observation

In addition, the thickness of glue film should be close to the width of discharge gap to avoid enlarging the micro hole because the melting point of resin adhesive is much lower than the stainless steel SUS304. One example of the thickness of glue film is shown in Fig. 6.8, which is measured from three locations by a surface profiler (CV-3100S4/MM, Mitutoyo). It is found that the thickness of glue film is similar to the gap width [79] in the condition of Table 6.1.

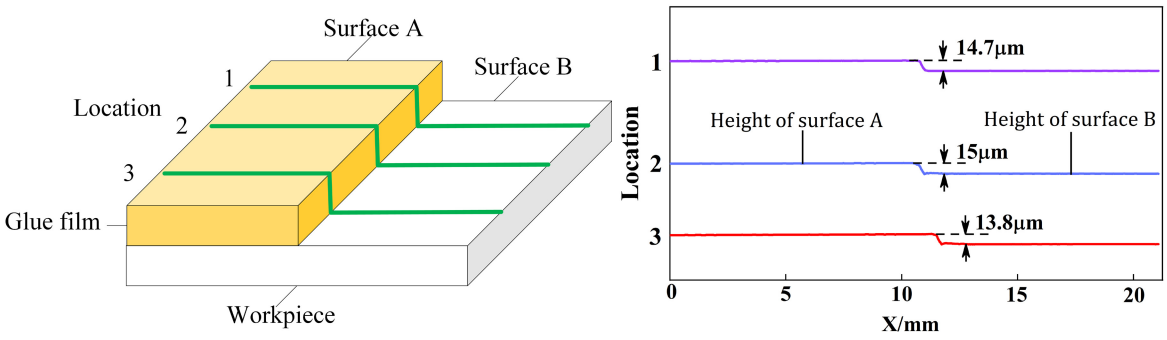

Fig. 6.8 Thickness of glue film

6.4 Performance of mist jet on shallow hole drilling

The shallow micro hole drillings with feed amount of 500μm in mist deionized water jet and deionized water jet were done to investigate the influence of flowrate water in the mist jet on the machining accuracy, machining speed and side gap width in two kinds of media.

6.4.1 Influence of water percentage in the mist jet on machining speed

The percentage of water and air in the mist jet dominates the physical property of mist jet. In order to find the optimized proportion ratio of water and air, the influence of flowrate of deionized water on the machining speed was investigated under a fixed air flowrate of 3480mL/min in the case of mist jet. The flowrate of deionized water is from 94ml/min to 284ml/min and the state of mist jet is shown in Fig. 6.9. It is found that in the flowrate of 194ml/min a straight mist jet can be obtained and shown in Fig. 6.9 (b), which has strong flushing effect on the gap area of micro hole. When the flowrate is lower than 94ml/min, low percentage of water leads to a short mist jet shown in in Fig. 6.9 (a), which is not enough to flush the interelectrode gap area of deep micro hole. When the flowrate is higher than 284ml/min shown in Fig. 6.9 (c), the high percentage of water results in a thick mist jet, which totally blocks the micro hole and is bad for the exchange of dielectric in the interelectrode gap area.

The drilling shallow hole micro with the feed amount of 500μm is done in different percentages of the deionized water. In each flowrate of the deionized water, three groups of the experiments were done. The machining speed is the average of three experiments. The relationship between the average machining speed with the flow rate of deionized water is shown in Fig. 6.10. The result shows that machining speed is the highest when the flowrate of deionized water is 194mL/min, which is consistent with the analyzation

on Fig. 6.9. It is evident that if the flowrate of deionized water is small, the percentage of water among the mist jet is so small that few mist drops enter into the gap and impact the dielectric liquid, resulting in low efficiency on the dielectric exchange. On the contrary, too much deionized water is difficult to be atomized by the compressed air so as that many big liquid drops exist in the mist jet to increase the viscosity of mist jet and decrease the shock on the dielectric liquid. Therefore, the low efficiency in the dielectric exchange leads to the low machining speed.

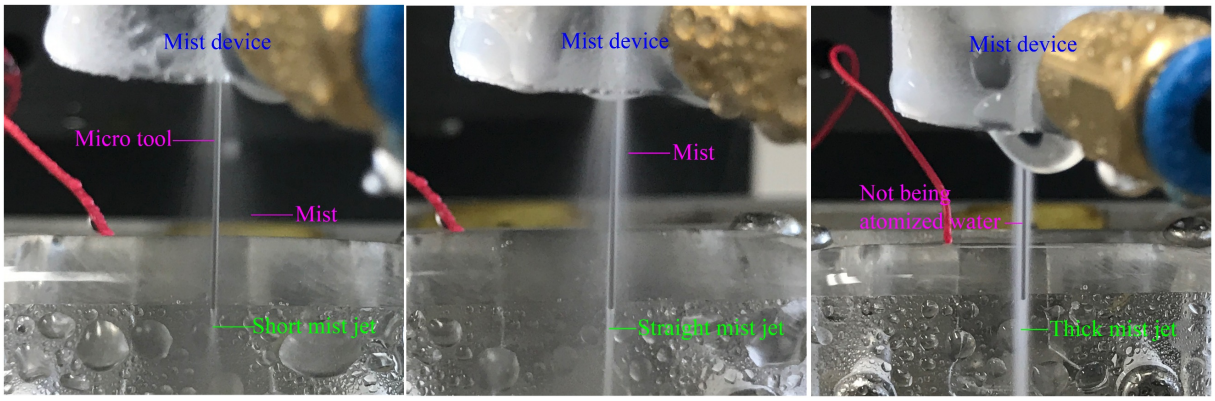

(a) Short mist jet (b) Straight mist jet (c) Thick mist jet

Fig. 6.9 Mist jets in different percentages of air and water

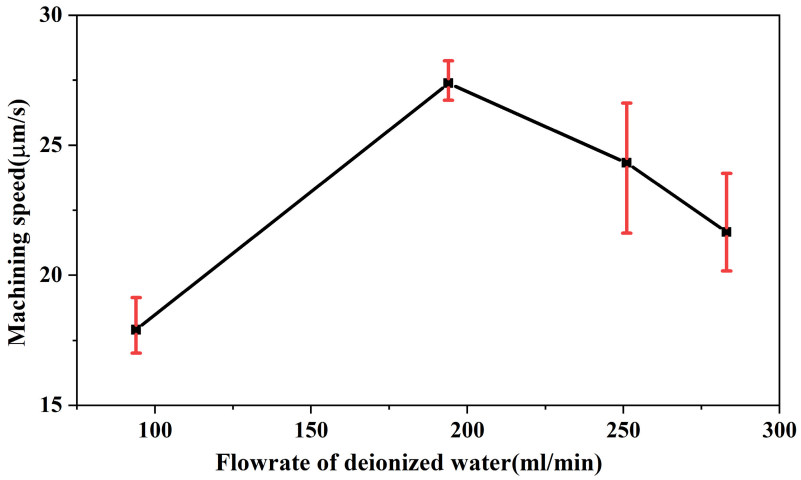

Fig. 6.10 Machining speeds in different flowrates of deionized water

6.4.2 Comparison of machining speed in mist jet and conventional water jet

To investigate machining speed in the mist jet and the conventional deionized water jet, the experiments have been carried out in two cases. The optimized percentage of air and water is used in the experiment with mist jet, which is obtained in section 6.4.1. In the experiment with water jet, the flowrate of the deionized water is same with that with mist jet. Each experiment under the same condition is repeated three times to decrease the

random error. The machining speed is shown in Fig. 6.11. It is found that the machining speed with mist jet is much larger than that with the water jet.

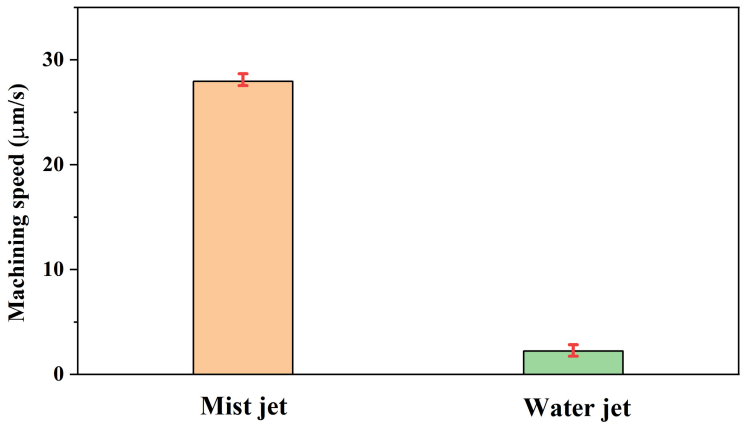

Fig. 6.11 Comparison of machining speeds with proposed and conventional methods

6.4.3 Suppression of electrolysis action by using mist jet

The electrolysis action can be decreased in the mist jet because the quick exchange of dielectric liquid decreases the hydrogen evolution reaction occurs in the vicinity of cathode. Therefore, the smaller entrance of micro hole is expected. In order to verify the supposition, the side gap width that reflects the radius difference between the drilled hole and the tool electrode was experimentally measured and evaluated as an index of suppression of electrolysis action and improving machining accuracy. The side gap width measured from the experiments in section 6.4.2 is shown in Fig. 6.12.

It is found that that the side gap width in the case of mist jet is about 5.2μm. But in the case of water jet is about 10.9μm, about two times larger than that in the case of mist jet. The results confirm the electrolysis action in enlarging the entrance of micro hole with water jet, which can be suppressed or weakened with proposed the mist jet.

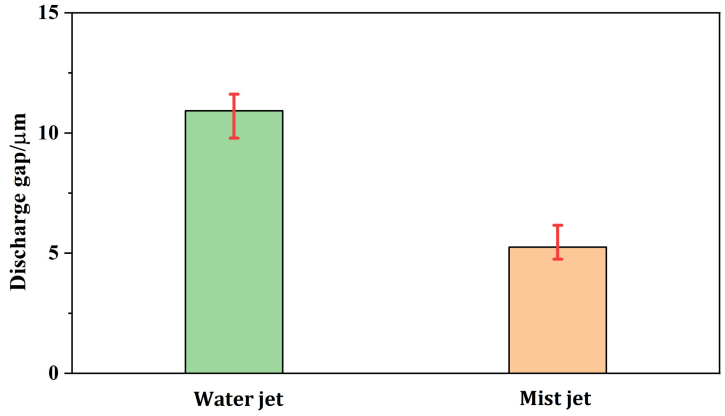

Fig. 6.12 Side gap width in the case of the mist jet and water jet

6.5 Performance of mist jet on deep micro hole drilling

The comparison experiments of deep micro hole drilling were conducted in the mist jet and water jet to investigate the performance of mist jet. The thickness of stainless steel SUS304 workpiece is 5mm. The feed curve of tool electrode during micro hole drilling with conventional water jet and mist jet is shown in Fig. 6.13 (a) and (b) respectively. The Fig. 6.13 (a) shows when feed depth of the micro tool reaches about 1.1mm, the micro tool cannot proceed any more, then retreats and fluctuates around 0.9mm for a long period of time with the water jet. The phenomenon of feeding limit of the tool electrode, called limitation of feeding depth in our research [63], commonly exists in the micro EDM drilling. Therefore, the machining speed seriously decreased in the fluctuation stage of the micro tool. However, by using the mist jet a through hole can be obtained. It seems that by using the mist jet the feeding limit disappears. The micro tool can continuously proceed until reaches the preset feed target. The result indicates that the deeper hole can be obtained at high machining speed by using mist jet.

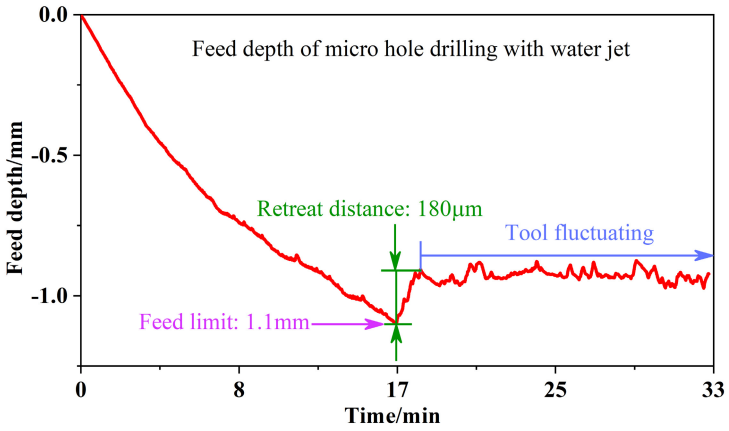

(a) In water jet

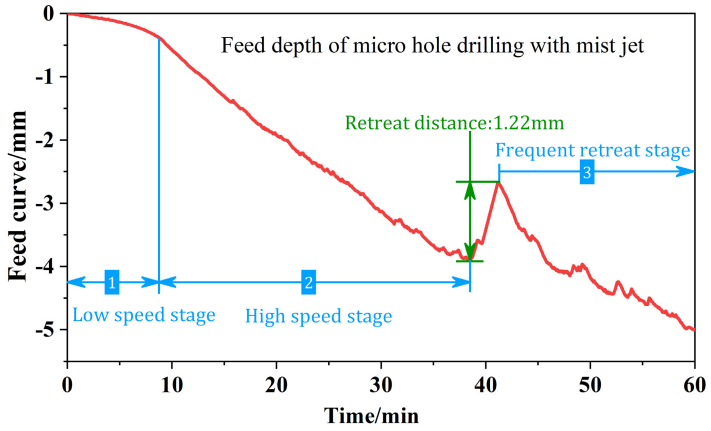

(b) In mist jet

Fig. 6.13 Feed depth of tool electrode during micro hole drilling

A big retreat of micro tool occurs in both cases as shown in Fig. 6.13. The retreat distance is much larger than the discharge gap (about 15μm [79]), which indicates that the consecutive short circuit occurs and makes the micro tool keep retreating until the insulation strength of gap area recovers. Compared to the water jet, the large retreat distance in mist jet reveals that debris also accumulates in the interelectrode and causes the consecutive short circuit. However, after the short circuit disappears, the micro tool continues to feed in mist jet. On the contrary, in water jet, the micro tool fluctuates around 0.9mm for a long period (about 16 minutes) and the machining speed decreases seriously. It reveals that the debris can be quickly exhausted by using the mist jet.

The drilling of micro hole in mist jet can be separated into three stages as shown in Fig. 6.13 (b): low speed stage, high speed stage and frequent retreat stage. The low machining speed at the beginning of machining may be due to the lateral vibration of micro tool caused by the impact of dielectric jet on electrode bottom. As shown in Fig. 6.14, the mist film on the side wall of micro tool after being flushed by the compressed air become the high-speed mist jet and forms a ring dielectric nappe. When the distance between the tool bottom with workpiece surface is less than 1mm according to the observation, a part of reflected dielectric jet can reach and impact the tool bottom. Since the micro tool rotates at high speed of 3000rpm, the dielectric film on the side wall is not totally uniform due to the equipment error and centrifugal effect. Therefore, the impact force of reflected dielectric jet on the tool bottom is different as F and F' shown in Fig. 6.14. The difference of their horizontal components (F_1 and F_1') leads to the later vibration of micro tool. Moreover, the vibration may be aggravated by the high-speed rotation of micro tool and vertical components (F_2 and F_2') because the fixed micro tool can be treated as a cantilever model. The lateral vibration leads to the low machining speed at the beginning of machining and a larger entrance shown in Fig. 6.15.

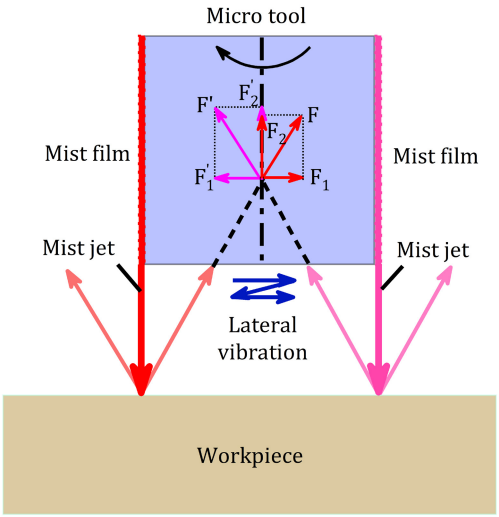

Fig. 6.14 Lateral vibration of micro tool

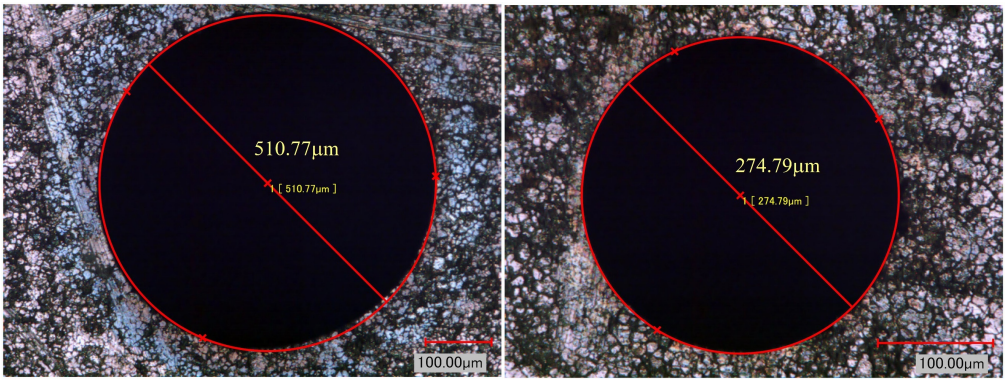

(a) Entrance (b) Exit

Fig. 6.15 Entrance and exit of 5mm through hole by using mist jet

Moreover, in order to verify the performance of mist jet in drilling deep hole, a deeper hole drilling was conducted in the stainless steel SUS304 workpiece with thickness of 15mm with the feed depth of 13.8mm, which is largest feed distance in this mist device due to the limitation of mist device. A blind hole with depth of 11.6mm is obtained and the feed curve of micro tool is shown in Fig. 6.16. The entrance of micro hole and micro tool after machining is shown in Fig. 6.17. The machining is also distributed into three stages: low speed stage, high speed stage and frequent retreat stage. It is found that the tool retreats frequently when the feed depth is larger than 7mm. Even so, the tool continues to proceed immediately after the consecutive short circuit disappears and no tool fluctuation is occurred as shown in Fig. 6.16. It indicates that by using the mist jet, the final depth of micro hole can be improved significantly. The deeper hole can be obtained in the faster speed by using the mist jet.

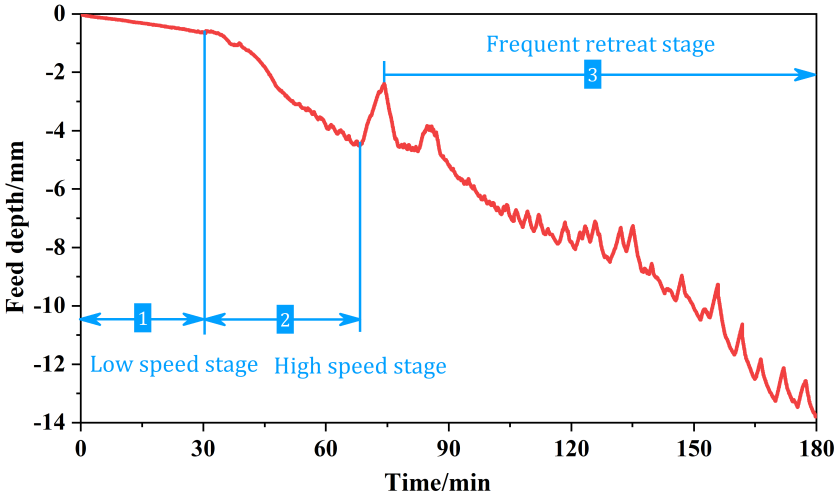

Fig. 6.16 Feed curve of micro tool

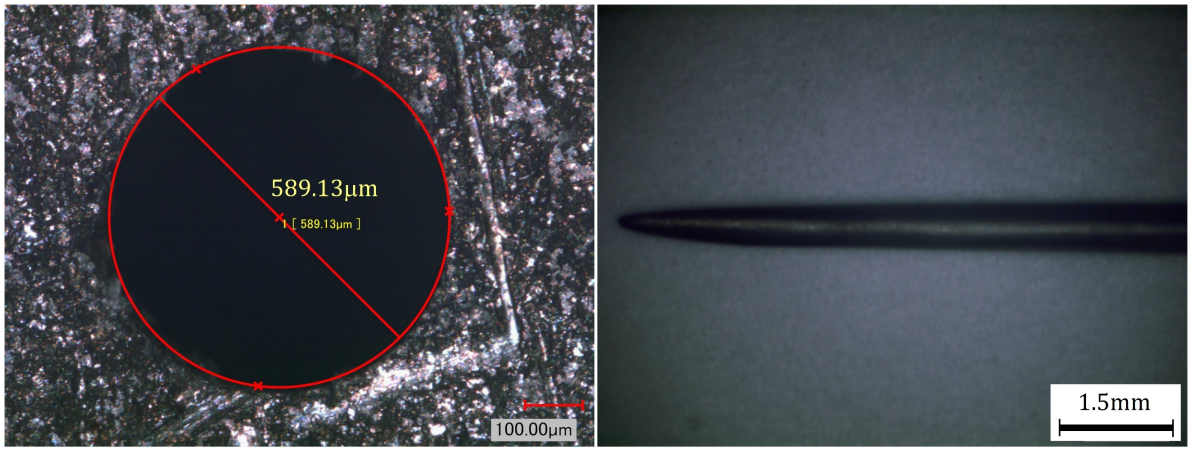

(a) Entrance of micro hole (b) Micro tool after machining

Fig. 6.17 Micro hole with feed depth of 13.8mm

6.6 Observation of phenomenon in interelectrode gap area

In order to find the difference in the behavior of debris and bubble between machining with the mist jet and the conventional water jet, observation of the phenomenon in the interelectrode gap area with a high-speed camera was carried out.

6.6.1 Behavior of debris

The observation of interelectrode gap area has been done in sandwich workpiece and blocked workpiece based on the stainless steel SUS304. The method is same as that introduced in section 3.3 of the chapter 3. The experimental condition is shown in Table 1. The frame rate is 4000rps and the shutter speed is 1/12000s. The images of interelectrode gap area in the feed depth of 400µm and 1.2mm are shown in Fig. 6.18 and 6.19 respectively. In Fig. 6.18 (a), the mist jet surrounding the micro tool causes the

diffuse reflection and decreases the intensity of illumination so that the gap area is not so clear. Since the melt point of resin adhesive is much lower than that of stainless steel SUS304, the glue film is melted more quickly in the discharging than the stainless steel SUS304 as shown in Fig. 6.18. Thus, the micro hole drilled in sandwich workpiece is slightly larger than that in blocked workpiece under the same conditions. The schematic of melt glue film is shown in Fig. 6.20. The area of glue film melted in the machining A' is larger than the desired area A. Although the micro hole in the observation is enlarged due to the glue film, it is still a blind hole according to the observation shown in Fig. 6.19, because no debris is leaked and found out of the gap area. Therefore, the observation result is reliable and can indicate the debris accumulation in mist jet and water jet.

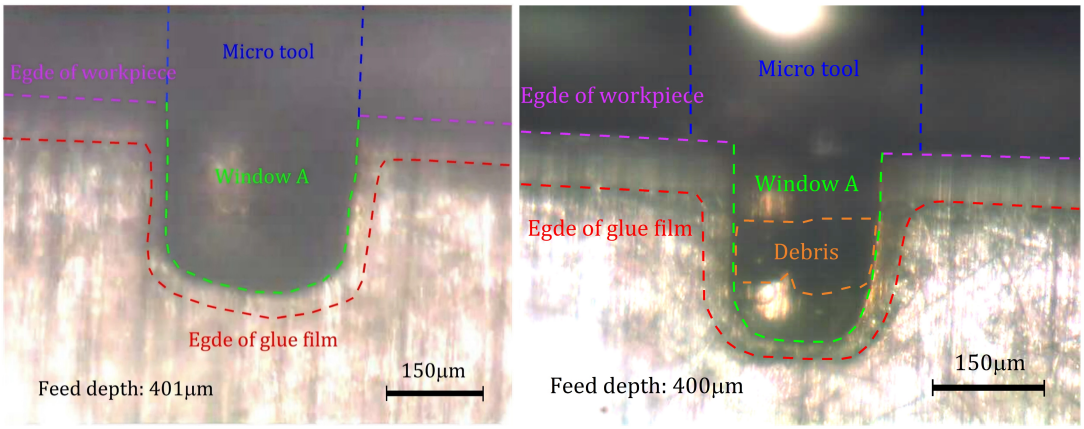

(a) In mist jet (b) In water jet

Fig. 6.18 Interelectrode gap in feed depth of 400μm

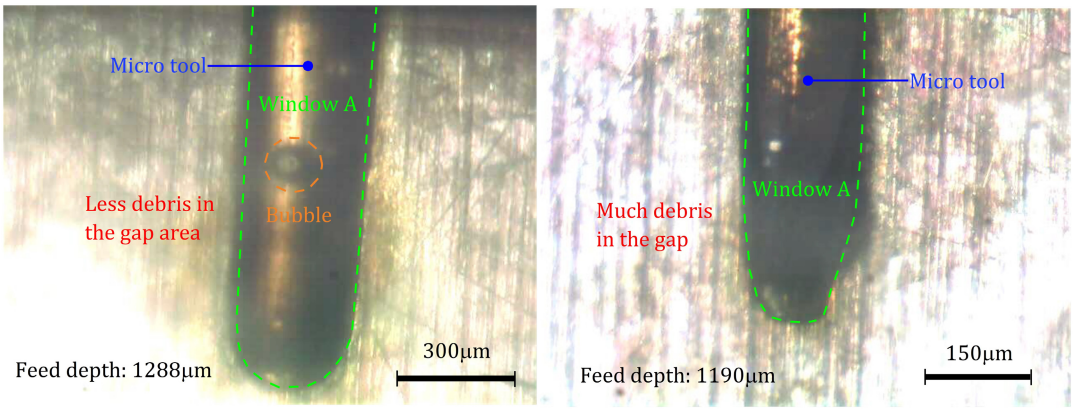

(a) In mist jet (b) In water jet

Fig. 6.19 Interelectrode gap in feed depth about 1.2mm

In the observation, only the interelectrode gap area in the area of window A (presented in Fig. 6.7 and 6.20) can be observed as shown in Fig. 6.19 (b). However, due to the lateral vibration of micro tool in the mist jet (explained in Fig. 6.14), the window A is enlarged, which is close to the size of micro tool as shown in Fig. 6.19 (a). It is found that the much

debris sticks on the surface on the micro hole in Fig. 6.18 (b). In Fig. 6.19 (b), more debris accumulates in the gap area and make the lower part of window A totally black. However, as shown in Fig. 6.19 (a), less debris accumulates in the gap area so that the surface of micro tool can be observed clearly. It indicates that by using the mist jet, the flushing effect on the gap area can be improved significantly and less debris accumulates in the gap area.

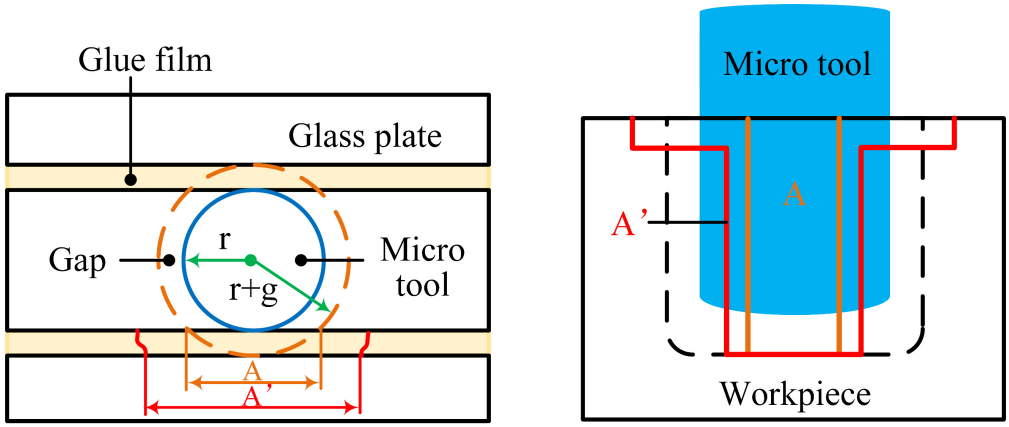

Fig. 6.20 Schematic of melted glue film

6.6.2 Behavior of bubble in the gap area of mist jet and water jet

The bubble behavior in the interelectrode gap area has been observed in mist jet and water jet respectively based on the SiC workpiece. Since the transparent SiC workpiece has excellent optical visibility and less debris is generated in the discharge process compared to the stainless steel SUS304 workpiece, it is very suitable to be used to observe the bubble behavior in the interelectrode gap area. In the observation with water jet, the frame rate is 4000rps and the shutter speed is 1/12000s. In the observation with mist jet, the frame rate is 4000rps and the shutter speed is 1/8000s.

It is found that in the gap area with water jet, the bubble merges with other bubbles to become a large bubble shown in Fig. 6.21 or grows up to a big bubble shown in Fig. 6.22. With the increase of hole depth, the bubble needs to go through longer distance from the bottom of micro hole to the entrance. Therefore, the bubble cannot escape from the gap area immediately and will stay in the gap area for a longer period, merge with other bubble or grow up to become a big bubble, which results in that less bubble escapes from gap area. Since the bubble escaping process has the function of flushing the gap area and improving the exchange of the dielectric liquid, less bubbles escaping from gap area with increase of hole depth lowers the flowing of dielectric liquid in the gap area and result in the debris accumulation as presented in Fig. 6.19 (b).

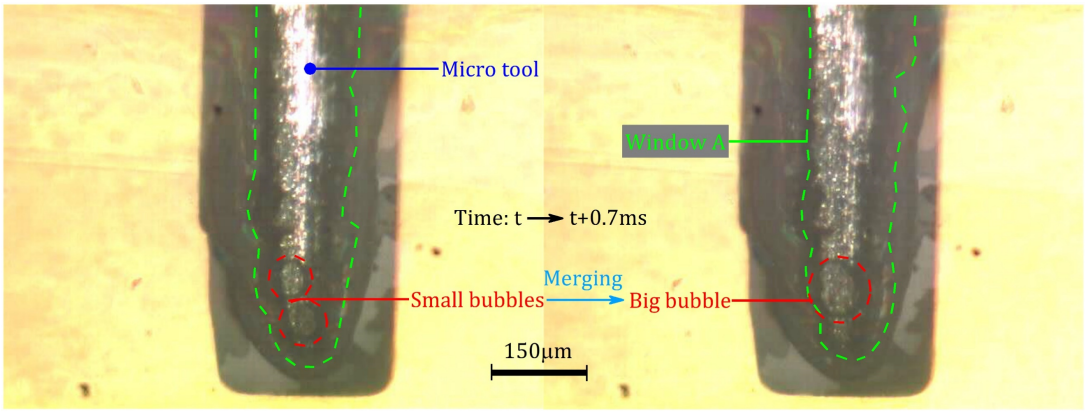

Fig. 6.21 Bubbles in feed depth of 777μm with water jet

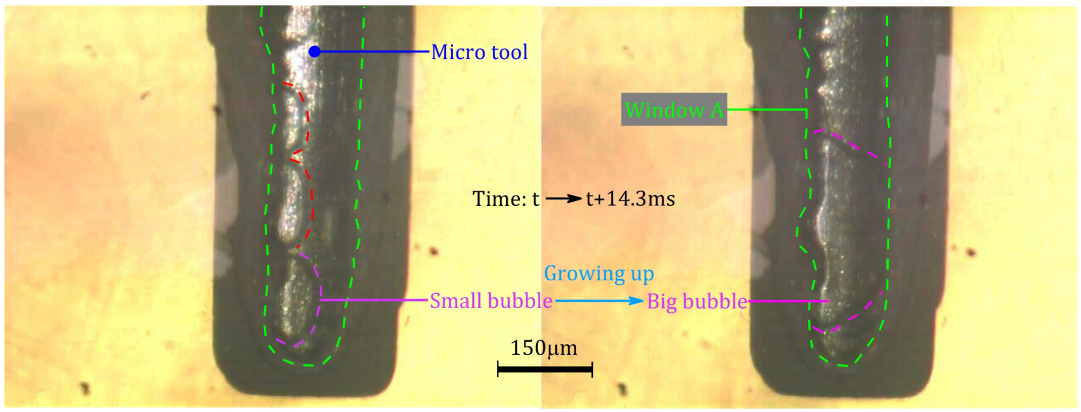

Fig. 6.22 Bubbles in feed depth of 1117μm with water jet

Bubbles in the interelectrode gap area with the mist jet are shown in Fig. 6.23 and 6.24. In Fig. 6.23, the mist jet causes the diffuse reflection and decreases the intensity of illumination so that the gap area is not so clear compared the images in Fig. 6.21 and 6.22. It is found that with the mist jet the bubble in the interelectrode gap area moves more quickly than that with the water jet.

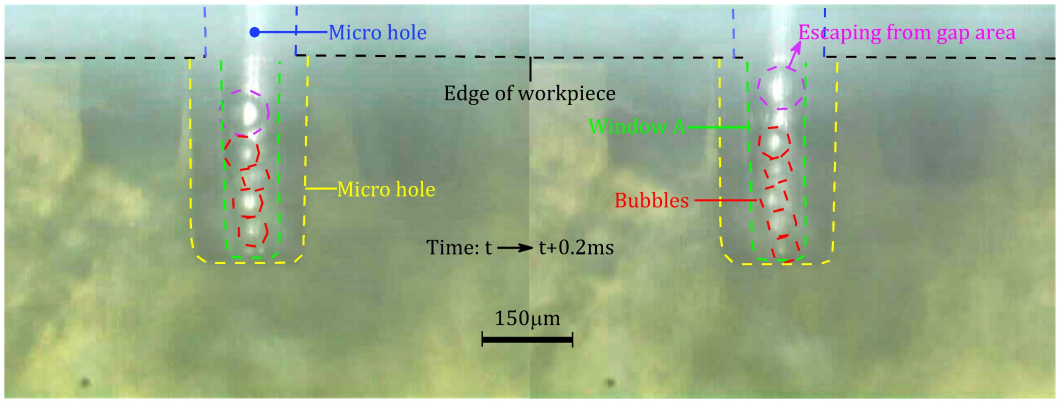

Fig. 6.23 Bubble in feed depth of 760μm with mist jet

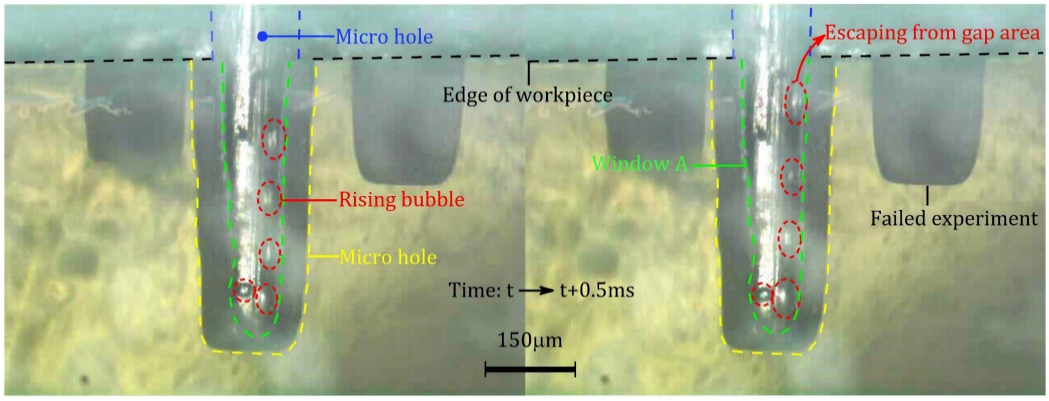

Fig. 6.24 Bubble in feed depth of 1090μm with mist jet

As shown in Fig. 6.23 and 6.24, the bubbles in the gap area is rising quickly towards the entrance of micro hole. It indicates that the dielectric liquid in the gap area is flowing quickly so that the bubbles also moves quickly and do not stay in the gap for a long period. Therefore, there is less possibility for the bubble growing up or merging with bubble to form a large bubble. It reveals the mist jet can bring surge to the dielectric liquid in the gap area to make the dielectric flow more quickly. The bubble flushes the gap more frequently so that less debris accumulates in the gap as presented in Fig. 6.19 (a).

6.7 Conclusions

In this chapter, the mist jet is applied in the micro EDM drilling. The advantages and principle of mist jet in suppression of electrolysis action, dispersion of debris colloform and improving the debris exhaust have been analyzed and discussed. A mist device was designed, fabricated and applied in three projects of experiments to investigate the performance of mist jet in the micro EDM drilling. Moreover, the interelectrode gap area has been directly observed based on the originally designed sandwich workpiece to verify the mentioned thoughts. Based on the experimental experiments, the following conclusions can be drawn：

(1) The electrolysis action in micro EDM drilling with conventional deionized water jet, which enlarges the entrance of micro hole and lowers the machining accuracy, can be suppressed by the mist jet because the deionized water surrounding the entrance of micro hole can be immediately flushed away by the mist jet with the high momentum. The micro hole with the smaller entrance can be obtained at the faster machining speed.

(2) The mist jet is significantly influenced by the percentage of water and air. In the

flowrate of air of 3480mL/min, the optimized machining speed can be obtained in the flowrate of water of 198mL/min.

(3) The deeper hole can be obtained at faster machining speed by using the mist jet. In this paper, a micro hole is obtained with feed depth of 13.8mm (hole depth: 11.6mm) and Φ300μm micro tool. It is expected that much deeper hole can be obtained in mist jet with a better mist device overcoming the limitation of the mist device presented in this paper in the further research.

(4) The observation of interelectrode gap area on debris shows that less debris accumulates in the gap area by using mist jet, which verifies the performance of mist jet on improving the debris exhaust.

(5) The observation of interelectrode gap area on bubble indicates that with mist jet the dielectric liquid flows more quickly due to the surge and bubbles can escape from gap area more quickly. Finally, the dielectric liquid exchanges more frequently and less debris accumulates in the gap area.

Chapter 7. Conclusions

The material removal in micro EDM depends on the repetitive single discharges. In the ideal machining environment, the discharge process seems simple. However, after focusing on the byproducts and their influences on the later discharge process, the whole process become very complex.

In a single discharge, the breakdown occurs firstly. The ignition is the only symbol to indicate the breakdown is finished. Then the discharge heat releases to evaporate the dielectric liquid and melt the material in the workpiece. The bubble and debris are generated from this process in 10μs after the breakdown. The discharge heat releasing and cooling definitely leads to the bubble oscillation (expansion and contraction), which actually acts as a vibration function on the gap area. Moreover, considering the bubble movement in the escaping from gap area, the bubble behavior has significant influence on the self-flushing effects to improve the dielectric exchange and debris exhaust. Therefore, once the bubble escaping frequency decreases with the increase of hole depth, the environment of gap area deteriorates seriously.

The conductive debris is not freely distributed in the gap area. Its physical properties such as small size in sub-microscale and electrical conductivity leads to its complex behavior in the dispersive system of gap area with strong electric field. An explanation based on the colloid chemistry is put forward to explain the behavior of debris. The charged conductive debris colloid will move directionally in the influence of electric field and be adsorbed on the surface of micro tool and micro hole. Only in the consecutive short circuit, when the electric field totally disappears, the adsorbed debris film can be separated from the surface of micro hole and micro tool and flushed out of gap area by movement of bubbles. This explanation is reasonable and can be used to explain the effectiveness of methods to improve the machining speed and debris exhaust such as ultrasonic vibration. Because the movement of conductive debris colloid is disturbed by using this method, it is not so easy to be absorbed in the surface of micro tool and micro hole. Therefore, the discharge in debris can be predicted and the machining limitation can be explained reasonably.

Based on the clarification on the behavior of bubble and debris, the influence of increase of hole depth on the machining speed can be explained easily. With the increase of hole depth, a big problem occurs that the bubble can not overflow out of gap area

immediately. Therefore, the bubble will accumulate in the gap area to grow up or merge with other bubble to become a larger bubble. The environment of gap area deteriorates seriously because of the debris accumulation. The behavior of debris will decrease the insulation strength of dielectric liquid seriously and cause the abnormal discharges and even links the cathode with anode directly resulting in the discharge in debris.

As a whole, the behavior of debris is harmful to the discharge process. The debris participating in discharge leads to the worthless waste of discharge energy and machining limitation in micro EDM. The behavior of debris in gap area destroys the premises to make sure the high machining accuracy in micro EDM that the discharge in narrow gap area. The behavior of debris enlarges the gap width by decreasing the gap width. The aggregated debris act as a wire to links the cathode and anode directly, resulting in the consecutive short circuit in micro hole drilling.

Therefore, the debris exhaust and dielectric exchange are important in micro EDM to make sure the machining speed and accuracy. In this research, a new solution is put forward to solve this problem by using the mist jet. Its performance in micro hole drilling has been verified in this research.

Furtherly, based on quantitative estimation on bubble behavior in micro EDM drilling, the further research in theoretical model may be built to simulate the movement of bubble and debris.

References

[1] Snoeys, R., Staelens, F., & Dekeyser, W. (1986). Current trends in non-conventional material removal processes. CIRP annals, 35(2), 467-480.

[2] El-Hofy, H. A. G. (2013). Fundamentals of machining processes: conventional and nonconventional processes. CRC press.

[3] Davim, J. P. (Ed.). (2008). Machining: fundamentals and recent advances. Springer Science & Business Media.

[4] Anonymous, History and development, in: The Techniques and ractice of Spark Erosion Machining, Sparcatron Limited, loucester, UK, 1965, p. 6.

[5] A.L. Livshits, Introduction, in: Electro-erosion Machining of Metals, Department of Scientific & Industrial Research, Butterworth & Co., London, 1960, p. x

[6] E.C. Jameson, Description and development of electrical discharge machining (EDM), in: Electrical Discharge Machining, Society of Manufacturing Engineers, Dearbern, Michigan, 2001, p. 12.

[7] L. Houman, Total EDM, in: E.C. Jameson (Ed.), Electrical Discharge Machining: Tooling, Methods and Applications, Society of Manufacturing Engineers, Dearbern, Michigan, 1983, pp. 5–19.

[8] S. Webzell, That first step into EDM, in: Machinery, 159, (4040) Findlay Publications Ltd, Kent, UK, November 2001, p. 41.

[9] Rajurkar, K. P., & Yu, Z. Y. (2000). 3d micro-edm using cad/cam. Cirp Annals, 49(1), 127-130.

[10] Yu, Z. Y., Masuzawa, T., & Fujino, M. (1998). Micro-EDM for three-dimensional cavities-development of uniform wear method. CIRP Annals, 47(1), 169-172.

[11] Singh, S., Maheshwari, S., & Pandey, P. C. (2004). Some investigations into the electric discharge machining of hardened tool steel using different electrode materials. Journal of materials processing technology, 149(1-3), 272-277.

[12] FREI, Charles. New methods of conditioning the dielectric liquid in EDM. 1992.

[13] Hinduja, S., & Kunieda, M. (2013). Modelling of ECM and EDM processes. CIRP Annals, 62(2), 775-797.

[14] Schumacher, B. M. (1990). About the role of debris in the gap during electrical discharge machining. CIRP annals, 39(1), 197-199.

[15] Yeo, S. H., Kurnia, W., & Tan, P. C. (2007). Electro-thermal modelling of anode and

cathode in micro-EDM. Journal of Physics D: Applied Physics, 40(8), 2513.
[16] Garg, R. K., Singh, K. K., Sachdeva, A., Sharma, V. S., Ojha, K., & Singh, S. (2010). Review of research work in sinking EDM and WEDM on metal matrix composite materials. The International Journal of Advanced Manufacturing Technology, 50(5-8), 611-624.
[17] Ho, K. H., Newman, S. T., Rahimifard, S., & Allen, R. D. (2004). State of the art in wire electrical discharge machining (WEDM). International Journal of Machine Tools and Manufacture, 44(12-13), 1247-1259.
[18] J. Qu, A.J. Shih, R.O. Scattergood, Development of the cylindrical wire electrical discharge machining process, part 1: concept, design, and material removal rate, J. Manuf. Sci. Eng. 124(3) (2002) 702–707.
[19] J. Qu, A.J. Shih, R.O. Scattergood, Development of the cylindrical wire electrical discharge machining process, part 2: surface integrity and roundness, J. Manuf. Sci. Eng. 124 (3) (2002)708–714.
[20] Lauwers B., Kruth J.P., Bleys P., Van Coppenolle B., Stenvens L., Derighetti R., 1998, Wire rupture prevention using on-line pulse localization in WEDM, Proc. of ISEM 12, 203-213..
[21] Pandey PC, Shan HS (1999) Modern machining process. Tata McGraw-Hill Publishing Company Ltd, ISBN 0070965536, 84–113.
[22] Luis CJ, Puertas I, Villa G (2005) Material removal rate and electrode wear study on the EDM of silicon carbide. J Mater Process Technol 164–165:889–896
[23] Altpeter, F., Perez, R., 2004, Relevant Topics in Wire Electrical Discharge Machining Control, J. of Materials Processing Technology, Vol. 149, Issues 1-3, 147-151.
[24] Han, F., Wachi, S., & Kunieda, M. (2004). Improvement of machining characteristics of micro-EDM using transistor type isopulse generator and servo feed control. Precision Engineering, 28(4), 378-385.
[25] Hara S, Nishioki N. Ultra-high speed discharge control for micro electric discharge machining. Initiatives of precision engineering of a millennium. Kluwer Academic Publisher; 2001. p. 194–8.
[26] Yan, M. T., & Chien, H. T. (2007). Monitoring and control of the micro wire-EDM process. International Journal of Machine Tools and Manufacture, 47(1), 148-157.
[27] Kunieda, M., Lauwers, B., Rajurkar, K. P., & Schumacher, B. M. (2005). Advancing EDM through fundamental insight into the process. CIRP annals, 54(2), 64-87.
[28] Chakraborty S, Dey V, Ghosh SK. A review on the use of dielectric fluids and their

effects in electrical discharge machining characteristics. Precision Engineering. 2015 Apr 1;40:1-6.
[29] Leão FN, Pashby IR. A review on the use of environmentally-friendly dielectric fluids in electrical discharge machining. Journal of Materials Processing Technology. 2004 Jun 10;149(1-3):341-6.
[30] Singh S, Bhardwaj A. Review to EDM by using water and powder-mixed dielectric fluid. J Miner Mater Charact Eng 2011;10(2):199–230.
[31] Kunieda M, Yoshida M, Taniguchi N. Electrical discharge machining in gas. CIRP Annals. 1997 Jan 1;46(1):143-6
[32] Bogaerts, A., Neyts, E., Gijbels, R., & Van der Mullen, J. (2002). Gas discharge plasmas and their applications. Spectrochimica Acta Part B: Atomic Spectroscopy, 57(4), 609-658.
[33] Zou R, Yu Z, Yan C, Li J, Liu X, Xu W. Micro electrical discharge machining in nitrogen plasma jet. Precision Engineering. 2018 Jan 1;51:198-207.
[34] Urabe, K., Morita, T., Tachibana, K., & Ganguly, B. N. (2010). Investigation of discharge mechanisms in helium plasma jet at atmospheric pressure by laser spectroscopic measurements. Journal of Physics D: Applied Physics, 43(9), 095201.
[35] Jiang, N., Ji, A., & Cao, Z. (2009). Atmospheric pressure plasma jet: Effect of electrode configuration, discharge behavior, and its formation mechanism. Journal of Applied Physics, 106(1), 013308.
[36] Kunieda M., Nakashima T., 1998, Factors Determining Discharge Location in EDM, IJEM, No.3,53-58.
[37] Kunieda M., Kojima H., 1990, On-line Detection of EDM Spark Locations by Multiple Connection of Branched Electric Wires, Annals of the CIRP, 39/1, 171-174.
[38] Obara H., 1992, Detection of Discharging Position on Wire EDM, Proc. ISEM 10, 404-409.
[39] Han F., Kunieda M., 2001, Chaos Found in Distribution of EDM Spark, Proc. of ISEM XIII,185-192.
[40] Masuzawa T. State of the art of micromachining. CIRP Annals-Manufacturing Technology. 2000 Jan 1;49(2):473-88
[41] The state-of-the-art EDM science, in: Tooling and Production D.R. Stovicek, The state-of-the-art EDM science, in: Tooling and Production, Nelson Publishing Inc., Ohio, US, 59(2) May1993, p. 42
[42] Ho, K. H., & Newman, S. T. (2003). State of the art electrical discharge machining

(EDM). International Journal of Machine Tools and Manufacture, 43(13), 1287-1300.
[43] Abbas NM, Solomon DG, Bahari MF. A review on current research trends in electrical discharge machining (EDM). International Journal of Machine Tools and Manufacture. 2007 Jun 1;47(7-8):1214-28.
[44] Reynaerts, D., & Van Brussel, H. (1997). Microstructuring of silicon by electro-discharge machining (EDM)—part I: theory. Sensors and Actuators A: Physical, 60(1-3), 212-218.
[45] Reynaerts, D., & Van Brussel, H. (1997). Microstructuring of silicon by electro-discharge machining (EDM)—part I: theory. Sensors and Actuators A: Physical, 60(1-3), 212-218.
[46] Masuzawa T, Fijino M, Kobayashi K. Wire Electro-discharge Grinding for Micromachining [J]. Annals of the CIRP,1985,34(1):431-434.
[47] van Osenbruggen, C., Luimes, G., van Dijk, A,,Siekman, J.G., 1965, Micro Spark Erosion as a Technique in Micro-miniaturization, Proc. of the IFAC/IFIP Symposium,Dies:
[48] Yu, Z. Y., Rajurkar, K. P., & Shen, H. (2002). High aspect ratio and complex shaped blind micro holes by micro EDM. CIRP annals, 51(1), 359-362.
[49] Fujino M., Okamoto N., Masuzawa T., 1995, Development of Multi-Purpose Micro processing Machine, Proceedings of ISEM XI, 613-620.
[50] Lazarenko, B.R., 1943, To invert the effect of wear on electric power contacts", Dissertation of The All-Union Institute for Electro Technique in Moscow/CCCP (in Russian).
[51] Motoki, M., Lee, C., Tanimura, T., 1967, Research on electrode Erosion Caused by Transient Arc Discharge in Dielectric Liquid, J. IEEJ, 87-943, 793-801 (in Japanese).
[52] Ikai, T., Hashiguchi, K., 1988, On the Tool Electrode Material with Low Erosion in the Electric Discharge Machining, T. IEEJ. D, 108-3, 338-343 (in Japanese).
[53] Mohri N., Suzuki M., Furuya M., Saito N., 1995, Electrode Wear Process in Electrical Discharge Machining, Annals of the CIRP, 44/1, 165-168.
[54] Kunieda M., Kobayashi T., 2004, Clarifying Mechanism of Determining Tool Electrode Wear Ratio in EDM Using Spectroscopic Measurement of Vapor Density, J. Materials Processing Technology, 149, 284-288.
[55] Xia H., Hashimoto, H., Kunieda M., Nishiwaki N., 1996, Measurement of Energy Distribution in Continuous EDM Process, J. of JSPE, 62, 8,1141-1145 (in Japanese).
[56] Van Dijck, F., 1973, Physico-Mathematical Analysis of the Electro Discharge

Machining Process, Dissertation of Katholieke Universiteit Leuven.
[57] Hayakawa, S., Yuzawa, M., Kunieda, M., Nishiwaki, N., 2001, Time Variation and Mechanism of Determining Power Distribution in Electrodes during EDM Process, IJEM, 6, 19-26.
[58] Yu Z Y，Masuzawa T，Fujino M. Micro-EDM for Three Dimensional Cavities，—Development of Uniform Wear Method[J]. Annals of the CIRP，1998，47(1): 169~172.
[59] A. Taylan, L. Blaine, Y.C. Yen, Manufacturing of dies and molds, Ann. CIRP 50 (2) (2001) 405–423
[60] Xu, J., Guo, B., Shan, D., Wang, Z., Li, M., & Fei, X. (2014). Micro-punching process of stainless steel foil with micro-die fabricated by micro-EDM. Microsystem technologies, 20(1), 83-89.
[61] Chern, G. L., Wu, Y. J. E., & Liu, S. F. (2006). Development of a micro-punching machine and study on the influence of vibration machining in micro-EDM. Journal of Materials Processing Technology, 180(1-3), 102-109.
[62] Yu Z，Rajurkar K P. Generation of Complex Micro Cavities by Micro EDM [J]. Transactions of North America Manufacturing Research Institute of SME，2000，233~238.
[63] Wataru NATSU, Takumu MIYAMOTO, Sha LI. Clarification and Solution of Depth-dependent Tool Wear and Removal Rate in Micro Electrical Discharge Drilling. Proceeding of the 13th euspen international conference.
[64] Yu ZY, Zhang Y, Li J, Luan J, Zhao F, Guo D. High aspect ratio micro hole drilling aided with ultrasonic vibration and planetary movement of electrode by micro-EDM. CIRP Annals-Manufacturing Technology. 2009 Jan 1;58(1):213-6
[65] Wansheng Z, Zhenlong W, Shichun D, Guanxin C, Hongyu W. Ultrasonic and electric discharge machining to deep and small hole on titanium alloy. Journal of Materials Processing Technology. 2002 Jan 15;120(1-3):101-6.
[66] Hung JC, Lin JK, Yan BH, Liu HS, Ho PH. Using a helical micro-tool in micro-EDM combined with ultrasonic vibration for micro hole machining. Journal of Micromechanics and Microengineering. 2006 Nov 13;16(12):2705.
[67] Yu ZY, Zhang Y, Li J, Luan J, Zhao F, Guo D. High aspect ratio micro hole drilling aided with ultrasonic vibration and planetary movement of electrode by micro-EDM. CIRP Annals-Manufacturing Technology. 2009 Jan 1;58(1):213-6.

[68] Ichikawa T, Natsu W. Investigation of machining mharacteristics of micro-EDM with ultrasonically vibrated machining fluid under ultra-small discharge Energy. International Journal of Electrical Machining. 2013;18:1-7.
[69] Ferraris E, Castiglioni V, Ceyssens F, Annoni M, Lauwers B, Reynaerts D. EDM drilling of ultra-high aspect ratio micro holes with insulated tools. CIRP Annals-Manufacturing Technology. 2013 Jan 1;62(1):191-4.
[70] Tanabe, R., Ito, Y., Mohri, N., & Masuzawa, T. (2011). Development of peeling tool for micro-EDM. CIRP annals, 60(1), 227-230.
[71] Ikeda, M.,1972, The Movement of a Bubble in the Gap Depending on the Single Electrical Discharge (1st report), J. JSEME, 6, 11, 12-26 (in Japanese).
[72] Miyajima J. Observation of Bubbles generated in EDM Gap. The Spring Meeting of JSPE. 1987 : 723.
[73] S. Hayakawa, Observation of flying debris scattered from discharge point in EDM process, in: Proceedings of the 16th International Symposium on Electro machining, ISEM XVI, 2010, pp. 121–125.
[74] Wang J, Han F, Cheng G, Zhao F. Debris and bubble movements during electrical discharge machning. International Journal of Machine Tools and Manufacture. 2012 Jul 1;58:11-8.
[75] Wang J, Han F. Simulation model of debris and bubble movement in consecutive-pulse discharge of electrical discharge machining. International Journal of Machine Tools and Manufacture. 2014 Feb 1;77:56-65.
[76] Kitamura T, Kunieda M, Abe K. High-speed imaging of EDM gap phenomena using transparent electrodes. Procedia CIRP. 2013 Jan 1;6:314-9.
[77] Kitamura, T., & Kunieda, M. (2014). Clarification of EDM gap phenomena using transparent electrodes. CIRP Annals, 63(1), 213-216.
[78] Kitamura T, Kunieda M, Abe K. Observation of relationship between bubbles and discharge locations in EDM using transparent electrodes. Precision Engineering. 2015 Apr 1;40:26-32.
[79] T. Miyamoto, M. Machida, W. Natsu: Influence of electrode material on EDM characteristics for micro deep hole, Proceedings of JSPE spring meeting 2015, (2015), pp.71-72. (in Japanese)
[80] Berger L. Dielectric strength of insulating materials. Carbon. 2006;1:2.
[81] Bian Y, Dong F, Zhang W, Wang H, Tan C, Zhang Z. 3D reconstruction of single rising

bubble in water using digital image processing and characteristic matrix. Particuology. 2013 Apr 1;11(2):170-83.
[82] Gonzalez RC, Wintz P. Digital image processing (3rd Edition). Prentice-Hall, Inc. 2007:649-61.
[83] Kern R. Sinker dielectric fundamentals. EDM Today 2009. January/February issue.
[84] Guitrau EB. WIRE EDM--AN OVERVIEW OF TECHNOLOGY AND TRENDS. Society of Manufacturing Engineers; 2000.
[85] Liu Y, Ji R, Zhang Y, Zhang H. Investigation of emulsion for die sinking EDM. The International Journal of Advanced Manufacturing Technology. 2010 Mar 1;47(1-4):403-9.
[86] Ekmekci B, Elkoca O, Erden A. A comparative study on the surface integrity of plastic mold steel due to electric discharge machining. Metallurgical and Materials Transactions B. 2005 Feb 1;36(1):117-24.
[87] Tzeng YF, Lee CY. Effects of powder characteristics on electrodischarge machining efficiency. The International Journal of advanced manufacturing technology. 2001 Apr 1;17(8):586-92.
[88] Chow HM, Yang LD, Lin CT, Chen YF. The use of SiC powder in water as dielectric for micro-slit EDM machining. Journal of materials processing technology. 2008 Jan 1;195(1-3):160-70.
[89] Liu Y, Ji R, Zhang Y, Zhang H. Investigation of emulsion for die sinking EDM. The International Journal of Advanced Manufacturing Technology. 2010 Mar 1;47(1-4):403-9.
[90] Kao CC, Tao J, Shih AJ. Near dry electrical discharge machining. International Journal of Machine Tools and Manufacture. 2007 Dec 1;47(15):2273-81.
[91] Cao Z, Liu Z, Ling J, Qiu M, Wang X. Deep-type hole machining by inner jetted aerosol dielectric ablation. The International Journal of Advanced Manufacturing Technology. 2015 Jun 1;78(9-12):1989-98.
[92] Lan-Rong C, Yan J, De-Jin H. Dressing of metal-bonded superabrasive grinding wheels by means of mist-jetting electrical discharge technology. journal of materials processing technology. 2009 Jan 19;209(2):779-84.
[93] MASAK T, KURIYAGAWA T. Study of precision micro-Electro-Discharge Machining (3rd Report): Analysis of micro-EDM process with deionized water. 2009. Vol. 43, No. 104:163-71.
[94] Li S, Natsu W, Masaki T, Yu ZY. Investigation on the influence of machining fluid on processing characteristics in micro-EDM. Advanced Materials Research 2012 (Vol. 479,

pp. 407-413). Trans Tech Publications.
[95] J. Murray, J. Sun, D. Patil, T. Wood and A. Clare: Physical and electrical characteristics of EDM debris, Journal of Materials Processing Technology, No.229(2016), pp.54-60.
[96] Rajagopalan, Raj, and Paul C. Hiemenz. "Principles of colloid and surface chemistry." Marcel Dekker, New-York 8247 (1997): 8.
[97] Ichikawa T, Natsu W. Investigation of machining characteristics of micro-EDM with ultrasonically vibrated machining fluid under ultra-small discharge Energy. International Journal of Electrical Machining. 2013;18:1-7.
[98] E. Suzuki. Development of high speed micro hole drilling machine by EDM, Journal of the Japan Society of Electrical Machining Engineers. 2013. Vol.47, No.114: 7-11. (In Japanese)

Achievements

Peer-reviewed journal papers

1. Guodong Li, Wateru Natsu, Zuyuan Yu. Investigation of depth-dependent characteristic in micro EDM drilling based on direct interelectrode area observation. International Journal of Electrical Machining. 2019, 24:33-38. (Chapter 2).

2. Guodong Li, Wataru Natsu, and Zuyuan Yu. Study on debris behavior and its influence on EDM characteristics in deep micro hole machining. Procedia CIRP 2018, 68: 578-581. (Part of chapter 2)

3. Guodong Li, Wateru Natsu, Zuyuan Yu. Study on quantitative estimation of bubble behavior in micro hole drilling with EDM. International Journal of Machine Tools and Manufacture. 2019, 140: 103437 (Chapter 3 and part of chapter 4)

4. Guodong Li, Wateru Natsu. Realization of micro EDM drilling with high machining speed and accuracy by using mist deionized water jet. Precision Engineering. (Chapter 5, accepted)

International conference papers

1. Guodong Li, Wataru Natsu, Zuyuan Yu. Observation of phenomenon in gap area during micro hole drilling with micro EDM. euspen's 17th International Conference & Exhibition, May 2017,Hannover, DE.

2. Guodong Li, Wataru Natsu, Zuyuan Yu. Clarification on the behavior of bubble in micro EDM drilling. The 17th International Conference on Precision Engineering. Nov 2018, Kamakura.

Domestic conference paper

1. Guodong Li, Wataru Natsu, Zuyuan Yu. Observation of phenomenon in gap area during the micro hole drilling with micro EDM[C] 精密工学会学術講演会講演論文集 2017 年度精密工学会春季大会, 2017: 695-696.

2. Guodong Li, Wataru Natsu, Zuyuan Yu. Study on Electrical Discharge Machining for Deep Micro hole with Atomized Dielectric Jet[C]//精密工学会学術講演会講演論文集 2017 年度精密工学会秋季大会, 2017: 875-876.

3. Guodong Li, Wataru Natsu, Zuyuan Yu. Investigating depth-dependence of bubble

behavior in micro deep hole drilling with micro EDM[C] 精密工学会学術講演会講演論文集 2018 年度精密工学会春季大会. The Japan Society for Precision Engineering, 2018: 887-888.

4. Guodong Li, Wataru Natsu, Zuyuan Yu. Depth dependent characteristics of discharge and their influence on micro deep hole drilling with EDM. 精密工学会学術講演会講演論文集 2018 年度精密工学会春季大会, 2018: 329-330.

5. Guodong Li, Wataru Natsu, Zuyuan Yu. Investigating depth-dependence of bubble behavior in micro deep hole drilling with micro EDM. [C] Proceedings of JSPE Semestrial Meeting 2018 JSPE Spring Conference. The Japan Society for Precision Engineering, 2017: 887-888.

6. Guodong Li, Wataru Natsu, Zuyuan Yu. Discharge characteristic influenced by debris concentration and bubble escaping speed in micro EDM drilling, [C] Proceedings of JSPE Semestrial Meeting 2019 JSPE Spring Conference. The Japan Society for Precision Engineering, 2019.

Acknowledgemets

In the end of the dissertation, it is time to express my sincere thanks to all the people helping me during my doctor period.

Sincerely thanks to Prof. Natsu for his unselfish devotion and help no matter in the research or daily life. I am so sorry that I give him so much troubles. His amiability and gentleness teach me how to face the life. His strictness and diligence teach me how to perform the research. I am honored to be your student.

Sincerely thanks to Secretary Sano for her kindness help on the daily work in the university.

Sincerely thanks to all the members in the Natsu Lab for their unselfish helps to solve the problems from daily life to the experiments. Thanks for your suggestions on the research conferences.

Sincerely thanks to M.S. Xing Huacheng for his unselfish in the daily life.

Sincerely thanks to the staffs from NAC company to support my experiments.

Sincerely thanks to the staffs from Keyence corporation to support the data measurement in my experiments.

Sincerely thanks to the staffs in the factory of TUAT to help and guide me how to use the machine tools.

Sincerely thanks to Prof. Yu in the DUT to always give me advices both in the research and life.

Sincerely thanks to Prof. Luo Hongping and Prof. Liu Guixian from Guangdong University of Technology to give me the supports in the research and life.

Sincerely thanks to Ph.D He Junfeng from Guangdong University of Technology to give me the supports in the research and life.

Sincerely thanks to my families for giving me support to overcome every obstacle.

Sincerely thanks to my fiancée Wang Yan for her endless softness and support to make me not alone any more.